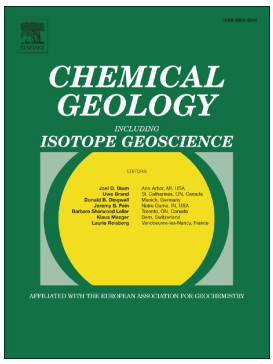

SHRIMP U–Pb–Th xenotime (YPO4) geochronology: A novel approach for the correction of SIMS matrix effects

A.J. Cross, I.S. Williams

PII: S0009-2541(17)30698-8
DOI: https://doi.org/10.1016/j.chemgeo.2017.12.017
Reference: CHEMGE 18588

To appear in: *Chemical Geology*

Received date: 29 April 2017
Revised date: 1 December 2017
Accepted date: 21 December 2017

Please cite this article as: A.J. Cross, I.S. Williams , SHRIMP U–Pb–Th xenotime (YPO4) geochronology: A novel approach for the correction of SIMS matrix effects. The address for the corresponding author was captured as affiliation for all authors. Please check if appropriate. Chemge(2017), https://doi.org/10.1016/j.chemgeo.2017.12.017

SHRIMP U–Pb–Th xenotime (YPO_4) geochronology: a novel approach for the correction of SIMS matrix effects

A.J. Cross[1, 2]* and I.S. Williams[1]

[1]Research School of Earth Sciences, The Australian National University, Canberra ACT 0200, Australia
[2]Geoscience Australia, GPO Box 378, Canberra, ACT 2601, Australia

*Corresponding author.
Email address: andrew.cross@ga.gov.au

Keywords: Geochronology, SIMS, SHRIMP, xenotime, U–Pb–Th matrix-effects

Abstract

Xenotime (YPO_4) occurs in a wide range of geological environments, but its potential to establish the timing of mineralisation and sediment diagenesis has been the focus of most recent studies. Xenotime in these settings usually has a relatively low uranium content (typically < 1000 ppm) compared to igneous xenotime and occurs as microscopic crystals (< 50 μm diameter), either individually or as outgrowths on zircon substrates. Large radius ion microprobes, such as the SHRIMP or Cameca 1270/1280, that have high sensitivity and spatial resolution, are well suited for U–Pb–Th analysis of xenotime from such environments. SIMS U–Pb–Th analyses of xenotime, however, are prone to significant U–Pb–Th matrix effects that are related to the wide natural range of U (0–6 wt%) and rare earth element (REE) (ΣREE: 12–22 wt%) concentrations in this mineral. For SHRIMP U–Pb–Th xenotime analyses, a 1 wt% increase in U concentration, relative to the U–Pb–Th calibration reference material, will on average cause a corresponding increase in the measured $^{206}Pb/^{238}U$ and $^{208}Pb/^{232}Th$ of approximately 15% and 14%, respectively. Similarly, a 1 wt% difference in ΣREE causes an increase of about 1.2% in $^{206}Pb/^{238}U$ and about 1.7% in $^{208}Pb/^{232}Th$. Correction for these chemically-induced matrix effects requires the concurrent analysis of three xenotime reference materials which have known ages and ranges of U and ΣREE contents that have been determined accurately by electron probe microanalysis. A least squares methodology is used to derive correction coefficients that relate the SHRIMP U–Pb–Th matrix effects to the U and ΣREE concentrations for the xenotime reference materials. Crucial to the success of this technique is the use of one dimensional (1-D) calibrations using $^{206}Pb^+/^{270}[UO_2]^+$ and $^{208}Pb^+/^{248}[ThO]^+$. Processing is carried out in two steps: (1) derivation of correction coefficients to

matrix-correct the $^{206}Pb^{+}/^{270}[UO_2]^{+}$ and $^{208}Pb^{+}/^{248}[ThO]^{+}$ ratios, and (2) processing of the matrix-corrected ratios to determine $^{206}Pb/^{238}U$ and $^{208}Pb/^{232}Th$.

1. Introduction

Xenotime (YPO_4) is a widespread but volumetrically minor mineral that can have numerous origins, such as: (1) igneous, in granites (e.g. Förster, 1998; Wark & Miller 1993; Schaltegger et al., 2005; Li et al., 2013) and pegmatites (Amli 1975; Demartin et al., 1991), (2) metamorphic, in metapelitic rocks (Franz et al., 1996; Bea & Montero 1999) and quartzitic rocks (Aleinikoff et al. 2012) (3) hydrothermal quartz veins (Brown et al., 2002; Cross et al., 2005), (4) authigenic overgrowths on detrital zircon (Rasmussen 1996; McNaughton et al., 1999) in siliciclastic sedimentary rocks (Aleinikoff et al., 2015), and (5) detrital mineral in placer deposits (Van Emden et al., 1997). The particular type of xenotime origin can be determined by trace element composition (England et al., 2001; Kositcin et al., 2003; Aleinikoff et al., 2010; 2015).

With typically low initial Pb concentrations, high U and Th contents, ability to self-anneal radiation damage (Harrison et al., 2002) and a closure temperature similar to that of zircon and monazite (~ 900ºC, Cherniak 2006), xenotime has many of the attributes of an excellent geochronometer. The small grain size of xenotime in hydrothermal environments or as outgrowths on detrital zircon (< 50 μm), combined with relatively low U and Th concentrations in these environments, has meant that geochronological studies have relied on large radius ion microprobes with high sensitivity and high spatial resolution such as the sensitive high resolution ion microprobe (SHRIMP) or Cameca 1270/1280. However, determination of Pb/U and Pb/Th ages of xenotime by secondary ion mass spectrometry (SIMS) is hampered by severe matrix effects (due to compositional differences between standard and unknown) that complicate isotopic analysis of this mineral (Fletcher et al., 2000; Fletcher et al., 2004; Li et al., 2013). The SHRIMP U–Pb matrix effect causes a breakdown in the basic assumption underpinning all SIMS $^{206}Pb/^{238}U$ ages, i.e. that the emission of secondary $^{206}Pb^{+}$ and $^{238}U_xO_x^{+}$ ions relative to the true $^{206}Pb/^{238}U$ in both the calibration reference material and unknown is identical.

Much of the success of the SHRIMP and Cameca (1270 or 1280) large radius ion microprobes in the application of U–Pb–Th dating is linked to the unique characteristics of zircon as a geochronometer. Nearly all zircon has a composition that is within a few weight percent of the

stoichiometric formula for the mineral. The most abundant trace element substitutions are Hf, Y and the heavy rare earth elements (HREE). Total REE and Y contents are typically <1 wt % and Hf concentrations average ~ 2 wt % (Hoskin and Schaltegger 2003). In contrast, xenotime has a wide range in composition. The HREE, which substitute for Y, can range up to ~ 10 wt %, while U and Th concentrations can range up to ~ 6 wt%. This range in chemical composition is the source of significant matrix effects which greatly complicate the SIMS U–Pb–Th analysis of this mineral. Here we outline a method to overcome these problems by using multiple reference xenotimes with a range of chemical compositions.

1.1 SHRIMP U–Pb–Th matrix effects

SIMS U–Pb–Th matrix effects result in a breakdown of the U–Pb–Th calibration procedure used to calculate $^{206}Pb/^{238}U$ and $^{208}Pb/^{232}Th$ from $^{206}Pb^{+}/^{238}U^{+}$ and $^{208}Pb^{+}/^{232}Th^{+}$. It is caused by differences in the ionisation efficiency of the U, Pb or Th isotopes (or a combination thereof) in crystals of the same mineral with either different chemical compositions, structural orientations, or degree of radiation damage, relative to the calibration standard.

Black et al. (1991) were perhaps the first to recognise an ion–probe instrumental bias in the $^{206}Pb/^{238}U$ ratios from high U zircons. Working on high U (2830–6760 ppm) zircons from mafic dykes in the Vestfold Hills of East Antarctica, Black et al. (1991) noted ~ 8% elevations in $^{206}Pb/^{238}U$ ages relative to $^{207}Pb/^{206}Pb$ ratios. These researchers attributed the apparent elevations in $^{206}Pb/^{238}U$ to an instrumental bias in the sputtering and ionisation efficiency of the $^{206}Pb^{+}$ and $^{238}U^{+}$ ions, between the matrix of the standard zircon, and high U zircons which were presumed to be metamict and therefore structurally damaged.

McLaren et al. (1994) also recognised an ion probe instrumental bias in the measurement of $^{206}Pb/^{238}U$ ratios from a single, high U zircon (SL14). These researchers, like Black et al. (1991), attributed this effect to U–induced structural contrasts with the standard, low U zircon SL13. In contrast, Williams and Hergt (2000) and Butera et al. (2001), have suggested that the elevated $^{206}Pb/^{238}U$ ratios, typical for ion probe analyses of high U zircon, are better interpreted as a U–induced instrumental bias rather than a microstructural one resulting from accumulated radiation damage. Butera et al. (2001) suggested that the U-induced matrix effect for zircon occurs only in crystals with over ~ 2500 ppm U. They suggested that for every ~ 1000 ppm over this threshold, there is approximately a 2% increase in the measured $^{206}Pb^{+}/^{238}U^{+}$. More recently, White and Ireland (2012) have suggested that elevated apparent $^{206}Pb/^{238}U$ ages associated with SHRIMP U–

Pb analysis of high-U zircon are directly related to the metamict (radiation damaged) nature of these zircons.

Although there are many published ion probe U–Pb–Th studies of monazite, only a few report U–Pb–Th matrix effects. For example, Stern and Sanborn (1998) and Stern and Berman (2000), reported elevations in monazite $^{206}Pb/^{238}U$ and $^{208}Pb/^{232}Th$ ratios of 6% and 8% respectively, which were attributed to Th concentration contrasts between the calibration standard and unknown. Zhu et al. (1998) also reported $^{206}Pb/^{238}U$ ion probe matrix effects which they thought stemmed from Th and/or Si concentration contrasts. Rasmussen & Fletcher (2002) and Fletcher et al. (2010) reported matrix effects for SHRIMP U–Pb–Th determinations of monazite. Crystal orientation can also cause significant SIMS U–Pb matrix effects and have been reported for the oxides baddeleyite (Wingate & Compston, 2000) and rutile (Taylor et al., 2012).

The wide range of chemical compositions in natural xenotime makes it particularly prone to U–Pb–Th matrix effects. Fletcher et al. (2000) noted a strong correlation between U concentration and $^{206}Pb^{+}/^{238}U^{+}$ ratios and suggested a method of U abundance scaling that attributed all $^{206}Pb/^{238}U$ age deviations to U. In a later paper, Fletcher et al. (2004) suggested that Th and ΣREE concentration contrasts in xenotime also result in $^{206}Pb/^{238}U$ and $^{208}Pb/^{232}Th$ age deviations. These researchers calculated correction factors for these elements by concurrently analysing three reference xenotime standards with differing compositions, and determined the correction factors for each element using a simple least squares routine. The correction factors calculated by Fletcher et al. (2004) for U, Th and ΣREE showed that for every 1 wt% abundance difference in these elements between the calibration standard and unknown, there is a corresponding 6.28%, 3.01% and 0.79% difference respectively in the measured $^{206}Pb/^{238}U$ ages. Correction factors for the same elements were also calculated for SHRIMP $^{208}Pb/^{232}Th$ xenotime ages and are 2.46%, 0.63% and 1.60% for U, Th and ΣREE respectively (Fletcher et al., 2004). More recently, Li et al. (2013), conducting experiments on a Cameca 1280, used a similar approach to Fletcher et al. (2004) and calculated broadly similar correction coefficients for U, Th and ΣREE for both $^{206}Pb/^{238}U$ and $^{208}Pb/^{232}Th$ xenotime ages. However, uncertainty regarding the reliability of SHRIMP $^{206}Pb/^{238}U$ and $^{208}Pb/^{232}Th$ xenotime ages has meant that most SHRIMP U–Pb xenotime dating experiments have been carried out on xenotimes > 1000 Ma where $^{207}Pb/^{206}Pb$ ages that are unaffected by matrix affects, can be used.

The aim of this study was to examine the limitations of SHRIMP xenotime U–Pb–Th dating and focusing on the effects, causes, and solutions to age deviations that result from matrix mismatches between U–Pb–Th calibration standards and unknowns. To do this, SHRIMP U–Pb–Th dating experiments were conducted on a number of xenotime samples of contrasting chemical composition that had been accurately dated by U–Pb ID–TIMS.

2. **Analytical methods and xenotime reference materials**

Xenotime crystal fragments and single crystals were mounted in epoxy resin and polished to reveal the sample interiors. Transmitted and reflected light photomicrographs were taken of the xenotime, followed by backscattered electron images using a Cambridge 360 scanning electron microscope at the Australian National University (ANU) Electron Microscopy Unit. ISOTOPIC ANALYSES WERE CARRIED OUT ON THE SHRIMP II AND SHRIMP-RG ION MICROPROBES LOCATED AT THE RESEARCH SCHOOL OF EARTH SCIENCES (RSES), ANU; electron probe microanalysis (EPMA) were conducted on a Cameca SX100 also located at RSES. In the following, EPMA refers to WAVELENGTH DISPERSIVE SPECTROMETRY DATA.

2.1. SHRIMP

Experiments conducted on SHRIMP II used a primary O_2^- beam with an ion current that ranged from 2 nA to 3.1 nA. Spot diameters were ~ 10 μm to 30 μm. For two experiments, the energy window was set to exclude 50% and 90%, respectively, of the low energy ions. This was done to remove the scattered ions interfering with the ^{204}Pb peak and also to test whether the high energy ions were less susceptible to U–Pb–Th matrix effects. Most of the experiments conducted on SHRIMP-RG were carried out under the analytical conditions needed for the analysis of diagenetic xenotime overgrowths and hydrothermal xenotime (i.e. ≤ 10 μm). To achieve this small spot size, the primary beam was focussed through a ~ 30 μm Köhler aperture, producing spot diameters between 5 and 7 μm. Initial trials on SHRIMP-RG using a 0.1 nA, O_2^- primary beam yielded a ^{206}Pb count rate of about 100 cps for analyses of the primary calibration standard MG-1 (~ 70 ppm ^{206}Pb; i.e. 14 cps/nA/ppm). However, there was concern that the low primary beam current perhaps was approaching the lower limit of stable analytical conditions such that poor individual $^{206}Pb^+/^{238}U^+$ spot precisions (~ 2%) resulted. Because of the higher O^- current achievable with the SHRIMP-RG duoplasmatron (O^-/O_2^- = 4), an O^- primary beam was used which resulted in an increase in the absolute ^{206}Pb count rate for MG-1 by a factor of ~ 3. The stronger primary current and better counting statistics offered by the O^- primary beam was judged to be the best balance between precision, sensitivity, and instrument stability. Under these conditions, primary O^- beam currents focussed through a 30 μm Köhler aperture ranged between ~ 0.8 and 1.2 nA. In contrast to SHRIMP II, SHRIMP-RG has a very low scattered ion background in the region of mass 204—only a single mass species enters the electrostatic analyser (ESA) at a given time. However, for SHRIMP II, the entire ion beam passes from the ESA into the magnet, where collisions between molecules and the flight tube result in scattering and a loss of energy. Because of the energy loss, the scattered

ions can be removed from the mass spectrum by energy filtering, as is routinely done during SHRIMP II analysis of monazite.

Several different sets of mass peaks were trialled throughout the various experiments to determine the optimum data acquisition sequence for xenotime U–Pb and Th–Pb analysis. A typical run table consisted of $^{194}[Y_2O]$, ^{204}Pb, background (measured 40 millimass units above ^{204}Pb), ^{206}Pb, ^{207}Pb, ^{208}Pb, ^{238}U, $^{248}[ThO]$, $^{254}[UO]$, $^{270}[UO_2]$ Some experiments included ^{232}Th and $^{264}[ThO_2]$ for independent $^{208}Pb/^{232}Th$ determinations. Additionally, with the aim of monitoring the matrix effects introduced by the HREE, some experiments included $^{190}[YbO]$, $^{177}[DyO]$ and $^{181}[HoO]$. Each of the analyses for the various analytical sessions consisted of 5 to 7 scans through the isotopic sequence. SHRIMP data were reduced, calculated and portrayed using Microsoft Excel® 2003, add-ins SQUID 2.50.11.02.03 (revision of Ludwig, 2009) and Isoplot 3.76.12.02.24 (revision of Ludwig, 2003). The decay constants used were those of Jaffey et al. (1971), together with present-day $^{238}U/^{235}U = 137.88$, following the recommendations of Steiger & Jäger (1977). Common-Pb corrections for unknowns were based on measured ^{204}Pb, and a Pb isotopic composition calculated using the Pb isotopic evolution model of Stacey & Kramers (1975) at a time corresponding to the estimated age of each unknown individual analysis. The result of this calculation is expressed in terms of common ^{206}Pb as a percentage of total measured ^{206}Pb ($^{206}Pb_c$). All isotopic ratios and dates cited in this publication are corrected for common Pb.

Ages derived from the pooling of multiple individual analyses are weighted means (with each constituent analysis weighted proportional to its inverse variance) unless otherwise specified. Uncertainties for pooled weighted mean $^{206}Pb/^{238}U$ and $^{208}Pb/^{232}Th$ ages include a session specific, 2σ error of the mean ('session to session error', 'calibration uncertainty' or 'external error') which is added in quadrature to the pooled $^{206}Pb/^{238}U$ and $^{208}Pb/^{232}Th$ age uncertainties.

This can be done via the equation: $2\sigma_{unc} = \sqrt{(a)^2 + (\frac{B}{100} * wm)^2}$

where 'a' is the pooled $^{206}Pb/^{238}U$ uncertainty, 'B' is the 2σ error of mean and 'wm' is the calculated weighted mean age. The session specific 2σ error of the mean is listed as a footnote in each of the SHRIMP U–Pb data tables presented.

The statistical coherence of calculated means was assessed using the Mean Square of Weighted Deviates (MSWD; McIntyre *et al.*, 1966) and the related probability of fit (POF), with the constituent analyses considered equivalent within their analytical uncertainties when the MSWD lies within the 95% confidence window defined in Table 1 of Mahon (1996) i.e. where POF > 0.025.

Uncertainties in ages derived from pooling of multiple individual analyses are quoted at the 95% confidence level unless otherwise indicated. For weighted means, the 95% confidence interval is defined as t-sigma (where t is Student's t for n–1 degrees of freedom, and n is the number of individual analyses in the population) when the MSWD of the pooled data is less than unity. When MSWD exceeds unity (but POF > 0.025), the 95% confidence interval is defined as t-sigma multiplied by the square root of the MSWD (Ludwig, 2003).

Discordance for the SHRIMP U–Pb ages reported here has been calculated using the equation:

$$\text{Disc. (\%)} = 100 \times [(^{207}\text{Pb}/^{206}\text{Pb date}) - (^{206}\text{Pb}/^{238}\text{U date})]/(^{206}\text{Pb}/^{238}\text{U date})$$

2.2 Electron probe microanalysis (EPMA)

Xenotime samples were analysed for Y, P, Si, Ca, Nd, Sm, Eu, Gd, Tb, Dy, Ho, Er, Tm, Yb, Lu, Th, and U by wavelength dispersive spectrometry (WDS) (Note that La, Ce and Pr were below the electron probe detection limits). All analyses were performed with a 25 kV electron beam regulated at 100 nA with a beam size of ~ 5 μm. The REE abundances were calibrated against synthetic REE phosphate standards and U oxide and Th oxide standards were used for U and Th calibration. Analyses were carried out using the analytical peaks and interference corrections as recommended by Pyle et al. (2002). Peak and background positions for each element were carefully chosen from EPMA scans of the three xenotime reference materials MG-1, Z6413 and BS-1. Appendix A contains the analytical conditions that were used for xenotime EPMA characterisation. With the exception of Lu, these data are comparable to the REE data set obtained by solution inductively coupled plasma-mass spectrometry (Aleinikoff et al., 2012) for MG-1 and BS-1.

2.3. Xenotime reference materials

SHRIMP xenotime U–Pb–Th experiments were conducted on fragments from three single-grain specimens, MG-1, BS-1, and Z6413. These samples have independent isotope dilution-thermal ionization mass spectrometry (ID-TIMS) U–Pb analyses and were used as reference materials. They were also used by Fletcher et al. (2004) and Li et al. (2013) in their studies of SIMS xenotime U–Pb–Th matrix effects. Two further xenotime samples were used to test the effectiveness of the derived U–Pb–Th matrix correction procedures, NY/PK 6-80 (Aleinikoff et al., 2012) and D43764, which is from the Yilgarn Craton, Western Australia.

BS-1 and MG-1 crystal fragments were obtained from Dr John Aleinikoff, USGS. Both crystals were originally provided by Dr. Miguel Basei, University of Sao Paulo, Brazil. These crystals

originated from metamorphic host rocks. BS-1 is from Bahia State, and MG-1 is from Ouro Preto, Minas Gerais State (pers. comm. Miguel Basei, 2005). Full descriptions of the original crystals are given in Fletcher et al. (2004). BS-1 has a ID-TIMS $^{206}Pb/^{238}U$ age of 508.9 ± 0.3 Ma (1σ) and a $^{207}Pb/^{206}Pb$ age of 505.5 ± 0.6 Ma (1σ) (Table 1) (Fletcher et al., 2004). A reference $^{206}Pb/^{238}U$ age of 509 Ma has been used in this study. ID–TIMS ages for MG-1 are near-concordant with a $^{206}Pb/^{238}U$ age of 490.0 ± 0.3 Ma (1σ) and a $^{207}Pb/^{206}Pb$ age of 491.8 ± 0.6 Ma (1σ) (Fletcher et al., 2004). A reference $^{206}Pb/^{238}U$ age of 490 Ma for MG-1 has been used in this study. For both MG-1 and BS-1, $^{208}Pb/^{232}Th$ ratios were calculated directly from the $^{206}Pb/^{238}U$ age assuming a closed isotopic system.

Z6413 fragments were obtained from Dr. Richard Stern, (formerly Geological Survey of Canada). This crystal is from a pegmatite from the Grenville Province, Canada (Stern and Rayner, 2003). Grain fragments are honey-yellow, clear and appear homogenous in backscattered electron images. Stern and Rayner (2003) report an ID–TIMS $^{206}Pb/^{238}U$ age of 994 ± 1 Ma (1σ) and $^{207}Pb/^{206}Pb$ age of 997 ± 1 Ma (1σ) (Table 1). A reference $^{206}Pb/^{238}U$ and $^{208}Pb/^{232}Th$ age of 994 Ma for Z6413 has been used in this study.

NY/PK 6-80 xenotime is derived from a monazite–xenotime gneiss from the Hudson Highlands of southeastern New York, USA (Aleinikoff & Grauch, 1990; Aleinikoff et al. 2012). Individual grains are mostly anhedral and range from 50 to 300 μm in diameter. Approximately 70% are clear and colourless, but ~ 30% are frosted and are pale green to brownish. Backscattered electron imaging shows that many crystals have distinct cores and rims as well as small monazite inclusions (< 1–5 μm) (Figure 1). NY/PK 6-80 was originally chosen for this study as it had ID-TIMS analyses that broadly suggested a crystallisation age of ~ 1000 Ma (see Appendix B). Although the data are spread beyond analytical uncertainty (MSWD = 12), twelve grains give a median age of 1000.1 +3.2/-4.8 Ma (96.1 % confidence) which was previously used in SHRIMP U–Pb xenotime experiments as the reference $^{206}Pb/^{238}U$ and $^{208}Pb/^{232}Th$ age for NY/PK 6-80. Subsequently, Aleinikoff et al. (2012) based on SHRIMP $^{207}Pb/^{206}Pb$ xenotime analyses, suggested that NY/PK 6-80 xenotime has experienced five separate growth periods. The cores were interpreted to have grown at 1034 ± 10 Ma and 1014 ± 3 Ma, while three periods of rim growth were interpreted at 999 ± 7 Ma, 961 ± 11 and 874 ± 11 Ma. The relative probability plot of the SHRIMP $^{207}Pb/^{206}Pb$ dates presented by Aleinikoff et al. (2012; Figure 3C) shows that the major mode for the analyses of the cores is at ~ 1012 Ma while the major mode for the analyses of the rims is at ~ 970 Ma. The SHRIMP U–Pb–Th analyses of NY/PK 6-80 cores and rims conducted during this study align well with these ages (see below) and consequently were used as reference $^{206}Pb/^{238}U$ and $^{208}Pb/^{232}Th$ values to assess the effectiveness of the matrix correction technique developed.

Sample D43764 is from a biotite schist from the Holleton region of the eastern Goldfields, Western Australia, and was procured from the Australian Museum. Xenotime crystals recovered from D43764 are yellow, euhedral dipyramids that range in size from 70 to 400 μm. The crystals are variably cracked and the majority are speckled with inclusions of monazite (<1 to 5 μm) that mostly occur in patches (Figure 1). There are no ID–TIMS data for this sample, but SHRIMP $^{207}Pb/^{206}Pb$ data collected during this study gave an age of 2622 ± 3 Ma (95 % confidence). This age has been corroborated by independent EPMA dating (Appendix C). Consequently, the $^{207}Pb/^{206}Pb$ age of 2622 Ma was used as the reference age for both $^{206}Pb/^{238}U$ and $^{208}Pb/^{232}Th$ ratios.

3. Results and Discussion

3.1. EPMA characterisation of xenotime reference materials

Representative EPMA data for MG-1, BS-1, Z6413, NY/PK 6-80 and D43764 are listed in Table 2. This table shows that there is a wide range in ΣREE and actinide concentrations among these samples. U_2O_3 contents range from 0.02 to 2.8 wt%, ThO_2 from 0.06 to 1.9 wt% and ΣREE_2O_3 from 15 to 20 wt%. Solution ICP-MS data for MG-1 and BS-1 is available in Aleinikoff et al. (2012a).

MG-1 is distinguished by lower ΣREE concentrations (~ 15 wt% ΣREE_2O_3) and also low to moderate U_2O_3 and ThO_2 contents, both of which are ~ 0.11 wt%. BS-1 contains the lowest levels of U among the reference xenotimes (~ 0.05 wt% U_2O_3) but moderate to high ThO_2 (~ 0.35 wt%) and high ΣREE_2O_3 contents of ~ 20 wt%. Three of the xenotime samples, Z6413, NY/PK 6-80 and D43764, have high U_2O_3 concentrations which are generally above ~ 1.4 wt%. Z6413 typically contains U_2O_3 of ~ 1.4 wt%, however some fragments were found to have concentrations of ~ 0.5 wt%. Z6413 is also characterised by moderate to low ThO_2 (0.26 wt%) and moderate to high ΣREE_2O_3 levels of ~ 18.5 wt%. There appears to be no discernible chemical difference between the cores and rims of NY/PK 6-80. This sample contains high U_2O_3 (~ 1.5 wt%), moderate to high ThO_2 (0.4 wt%) and high ΣREE_2O_3 levels (~ 20 wt%). Sample D43764 contains the highest ThO_2 concentrations amongst the reference xenotimes (~ 1 wt%) as well as high U_2O_3 (~ 1.6 wt%) and moderate to high ΣREE_2O_3 (~ 18.5 wt%). Z6413 and NY/PK 6-80 have the highest U/Th ratios (~ 6 and ~ 4, respectively) whereas D43764 has a U/Th ratio of ~ 1.6. BS-1 has the lowest U/Th ratio of ~ 0.15 and MG-1 has a ratio of ~ 1.

3.2 SHRIMP U–Th–Pb xenotime calibration

In determining the most suitable SHRIMP $^{206}Pb/^{238}U$ xenotime calibration method, all nine combinations of $Pb/U[O_x]:U[O_x]$ /$U[O_x]$ were trialled. Although two experiments conducted on SHRIMP II showed that the ratio pair, Pb/U:UO/U performed best overall for the three xenotime standards MG-1, BS-1 and Z6413, significant contrasts in slope between these reference materials occurred for all $Pb/U[O_x]:U[O_x]/U[O_x]$ ratio combinations in each of the SHRIMP-RG experiments. In contrast, all data sets collected on SHRIMP II and SHRIMP-RG gave good results when the 1-dimensional $^{206}Pb^+/^{270}[UO_2]^+$ calibration was used to calculate $^{206}Pb/^{238}U$ ratios (see below). Accordingly, calibration for all SHRIMP $^{206}Pb/^{238}U$ xenotime ages reported here was done using a $^{206}Pb^+/^{270}[UO_2]^+$, 1-D calibration. This SHRIMP $^{206}Pb/^{238}U$ calibration method has also been used successfully for SHRIMP U–Pb monazite dating (Fletcher et al., 2010; Huston et al., 2016) and reported for SHRIMP U–Pb xenotime analysis by Cross and Williams (2008). The 1-D calibration approach has also successfully been applied to SHRIMP $^{208}Pb/^{232}Th$ geochronology. Fletcher et al. (2010), recommend using SHRIMP $^{208}Pb^+/^{264}[ThO_2]^+$ ratios for monazite $^{208}Pb/^{232}Th$ ages, while Huston et al. (2016) have used SHRIMP $^{208}Pb^+/^{264}[ThO_2]^+$ ratios for the determination of allanite $^{208}Pb/^{232}Th$ ages.

The secondary ion energy profiles for $^{206}Pb^+$, $^{238}U^+$, $^{254}[UO]^+$ and $^{270}[UO_2]^+$ also support the calculation of $^{206}Pb/^{238}U$ from the $^{206}Pb^+/^{270}[UO_2]^+$ ratios (Figure 2a, b). Energy distributions for $^{206}Pb^+$ and $U[O_x]^+$ species, were measured on SHRIMP II and SHRIMP-RG and show similar trends to those obtained for monazite (Harrison et al. 1995 and Stern & Berman 2000). Specifically, the energy profile for $^{270}[UO_2]^+$ most closely parallels that of the $^{206}Pb^+$ ion distribution. The $^{254}[UO]^+$ ions also show a close but lesser similarity to the $^{206}Pb^+$ profile, and the $^{238}U^+$ ions have a broader energy distribution in comparison to the $^{206}Pb^+$ and $U[O_x]^+$ ion distributions.

Calculating $^{206}Pb/^{238}U$ from $^{206}Pb^+/^{270}[UO_2]^+$ ratios is straightforward. The $^{206}Pb^+/^{270}[UO_2]^+$ ratio of the unknown is divided by the Biweight (or average) $^{206}Pb^+/^{270}[UO_2]^+$ of the primary calibration reference material, which is in turn multiplied by the reference $^{206}Pb/^{238}U$ ratio of the primary calibration reference material (see below).

$$^{206}Pb/^{238}U_{(unk)}=(^{206}Pb^+/^{270}[UO_2]^+)_{unk}/av.(^{206}Pb^+/^{270}[UO_2]^+)_{std}*(^{206}Pb/^{238}U\_ref)_{std}$$

3.3 Independent $^{208}Pb/^{232}Th$ age calculations

The calculation of $^{208}Pb/^{232}Th$ ages from the reference xenotime samples can be used to assess the U–Pb–Th concordance of the target mineral, and thereby help to assess the xenotime matrix effect.

The significant matrix effects of SHRIMP xenotime $^{206}Pb^{+}/^{238}U_x^{+}$ ratios (see below) preclude the calculation of derivative $^{208}Pb/^{232}Th$ ages that are based on $^{206}Pb/^{238}U$, $^{208}Pb^{+}/^{206}Pb^{+}$ and $^{248}[ThO]^{+}/^{254}[UO]^{+}$ ratios as described for monazite by Williams et al. (1996). Therefore, independent $^{208}Pb/^{232}Th$ ratio calibration is necessary.

For the independent $^{208}Pb/^{232}Th$ age calibration, combinations of $^{208}Pb/^{232}Th$: $^{248}[ThO]/^{232}Th$ and $^{208}Pb/^{248}[ThO]$: $^{248}[ThO]/^{232}Th$ were trialled but variations in slope exist between the xenotime reference materials and these calibration pairs. This is similar to the findings of Fletcher et al. (2004) who found that the $^{208}Pb/^{232}Th$ calibration is very sensitive to the choice of calibration slope, which subsequently yielded inferior results to the $^{206}Pb/^{238}U$ age calculations and matrix corrections. In contrast, 1-D $^{208}Pb/^{232}Th$ calibrations using $^{208}Pb^{+}/^{248}[ThO]^{+}$ ratios gave the best results with 1σ external spot-to-spot error (commonly referred to the 1σ reproducibility) between 1.0% and 3.5% (1σ), which is similar to that for the 1-D $^{206}Pb^{+}/^{270}[UO_2]^{+}$ calibration. Accordingly, $^{208}Pb/^{232}Th$ ratios were calculated from the $^{208}Pb^{+}/^{248}[ThO]^{+}$ ratios in the same way xenotime $^{206}Pb/^{238}U$ ratios were derived from $^{206}Pb^{+}/^{270}[UO_2]^{+}$.

3.4 Quantitative elemental SIMS xenotime analysis

The SHRIMP U–Pb–Th xenotime matrix correction technique detailed below depends critically upon the accurate determination of xenotime chemical composition. However, the quantification of elemental concentrations of geological materials by SIMS is also significantly hampered by matrix effects. Although theoretical models have been used to overcome this problem (e.g. Andersen and Hinthorne, 1973), the best results have come from empirical approaches that use matrix matched standards and relative sensitivity factors (RSF). The RSF approach as explained by Benninghoven et al (1987) (pages 290–291) as follows. RSF are calculated from the ratio of the practical sensitivity of the elements of interest, where the practical sensitivity of element 'A' i.e. $[S_p(A)]$ is defined as: cps/nA/concentration (ppm). Therefore the RSF of element A with respect to element R is $[S_r(A)] = S_p(A)/S_p(R)$. Therefore, the concentration of element 'A' can be calculated from the ratio of the ion currents of elements A and R and the known concentration of the reference element R in the sample (usually measured by EPMA) according to the equation:

$$C(A) = 1/S_r(A) * (A^{+}/R^{+})* R \text{ (ppm)}$$

where C(A) is the concentration of element A, A^+ and R^+ are the ion currents of elements A and R and R (ppm) is the known concentration of element R. The procedure used for the technique described above involves the determination of RSF from standards of known composition which are then compared to 'unknown' samples that ideally are matrix–matched.

This approach deviates from that typically used for U abundance determinations for SHRIMP zircon analysis. For that method, a comparison is made between a matrix matched standard zircon of known composition and the 'unknown' zircon. The method assumes that the Zr content of the vast majority of zircon is constant within a few wt% and as such Zr can be used as a reference element, without independent EPMA analysis. The method involves a calibration between $^{196}[Zr_2O]^+/^{238}U^+$ and $^{254}[UO]^+/^{238}U^+$ which obeys a power law of the form $y = ax^{0.66}$ (Claouè-Long et al. 1995). Ireland & Bukovanska (2003) state that for SHRIMP analyses of the standard zircon SL13, U determinations are generally within 10% of the long term average which approximately equates to the known range of U in this mineral.

The range of Y abundance and the substituting HREE in xenotime means that there is no element of near-constant concentration that can be used as a reference from which to calculate elemental abundances. For example, the EPMA data displayed in Table 2 show that Y_2O_3 concentrations can range from 39 to 47 wt% for the reference xenotime samples used as a part of this study. Therefore, SHRIMP-based elemental abundance calculations in xenotime using Y as a reference element (without external EPMA analysis) will be biased by the actual Y concentration contrast between the standard and unknown.

With the above considerations in mind, Fletcher et al. (2004) argued that first order U abundance estimates were achievable via a method of U abundance scaling. This method relies on an observed correlation between $^{254}[UO]^+/^{194}[Y_2O]^+$ ratios and EPMA U concentrations determined from the same locations (see Fig. 6, Fletcher et al., 2004). U abundances are then derived by calculation of a U sensitivity factor, which is simply the average EPMA U concentration of the standard, divided by the average $^{254}[UO]^+/^{194}[Y_2O]^+$ of the standard. The U concentration of an unknown is then calculated by multiplying the sensitivity factor by the $^{254}[UO]^+/^{194}[Y_2O]^+$ of the unknown.

3.4.1 EPMA and SIMS elemental quantification

In an effort to determine the most suitable SIMS elemental quantification method for xenotime, the method of U abundance scaling proposed by Fletcher et al. (2004) was trialled against quantification via RSF as explained above, using both Y and Ho as reference elements. With these

methods, U concentrations were calculated from SHRIMP analyses of the reference xenotimes and compared to EPMA U abundances determined at each spot location prior to SHRIMP analysis.

For determination of U abundance using the scaling method of Fletcher et al. (2004), MG-1 was used as the U standard and the $^{270}[UO_2]^+$ molecule as a proxy for U concentration. Nine EPMA analyses of fragments from MG-1 have an average U concentration of 965 ± 65 ppm (2σ, SDOM; Standard Deviation of the Mean), which was used as the reference U concentration of MG-1 for this experiment. The reference U value for MG-1 has a 2σ variation of 6.7%, therefore U abundance calculations for 'unknown' xenotimes at best can only be expected to be accurate to this level.

MG-1 was also used as the standard for U abundance determinations using RSF, i.e. $RSF_{(U–Y)}$ and $RSF_{(U–Ho)}$. Y was measured as $^{194}[Y_2O]$, Ho as $^{181}[HoO]$ and U as $^{270}[UO_2]$. The average of nine MG-1, EPMA and SHRIMP analyses was used to determine the RSF, where $RSF_{(U–Y)}$ has a value of 45.96 and $RSF_{(U–Ho)}$ = 0.39. Therefore, the $^{270}[UO_2]^+$ molecule is more efficiently ionised than $^{194}[Y_2O]^+$ but not as efficiently as $^{181}[HoO]^+$. For the $RSF_{(U–Y)}$ and $RSF_{(U–Ho)}$, Y and Ho concentrations were determined by EPMA prior to subsequent SHRIMP analysis at the same location. Table 3 shows the comparison between the xenotime EPMA U abundance measurements for the reference xenotimes (MG-1, BS-1, Z6413 and NY/PK 6-80) with the SHRIMP-based U determinations. The EPMA U xenotime data clearly show the limitations of EPMA for U. Although the xenotime samples with U concentrations greater than ~ 1 wt% have individual uncertainty estimates of 6% to 7% (σ) (i.e. Z6413 and NY/PK 6-80), the xenotime with U concentrations significantly below ~ 1000 ppm have very imprecise U determinations. For example, EPMA U determinations of BS-1 range between 150 ppm and 570 ppm, and have individual 1σ precision estimates of 30% to 114%.

The three different SHRIMP xenotime U abundance determination methods shown in Table 3 are best assessed with reference to the results for Z6413 and NY/PK 6-80. Comparisons between the results of MG-1 are excluded as in each of the methods, MG-1 was used as the calibration standard. The highly imprecise EPMA U determinations for BS-1 result in all three of the SHRIMP-based U abundance methods falling well within the analytical errors of the EPMA determinations. Therefore, the relative merits of the three SHRIMP based techniques for estimating U concentration for BS-1 cannot be assessed independently. The comparison between the three SHRIMP-based methods of U concentration determination for Z6413 and NY/PK 6-80 show that $RSF_{(U–Ho)}$ performs the best overall, with individual U determinations generally within 5% of the EPMA value. Furthermore, the SHRIMP U abundance determinations using $RSF_{(U-Y)}$ are generally more accurate than the U abundance scaling method of Fletcher et al. (2004) by approximately 6 to 7%.

The better results of $RSF_{(U–Y)}$ in comparison to the U scaling method of Fletcher et al. (2004) are partly explained by the ~ 3 to 5 wt % difference in Y concentration that Z6413 and NY/PK 6-80 have with the standard MG-1, that is compensated for with $RSF_{(U–Y)}$. However, the superior results of $RSF_{(U–Ho)}$ over $RSF_{(U–Y)}$ are less easily explained. It might be that the ionisation of Y varies in the reference xenotimes, i.e. that the $^{194}[Y_2O]^+$ molecules are subject to matrix effects. This may be supported by the findings of Zinner & Crozaz (1986) who suggest that RSF for major elements are more affected by the matrix than for trace elements. Although the concentration of Ho in xenotime is not in trace proportions (usually about 1 wt%) its low concentration compared to Y may mean that Ho is relatively insensitive to matrix effects.

The up to 10% variation in Y content between different xenotime grains precludes this element from being used as a reference without knowledge of its true concentration. Therefore the U scaling method proposed by Fletcher et al. (2004) should be avoided. SHRIMP elemental quantification using $RSF_{(U–Ho)}$ can reasonably be expected to be within 5–10% of the actual value, whereas $RSF_{(U-Y)}$ can be expected to be within 15–20% of the real concentration.

As discussed above, the SIMS quantification of elemental abundances in xenotime is best determined with RSF that are normalised to either Ho or Y that have been determined independently by EPMA. The abundance levels of the significant REE in xenotime (i.e. Nd–Yb) and good precision achievable with EPMA for these elements mean that their analysis is most efficiently carried out by this technique prior to SHRIMP analysis. The abundance of U in concentrations of ~ 1000 ppm or greater can be determined accurately by EPMA. However, for xenotime with significantly lower levels of U, the use of $RSF_{(U–Ho)}$ or $RSF_{(U–Y)}$ is preferred.

Accurately targeting the SHRIMP spot at the same sample location as analysed by the EPMA requires great care in recording the location of the EPMA spot. Using an Au coat for EPMA analysis greatly helps this task as the electron probe beam ‘welds’ the Au onto the sample surface leaving a bright spot which is easily photographed and is clearly seen on the SHRIMP video monitor.

A Monte Carlo simulation of the EPMA excitation volume using the Casino program (V 2.4.2) for an average xenotime matrix using a ~ 5 µm diameter, 25 kV electron beam, shows that ~ 99 % of the electrons penetrate to a depth of ~ 2.4 µm. By contrast, it is estimated that the SHRIMP primary beam when focussed through a 30 µm Köhler aperture sputters a region of approximately 5–7 µm in diameter by 0.5–1 µm in depth. Therefore, when using the combined analytical results from the electron probe and SHRIMP to determine elemental abundances, it is assumed that the xenotime samples are homogenous at the maximum combined sampling scale of both methods, i.e. the

analysed xenotime grains are homogenous at a scale equivalent to a 7 µm diameter spot that penetrates 2.4 µm into the sample. Modelling the excitation volume of the electron microprobe analysis as a sphere and the sampled volume of the SHRIMP spot as a cylinder, equates to a total sample volume of ~ 45 μm^3.

3.5 SHRIMP xenotime Th/U ratios

For this study, SHRIMP xenotime Th/U ratios were determined from independently calibrated $^{206}Pb/^{238}U$ and $^{208}Pb/^{232}Th$ ratios. More typically, a calibration factor is used to correct the measured $^{248}[ThO]^+/^{254}[UO]^+$ ratios to their true Th/U. The Th/U calibration factor is calculated from $^{208}Pb^+/^{206}Pb^+$, $^{248}[ThO]^+/^{254}[UO]^+$ ratios and the known age of the reference material (Williams et al., 1996). For SHRIMP U–Pb zircon analysis, the Th/U calibration factor is consistent across analytical sessions. In contrast, Th/U calibration factors for SHRIMP U–Pb xenotime analyses, as for monazite, differ slightly between instruments, analytical sessions and reference materials (Table 4). Table 4 displays the Th/U calibration factors for ten SHRIMP U–Pb–Th xenotime sessions calculated for MG-1, BS-1 and Z6413. The Th/U calibration factors calculated from SHRIMP-RG data are, on average, ~ 9% higher than those from SHRIMP II. Average Th/U calibration factors for the SHRIMP II data differ by 4.4%. This is probably related, in part, to the different energy ranges of the $^{248}[ThO]^+$ and $^{254}[UO]^+$ ions as the secondary ion beam was energy filtered by 50 and 90%, respectively, in two of the three SHRIMP II sessions (Table 4). The calibration factors for the three SHRIMP II sessions vary between the three reference materials by between 0.5 and 1.4%, whereas the Th/U calibration factors for the seven SHRIMP-RG sessions are internally variable by 1.2–3.4%.

The variation in SHRIMP xenotime Th/U calibration factors is dependent on the instrument used and the analytical conditions employed. Xenotime Th/U calibration factors calculated from two separate SHRIMP II instruments using an unfiltered secondary ion beam (i.e. Fletcher et al. 2004 and this study) are within 1.1% of each other and as such, are reasonably consistent. However, energy filtering appears to reduce the Th/U calibration factor. The variation of the xenotime Th/U correction factors between sessions demonstrates that this correction should be routinely determined when $^{206}Pb/^{238}U$ and $^{208}Pb/^{232}Th$ ages are not directly calibrated.

Fletcher et al. (2004) were concerned about a variation of 3.5% in the Th/U calibration factor determined from different xenotime reference materials and analytical sessions, which was tentatively attributed to a matrix effect. Variations in the Th/U calibration factor between SHRIMP U–Pb analytical sessions also occurs for monazite and varies by 6% (Stern & Berman 2000).

Intriguingly, the Th/U calibration factors for the different xenotime standards analysed in the ten SHRIMP sessions shown in Table 4 are internally similar and indicate that the $^{208}Pb^{+}/^{206}Pb^{+}$ vs. $^{248}[ThO]^{+}/^{254}[UO]^{+}$ calibration is significantly less susceptible to the pronounced $^{206}Pb/^{238}U$ and $^{208}Pb/^{232}Th$ matrix effects that complicate SHRIMP studies of this mineral (see below).

3.6 SHRIMP U–Th–Pb xenotime age determinations of the reference materials

Chemical contrasts between the xenotime reference materials were found to cause significant U–Pb–Th matrix effects (ME). In general, a high U xenotime, when calibrated against a low to moderate U reference material, results in elevated $^{206}Pb/^{238}U$ and $^{208}Pb/^{232}Th$ ratios for the unknown sample, producing reversely discordant U–Pb compositions (Figure 3a). The opposite occurs when a xenotime with low to moderate U concentrations was calibrated against a high U xenotime reference material, that is, the 'unknown' sample appears normally discordant (Figure 3b).

Figure 4a compares the independently calculated $^{206}Pb/^{238}U$ and $^{208}Pb/^{232}Th$ ages as well as the $^{207}Pb/^{206}Pb$ ages for the high U xenotime reference material, Z6413, calibrated against MG-1 (low-moderate U) using SHRIMP II. This graph shows that the independently calibrated $^{206}Pb/^{238}U$ and $^{208}Pb/^{232}Th$ ages for Z6413 are highly correlated (R^2 = 0.98) and similarly elevated by approximately 14% relative to the reference age for this sample. Additionally, the $^{207}Pb/^{206}Pb$ ages for Z6413 appear to be unaffected by matrix contrasts and lie within error of the reference age. SHRIMP U–Pb–Th xenotime ME are also evident between xenotimes with contrasting Th and/or ΣREE concentrations. Figure 4b shows that the $^{206}Pb/^{238}U$ and $^{208}Pb/^{232}Th$ ages for BS-1 (low U, high Th and high ΣREE) when calibrated against MG-1 are elevated by between 5 and 6%.

A significant finding of this study has been to demonstrate that both $^{206}Pb/^{238}U$ and $^{208}Pb/^{232}Th$ SHRIMP xenotime ages are similarly affected by matrix contrasts between the calibration standard and unknown. Figures 4a and 4b show the close relationship between the matrix uncorrected $^{206}Pb/^{238}U$ and $^{208}Pb/^{232}Th$ ages. In each of these cases, the individual, independently calibrated $^{206}Pb/^{238}U$ and $^{208}Pb/^{232}Th$ ages for Z6413 and BS-1 are within error of each other. $^{206}Pb/^{238}U$-$^{208}Pb/^{232}Th$ concordia diagrams also demonstrate this. Figures 5a and 5b show $^{206}Pb/^{238}U$-$^{208}Pb/^{232}Th$ concordia diagrams for Z6413 and BS-1, and demonstrate that these samples have concordant to near-concordant compositions that are, however, significantly elevated above their reference ages.

3.6.1 Xenotime composition and SHRIMP U–Pb–Th matrix effects

In agreement with previous studies by Fletcher et al. (2000) and Fletcher et al. (2004), SHRIMP U–Pb–Th xenotime determinations are strongly influenced by contrasts in chemical composition, particularly U concentration. Table 5 shows the averaged contrasts in U, Th and ΣREE between the xenotimes used in this study and the calibration reference material, MG-1, and their typical SHRIMP U–Pb–Th fractionations. The xenotime samples with the highest observed U–Pb–Th fractionations are Z6413, NY/PK 6-80 and D43764, which have average, elevated fractionations of between 16 and 24%. Each of these samples has U contents that are between ~ 1.1 and 1.4 wt% in excess of the average MG-1 U concentration. The influence of U on U–Pb–Th ages can also be seen at the spot-to-spot level. Xenotime samples with high U show strong positive correlations between the $^{206}Pb^{+}/^{270}[UO_2]^{+}$ and $^{208}Pb^{+}/^{248}[ThO]^{+}$ ratios with $^{254}[UO]^{+}/^{194}[Y_2O]^{+}$ ratios (Figure 6a-b), as well as with independent EPMA analyses made prior to, and at the same spot location as, the SHRIMP analyses (Figure 6c-d). Interestingly, $^{206}Pb^{+}/^{270}[UO_2]^{+}$ and $^{208}Pb^{+}/^{248}[ThO]^{+}$ ratios from xenotime with high, variable U concentrations also have significant positive correlations with $^{190}[YbO]^{+}/^{194}[Y_2O]^{+}$ and $^{177}[DyO]^{+}/^{194}[Y_2O]^{+}$ ratios that are not apparent in the reference materials MG-1 and BS-1 (Figure 7a-d). This might indicate that the matrix effects that cause variations in the $^{206}Pb^{+}/^{270}[UO_2]^{+}$ and $^{208}Pb^{+}/^{248}[ThO]^{+}$ ratios also cause corresponding variations in the $^{190}[YbO]^{+}/^{194}[Y_2O]^{+}$ and $^{177}[DyO]^{+}/^{194}[Y_2O]^{+}$ ratios.

It is likely that the dominant control on the SHRIMP U–Pb–Th matrix effects is a mismatch in U content between calibration reference material and unknown. The dominance of the xenotime U-dependant matrix effects may mask, or dilute, any observable spot–to–spot effect arising from concentration contrasts in Th and/or ΣREE, which were not observed. However, the influence on $^{206}Pb^{+}/^{270}[UO_2]^{+}$ and $^{208}Pb^{+}/^{248}[ThO]^{+}$ ratios caused by matrix mismatches between Th and/or ΣREE concentrations is evident in the elevated $^{206}Pb/^{238}U$ and $^{208}Pb/^{232}Th$ ratios observed in BS-1 analyses that were calibrated against MG-1 (Figure 4b and Table 5).

The wide range of actinide and REE contents in xenotime means that matching concentrations of U and possibly Th and ΣREE between U–Pb–Th reference materials and unknowns is virtually impossible. This means that for SHRIMP xenotime U–Pb–Th dating to be effective, alternative SHRIMP analytical conditions or matrix correction procedures need to be adopted that can correct $^{206}Pb/^{238}U$ and/or $^{208}Pb/^{232}Th$ ratios over a wide range of xenotime compositions.

Two approaches were used in attempting to remove or correct for the SHRIMP U–Pb–Th matrix effects: (1) energy filtering and (2) empirically based U–Pb–Th matrix corrections.

3.6.2 Energy Filtering

The isotopic and chemical composition of the SIMS secondary ion beam typically differs from that of the target. Indeed, fractionation of the secondary ion beam is considered a basic feature of the SIMS sputtering and ionisation process (Shimizu & Hart, 1982). Shimizu & Hart (1982) recognised that both isotopic and chemical fractionation of the secondary ion beam is to a large extent energy dependent and less obvious in the high energy secondary ion population. These researchers suggested that chemical and isotopic fractionation of the secondary ion beam could be reduced, or even eliminated, by energy filtering.

With the aim of reducing the SHRIMP U–Pb–Th matrix effects observed amongst the reference xenotime samples, energy filtering of the secondary ion beam was trialled by removing 50 and 90% of the total secondary ion beam during SHRIMP II U–Pb–Th xenotime analysis. These experiments failed to influence the xenotime U–Pb–Th matrix effect, suggesting that significant xenotime U–Pb–Th matrix effects are not secondary ion energy-dependant (Table 6).

3.6.3 SHRIMP U–Pb–Th xenotime matrix correction: multi-element least squares methodology

The SHRIMP U–Pb–Th matrix correction technique developed determines the combination of correction coefficients for the elemental contrasts between the reference materials to correct for SHRIMP U–Pb–Th matrix effects using a least squares methodology. This procedure has two stages. The first corrects the $^{206}Pb^{+}/^{270}[UO_2]^{+}$ and $^{208}Pb^{+}/^{248}[ThO]^{+}$ ratios for chemical matrix effects, and the second uses the matrix corrected ratios to derive $^{206}Pb/^{238}U$ and $^{208}Pb/^{232}Th$ ages using 1-D, $^{206}Pb^{+}/^{270}[UO_2]^{+}$ and $^{208}Pb^{+}/^{248}[ThO]^{+}$ calibrations.

The first stage of this procedure relates SHRIMP U–Pb–Th matrix effects to concentration contrasts in U, Th and ΣREE between the three xenotime reference materials (in this case, MG-1, BS-1, and Z6423) in order to derive correction coefficients (f(U), f(Th) and f(ΣREE)) for the $^{206}Pb^{+}/^{270}[UO_2]^{+}$ and $^{208}Pb^{+}/^{248}[ThO]^{+}$ ratios. All elemental concentrations for these equations were measured by EPMA.

See Appendix D for a detailed description of the matrix correction methodology.

3.6.4 SHRIMP U–Pb–Th xenotime matrix correction: results

Combinations of U, Th and ΣREE were trialled as variables in the least squares methodology primarily to determine which was the most effective in quantifying and correcting for the SHRIMP U–Pb–Th matrix effects. Additionally, Ca and Si concentrations were also trialled, as these elements can occur in concentrations of up to 1000s of ppm, are responsible for actinide substitution

into the xenotime lattice, and therefore may themselves impact on the matrix effects. The best results were obtained using (U, Th, ΣREE) and (U, ΣREE). Trials which included Ca and Si gave poor results, indicating that these elements have little or no detectable influence on xenotime matrix effects. Additionally, trials which used only U and Th as variables yielded poor results.

The assumption underpinning the least squares approach is that contrasts in xenotime U, ΣREE and Th contents are all responsible for SHRIMP U–Pb–Th matrix effects. This premise is also used by Fletcher et al. (2004) and Li et al. (2013) in developing their U, Th and ΣREE relative correction factors. Although U has been demonstrated to have a major impact on SHRIMP U–Pb–Th matrix effects, ΣREE and Th have not. Th was shown by Stern & Sanborn (1998) and Stern & Berman (2000) to cause SHRIMP $^{206}Pb/^{238}U$ matrix effects in monazite and therefore, by inference, might also cause xenotime matrix effects. Total REE concentrations in xenotime can vary by as much as ~ 10 wt% and could, therefore, be a significant cause of matrix contrasts between different xenotimes.

The correction coefficients for nine SHRIMP U–Pb–Th xenotime sessions conducted during this study are displayed in Table 7. These data indicate that: (1) correction coefficients for U, Th and ΣREE vary for both $^{206}Pb^{+}/^{270}[UO_2]^{+}$ and $^{208}Pb^{+}/^{248}[ThO]^{+}$ ratios from session to session, and (2) coefficients for U typically dominate the matrix correction for both $^{206}Pb^{+}/^{270}[UO_2]^{+}$ and $^{208}Pb^{+}/^{248}[ThO]^{+}$ ratios. The U and ΣREE correction coefficients are all positive but the Th coefficients for both $^{206}Pb^{+}/^{270}[UO_2]^{+}$ and $^{208}Pb^{+}/^{248}[ThO]^{+}$ ratios range between positive and negative values. The range in the correction coefficients for Th implies that differences in the SHRIMP instrumental conditions between analytical sessions can cause Th contrasts between the reference materials to have either a positive or negative influence on the $^{206}Pb^{+}/^{270}[UO_2]^{+}$ and $^{208}Pb^{+}/^{248}[ThO]^{+}$ ratios. It is unrealistic to consider that differences in instrumental conditions alone, from session to session, are responsible for this. A better interpretation of these results is that Th plays either an undetectable or insignificant role in SHRIMP xenotime U–Pb–Th ME.

To test the influence of Th on matrix corrections, Th was omitted from the least squares methodology such that only f(U) and f(ΣREE) were determined for the nine SHRIMP sessions and are displayed in Table 8. These results show that f(U) and f(ΣREE) for both $^{206}Pb^{+}/^{270}[UO_2]^{+}$ and $^{208}Pb^{+}/^{248}[ThO]^{+}$ ratios are reasonably consistent from session to session and between different instruments. For the $^{206}Pb^{+}/^{270}[UO_2]^{+}$ ratios, f(U) ranges between 0.0925 and 0.1188 and has a Biweight mean value of 0.1030, whereas f(ΣREE) ranges between 0.0061 and 0.137, with a Biweight mean of 0.0093. For the $^{208}Pb^{+}/^{248}[ThO]^{+}$ data, f(U) ranges between 0.0800 and 0.1040 (Biweight mean = 0.0923), whereas f(ΣREE) ranges between 0.0082 and 0.0211 (Biweight mean = 0.0133). The correction coefficients shown in Table 8 on average show that a 1 wt% change in U concentration causes a corresponding 15 and 14% change in SHRIMP xenotime $^{206}Pb/^{238}U$ and

$^{208}Pb/^{232}Th$ ratios respectively. A 1 wt% change in ΣREE causes a corresponding 1.2 and 1.7% change in $^{206}Pb/^{238}U$ and $^{208}Pb/^{232}Th$.

3.6.5 Results of experiment SHII-(Dec-05) – SHRIMP II

Two experiments were conducted to test the effectiveness of the U–ΣREE least squares methodology in correcting SHRIMP U–Pb–Th ME using xenotime grains from NY/PK 6-80 and D43764, which were treated as 'unknowns'. These were session SHII-(Dec-05) and session RG-(Jun-06).

Experiment SHII-(DEC-05) was designed to test the U–ΣREE least squares matrix correction method using MG-1, Z6413 and BS-1 as reference materials and NY/PK 6-80 as the unknown. To reduce the acquisition time for each analysis, and increase the number of analyses carried out during the experiment, ^{207}Pb was not measured. U and ΣREE concentrations were determined by EPMA analysis prior to SHRIMP U–Pb–Th analyses.

Forty-one analyses were carried out on the three reference materials during this session. The matrix uncorrected U–Pb–Th ratios calibrated to MG-1 show them to be mutually concordant but elevated in comparison to their reference $^{206}Pb/^{238}U$ages. Matrix uncorrected U–Pb–Th ratios for BS-1 are elevated by ~ 5% whereas analyses for Z6413, are elevated by approximately ~ 21% (Table 6).

The matrix correction factors, f(U) and f(ΣREE) for this session are displayed in Table 8 and, once applied to the $^{206}Pb^{+}/^{270}[UO_2]^{+}$ and $^{208}Pb^{+}/^{248}[ThO]^{+}$ ratios, correct the U- and ΣREE-matrix effects. Fourteen analyses of BS-1 (ID-TIMS age = 508.9 ± 0.3 Ma) combine to give a SHRIMP $^{206}Pb/^{238}U$ age of 508 ± 9 Ma (MSWD = 0.77, POF = 0.69), and a $^{208}Pb/^{232}Th$ age of 508 ± 11 Ma (MSWD = 0.67, POF = 0.79). For Z6413 (ID-TIMS age = 994 ± 1 Ma), 12 analyses combine to give a SHRIMP $^{206}Pb/^{238}U$ age of 994 ± 18 Ma (MSWD = 0.34, POF = 0.98), and a $^{208}Pb/^{232}Th$ age of 991 ± 23 Ma (MSWD = 0.87, POF = 0.57).

Twenty-five SHRIMP U–Pb–Th analyses were carried out on crystals from NY/PK 6-80 and comprised 16 analyses of the cores and nine analyses of the rims. The SHRIMP $^{206}Pb/^{238}U$ and $^{208}Pb/^{232}Th$ results were assessed assuming that NY/PK 6-80 cores have a mean age of approximately 1012 Ma and the rims, a mean age of approximately 970 Ma (see above). The independently calibrated $^{206}Pb/^{238}U$ and $^{208}Pb/^{232}Th$ matrix uncorrected dates for both the cores and rims are all concordant within experimental error but on average, elevated by approximately 27% above their assumed ages (Figure 8). Following U and ΣREE matrix correction, all 16 analyses of the cores have the same $^{206}Pb/^{238}U$ age within their uncertainties (MSWD = 1.35, POF = 0.16) and

give an age of 1006 ± 19 Ma. The same grains give a $^{208}Pb/^{232}Th$ age of 1011 ± 23 Ma (MSWD = 1.12, POF = 0.33), which is identical within analytical uncertainty to the $^{206}Pb/^{238}U$ result (MSWD = 0.11, POF = 0.74; Figure 8). The nine analyses of the rims also have identical $^{206}Pb/^{238}U$ and $^{208}Pb/^{232}Th$ ages within uncertainty (MSWD = 0.12, POF = 0.72). The $^{206}Pb/^{238}U$ results for the rims give an age of 971 ± 26 Ma (MSWD = 1.89, POF = 0.06) while the $^{208}Pb/^{232}Th$ results give an age of 978 ± 30 Ma (MSWD = 1.57, POF = 0.13) (Figure 8, Appendix E.1–E.4). Notably, the $^{206}Pb/^{238}U$ data demonstrate that the ages of the cores and rims are statistically distinguishable (MSWD = 6.35, POF = 0.01).

The usefulness of this data set in resolving the various age components identified by Aleinikoff et al. (2012) in NY/PK 6-80 is limited as ^{207}Pb was not measured. Therefore, $^{207}Pb/^{206}Pb$ ages which are more precise than either $^{206}Pb/^{238}U$ or $^{208}Pb/^{232}Th$ ages in xenotime greater than about 1000 Ma, cannot be used. The larger uncertainties of the $^{206}Pb/^{238}U$ and $^{208}Pb/^{232}Th$ results are dominated by the external spot-to-spot error (or reproducibility) of the primary calibration standard (MG-1) which for this session, was 2.07% (1σ; $^{206}Pb/^{238}U$) and 2.44% (1σ; $^{208}Pb/^{232}Th$). This resulted in 95% confidence uncertainties for the weighted mean $^{206}Pb/^{238}U$ ages of 1.9% and 2.7% (cores and rims respectively) and 2.3% and 3.1% for the $^{208}Pb/^{232}Th$ ages (cores and rims respectively). However, the matrix corrected $^{206}Pb/^{238}U$ results in particular gave positive results as (1) the ages of the cores and rims are statistical distinguishable and (2) the weighted mean ages of the cores and rims accord with the dominant SHRIMP $^{207}Pb/^{206}Pb$ age modes for NY/PK 6-80 cores and rims reported by Aleinikoff et al. (2012) (i.e. ~ 1012 Ma and ~ 970 Ma, see above).

3.6.6 Results of experiment RG-(Jun-06) – SHRIMP-RG

Experiment RG-(Jun-06) was conducted using SHRIMP-RG and designed to test the U–ΣREE least squares matrix correction method using MG-1, Z6413 and BS-1 as reference materials and xenotime D43764 (2622 ± 3 Ma) as the 'unknown'. Concentrations of U and ΣREE were determined by EPMA prior to the SHRIMP U–Pb–Th analyses. Twenty-five U–Pb–Th isotopic compositions were measured by SHRIMP on the reference materials MG-1, BS-1 and Z6413. Calibrated to MG-1, the matrix uncorrected U–Pb–Th ratios for BS-1 and Z6413 are concordant but elevated compared with their reference U–Pb–Th ratios by ~ 4 and ~ 16% respectively.

The matrix correction factors f(U) and f(ΣREE) for this session are presented in Table 8 and are effective in correcting for the U and ΣREE matrix effects for BS-1 and Z6413. Seven analyses of BS-1 (ID-TIMS age = 508.9 ± 0.3 Ma) combine to give a $^{206}Pb/^{238}U$ age of 512 ± 19 Ma (MSWD = 0.19, POF = 0.98), while eight analyses give a $^{208}Pb/^{232}Th$ age of 508 ± 11 Ma (MSWD = 1.36, POF

= 0.22). SHRIMP $^{206}Pb/^{238}U$ ages for Z6413 (ID-TIMS age = 994 ± 1 Ma) comprise eight analyses that give an age of 996 ± 29 Ma (MSWD = 0.37, POF = 0.92). The $^{208}Pb/^{232}Th$ analyses of Z6413 are, however, significantly scattered beyond their uncertainties (MSWD = 7.2). Excluding the highest and lowest analyses removes the dispersion (MSWD = 2.46, POF = 0.03) and gives an age of 992 ± 27 Ma.

Nineteen SHRIMP U–Pb–Th analyses were made on sample D43764. Common Pb contents are uniformly low (<0.01% common ^{206}Pb). The $^{207}Pb/^{206}Pb$ age results include a discordant analysis and another with a large uncertainty that is also significantly lower than the dominant population. These analyses were excluded from age interpretations. The remaining 17 analyses are dispersed beyond their analytical uncertainties (MSWD = 2.4). Excluding the highest two analyses, removes the scatter (MSWD = 1.46, POF = 0.12) and gives a $^{207}Pb/^{206}Pb$ age of 2622 ± 3 Ma which is within error of the EPMA determined chemical U–Th–Pb age for this sample (2637 ± 22 Ma, see Appendix C). Contrasting with these results are the independently determined $^{206}Pb/^{238}U$ and $^{208}Pb/^{232}Th$ ages that are, on average, elevated by ~ 16% compared to the $^{207}Pb/^{206}Pb$ age for this sample. When plotted on a U–Pb–Th concordia, the matrix uncorrected $^{206}Pb/^{238}U$ and $^{208}Pb/^{232}Th$ ratios are near-concordant but elevated above the reference age (Figure 9) and when plotted on a Tera-Wasserburg concordia, the $^{206}Pb/^{238}U$ compositions are shown to be significantly reversely discordant (Figure 10a).

The U- and ΣREE-matrix-corrected $^{206}Pb/^{238}U$ data contain one analysis that is significantly lower than the others and was removed from interpretations. Another analysis with a large uncertainty was also removed from interpretations. The remaining 17 analyses are concordant with their $^{207}Pb/^{206}Pb$ ratios (Figure 10b) and have the same $^{206}Pb/^{238}U$ within their uncertainties (MSWD = 0.50, POF = 0.95) and combine to give an age of 2616 ± 53 Ma. The 19 U and ΣREE matrix corrected $^{208}Pb/^{232}Th$ data include two analyses that are significantly lower than the dominant population and were accordingly removed from interpretations. The remaining 17 analyses have the same $^{208}Pb/^{232}Th$ (MSWD = 1.18, POF = 0.28) and give an age of 2588 ± 42 Ma (Figure 9, Appendix E.5–E.8).

4. Implications

The results of experiments RG-(Jun-06) and SHII-(DEC-05) in successfully correcting the SHRIMP U–Pb–Th matrix effects in NY/PK 6-80 and D43764 demonstrate that the least squares methodology developed in this study appropriately corrects for U and ΣREE contrasts in xenotime. It is not necessary to include Th in the $^{206}Pb/^{238}U$ and $^{208}Pb/^{232}Th$ matrix effects correction as

Fletcher et al. (2004) and Li et al. (2013) have done previously. The additional uncertainties associated with this approach, namely the uncertainty associated with the U and ΣREE correction, EPMA analyses and the elemental determinations, result in 95% confidence precision estimates of between 1.5 and 3.0%.

An essential part of the success of the SHRIMP U–Pb–Th xenotime matrix correction procedure is the use of the 1-D $^{206}Pb^{+}/^{270}[UO_2]^{+}$ and $^{208}Pb^{+}/^{248}[ThO]^{+}$ calibrations. By comparison, when xenotime $^{206}Pb/^{238}U$ and $^{208}Pb/^{232}Th$ ratios were calculated from the Pb^{+}/U^{+} versus UO^{+}/U^{+} calibration (or any combination of $Pb/U[O_x]:U[O_x]/U[O_x]$ and/or $Pb/Th[O_x]:Th[O_x]/Th[O_x]$), the matrix correction routine performed poorly. The better results obtained by the xenotime U–Pb–Th matrix correction procedure when using 1-D calibrations is because they are independent of the variations in slope that commonly exist between different xenotime samples and combinations of xenotime $Pb/U[O_x]:U[O_x]/U[O_x]$ calibrations.

Although U and ΣREE are presented above as plausible causes of U–Pb–Th matrix effects in xenotime, it is important to note that the combination of U, Th and ΣREE, when used in the above matrix correction procedure, produces comparable results. The positive and negative correction coefficients for Th (f(Th)) shown in Table (7) indicate that the Th-related SHRIMP U–Pb–Th matrix effects are not significant. Furthermore, even though sample D43764 contains on average, 1 wt% ThO_2, the correction coefficients for U and ΣREE alone adequately correct the SHRIMP U–Pb–Th matrix effects in this sample. These results do not exclude Th as potential cause of SHRIMP U–Pb–Th matrix effects in xenotime, rather they suggest that Th contrasts between the calibration standard and unknown of approximately 1 wt% appear to have no effect on $^{206}Pb/^{238}U$ or $^{208}Pb/^{232}Th$ ratios. The majority of published xenotime EPMA analyses record Th concentrations of typically < 1 wt%, indicating that for most xenotime Th will have little to no effect on U–Pb–Th xenotime ratios measured by SHRIMP.

The strong inference that a mismatch in xenotime U and ΣREE contents between the calibration reference materials and unknowns causes SHRIMP xenotime U–Pb–Th matrix effects explains the 4–5% elevation of $^{206}Pb/^{238}U$ and $^{208}Pb/^{232}Th$ ratios measured in BS-1 relative to MG-1 (when used as the calibration reference material). The low concentrations of U in BS-1 (~ 400 ppm) excludes U as a factor causing $^{206}Pb/^{238}U$ or $^{208}Pb/^{232}Th$ fractionation. The SHRIMP U–Pb–Th matrix effects in BS-1 are better interpreted as arising from its relatively high ΣREE concentration, which is approximately 4 wt% higher than that in the U–Pb–Th calibration standard MG-1.

4.1 Causes of SHRIMP xenotime U–Pb–Th ME

The correction coefficients for U and ΣREE shown in Table 8 for nine separate SHRIMP sessions, although internally variable, show a consistent pattern. For both the $^{206}Pb/^{238}U$ and $^{208}Pb/^{232}Th$ results, U is the dominant cause of matrix effects, whereas ΣREE plays a subordinate role. For both the $^{206}Pb/^{238}U$ and $^{208}Pb/^{232}Th$ data, the correction coefficients for U and ΣREE appear to be reasonably consistent across the different instruments and operating conditions. For example, the correction coefficients for session SHII-(Dec-05) are typical for the entire data set, even though this session was run under very different instrumental conditions compared to the eight other SHRIMP-RG sessions. Even energy filtering involving removal ~ 90% of the secondary ions during this session failed to reduce the U–Pb–Th matrix effects, or to significantly alter the U and ΣREE correction coefficients. The inference from this, as well as the general consistency of the U and ΣREE correction coefficients, is that xenotime U–Pb–Th matrix effects are probably caused at the site of sputtering and ionisation, which is consistent with a suggestion of Williams (1998) concerning SIMS matrix effects.

The consistency of relative correction factors for U and ΣREE observed for different instruments and operating conditions is probably a function of the identical primary column and secondary ion extraction configuration used in both instruments. It is for this reason that xenotime U and ΣREE related U–Pb–Th matrix effects can be expected to behave similarly between different SHRIMP II and SHRIMP-RG instruments. Generally it is expected that the average correction coefficients for U and ΣREE shown in Table 8 will apply broadly between different instruments. An important finding of this study has been that the U and ΣREE-related xenotime U–Pb–Th matrix effects should be determined and corrected for each analytical session in the same manner as the $^{206}Pb/^{238}U$ calibration is routinely established for each SHRIMP U–Pb session.

Two lines of evidence suggest that it is the relative ionisation of the Pb^+ ions between xenotime grains with contrasting U and ΣREE that results in the SHRIMP U–Pb–Th matrix effects: These are 1) the similarity in the Th/U calibration factor between the reference materials and 2) the independently determined $^{206}Pb/^{238}U$ and $^{208}Pb/^{232}Th$ ratios. Our results show that SHRIMP xenotime Th/U calibration factors are virtually unaffected by matrix contrasts. This is particularly the case for session SHII-(Dec-05) where the Th/U calibration factors for the three reference materials have an internal variation of 0.46% (Table 4), yet the $^{206}Pb/^{238}U$ matrix effects for the reference material Z6413 are on average, elevated by 21% above its reference value (Table 6). If it is the relative ionisation of the $^{254}[U_xO_x]^+$ and $[^{232}Th_xO_x]^+$ molecules that result in SHRIMP U–Pb matrix effects, then the Th/U calibration factors for the three reference materials used here would be significantly different. However, a relative increase or decrease in the ionisation of the Pb^+ isotopes will not result in any noticeable isotopic matrix effects as ions of all Pb isotopes would be equally

affected. The change in the ionisation and transmission of the Pb^+ ions relative to U and ΣREE contrasts appears not to have a noticeable effect on the $^{207}Pb/^{206}Pb$ ratios.

The concordance between independently calculated $^{206}Pb/^{238}U$ and $^{208}Pb/^{232}Th$ is striking (Figures 4a and 4b). Similar to the above argument, if it is the emission of the $^{254}[U_xO_x]^+$ and $[^{232}Th_xO_x]^+$ that results in matrix effects, these molecules would have to be differentially fractionated by the matrix effects in such a way that they consistently give concordant, albeit elevated, U–Pb–Th ratios. An increase in the emission of Pb^+ ions is a more plausible cause of SHRIMP U–Pb–Th xenotime, U- and ΣREE-related matrix effects.

4.2 SHRIMP U–Pb–Th matrix effects *in xenotime, zircon and monazite*

The chemically-induced xenotime U–Pb–Th SHRIMP fractionations of up to 24% observed in this study exceed the U–Pb–Th matrix effects that have been reported for monazite and zircon, which range between 1 and 5%. The magnitude of the U–Pb–Th fractionations in xenotime is directly related to the high U concentrations that are commonly associated with this mineral. Xenotime U concentrations measured from samples used in this study range from ~ 0.04 to 2 wt%, whereas the range reported in the literature is from <0.01 to 6 wt%. Additionally, U concentrations can differ significantly within a single crystal and also within a single population of crystals. For example, fragments from the single crystal reference material Z6413 have a U range of ~ 1 wt%, and in NY/PK 6-80, U concentrations were found to differ by ~ 1.5 wt%. In contrast, the U concentrations in zircon and monazite are considerably lower. For monazite, U concentrations rarely exceed 0.5 wt% (Overstreet 1967) and are more commonly <1000 ppm, whereas for zircon, U concentrations are typically <1500 ppm. Therefore, U–induced SHRIMP U–Pb–Th ME are less likely and are expected to be minor in monazite and zircon, compared with xenotime, as observed.

The role of the REEs in SHRIMP U–Pb–Th fractionation is less straightforward. Monazite typically has ΣREE concentrations of between 35 and 55 wt%. The dominant component is the LREE, in particular La, Ce and Nd. For the few studies that have recognised SHRIMP U–Pb–Th matrix effects in this mineral, the causal elements were thought to be U and/or Th (Rasmussen & Fletcher 2002; Stern & Berman 2000) and the LREE (Fletcher et al. 2010).

Like xenotime, zircon (isostructural with xenotime) is typically enriched in the HREE, with the total concentration rarely exceeding 0.5 wt% (from Table 1 in: Hoskin & Schaltegger, 2003). For zircon, only one study has examined a possible link between $^{206}Pb/^{238}U$ matrix effects and REE concentrations. This study, by Black et al. (2004), suggested that $^{206}Pb/^{238}U$ matrix effects of ~ 1% were caused by matrix mismatches in the trace elements Y, P and REE between the calibration reference materials and unknowns. An interesting finding of this research was that the zircons with

the highest concentration of trace elements had reduced, not elevated $^{206}Pb/^{238}U$ ratios. However, for xenotime, where the ΣREE concentration typically ranges between 13 and 22 wt% (dominated by the HREE, Gd, Dy, Er and Yb), it is the crystals with the higher HREE concentrations which have elevated $^{206}Pb/^{238}U$ ratios. The results of this study suggest that, on average, a 1 wt% increase in the ΣREE between the calibration standard and unknown results in a $^{206}Pb/^{238}U$ increase of approximately 1.2%.

4.3 FUTURE SHRIMP U–Pb–Th xenotime studies

An accurate knowledge of xenotime composition is crucial for correcting the significant U–Pb–Th matrix effects associated with SHRIMP xenotime analysis. Two factors complicate any SIMS-based elemental quantification of xenotime. Firstly, there is no element in xenotime with a relatively consistent concentration that can be used as a reference to normalise SIMS-based estimates of the concentrations of other elements. Also, it appears that xenotime chemical matrix contrasts that influence the ionisation and emission of the Pb^+ ions also affect the ionisation of Y and some REE. This was demonstrated by the strong positive correlations between SHRIMP xenotime $^{206}Pb^+/^{270}(UO_2^+)$ and $^{208}Pb^+ /^{232}ThO^+$ ratios with $^{190}(YbO^+)/^{194}(Y_2O^+)$, $^{177}(DyO^+)/^{194}(Y_2O^+)$ ratios (Figure 7a-d). These limitations of the SIMS elemental quantification of xenotime support xenotime elemental quantification by EPMA or EPMA-assisted procedures such as via relative sensitivity factors (RSF) as explained in section 3.4.

EPMA results from this study show that ΣREE concentrations can be estimated accurately from the four major REE constituents of xenotime (Gd, Dy, Er and Yb). Figure 11 shows the good correlation between ΣGdDyErYb and ΣREE in xenotime for the reference materials used in this study ($R^2 = 0.93$). The ΣGdDyErYb concentrations for the xenotime plotted in Figure 11 are accurate to within a range of ± 2% of their ΣREE concentrations and hence can serve as a good proxy. Therefore, REE quantification for xenotime necessary to carry out SHRIMP U–Pb–Th matrix corrections could be reduced to analysing Gd, Dy, Er and Yb by EPMA. Additionally, it is recommended that Ho is also analysed by EPMA to serve as a reference for the determination of xenotime U concentration via $RSF_{(U\text{-}Ho)}$.

5. Conclusions

The wide range in the chemical composition of xenotime, particularly in U and ΣREE, results in significant difficulties for SHRIMP analysis for both the determination of U–Pb–Th ratios and quantitative elemental analysis.

For SHRIMP U–Pb–Th xenotime analysis, chemical contrasts in U, and to a lesser extent ΣREE, between the primary calibration reference material and unknown can result in U–Pb–Th matrix effects of up to ~ 24%. For xenotime, it appears likely that it is the differing secondary emission of the Pb^+ ions that causes the U–Pb–Th matrix effects. Accordingly, it appears that the formation and emission of Pb^+ ions during SHRIMP U–Pb–Th analysis is not only a function of the Pb concentration in the target, but also the concentration of U and ΣREE. Additionally, the ionisation and emission of Y, Yb and Dy also appears to be affected by the composition of the xenotime matrix. To correct for the SHRIMP U–Pb–Th xenotime matrix effects, a detailed knowledge of the chemical composition of the xenotime standards and unknowns at each analytical spot is required. For this task, EPMA analysis is recommended. In addition, U abundance can be estimated accurately using $RSF_{(U\text{-}Ho)}$. The SHRIMP U–Pb–Th matrix correction technique developed herein requires the concurrent analysis of three xenotime reference materials, with concordant U–Pb–Th compositions and different U and ΣREE concentrations, for each analytical session.

The SHRIMP-RG is well-suited to SHRIMP U–Pb xenotime analysis as its design removes molecular interferences or 'scattered ions' on or near the ^{204}Pb peak. Although these 'scattered ions' can be removed by energy filtering or by the insertion of the retardation lens (typically used during SHRIMP II U–Pb–Th xenotime analysis), the former in particular results in a significant loss of sensitivity. This loss is an important consideration as SHRIMP analysis of microscopic (~ 5–10 μm) xenotime demands the smallest diameter SHRIMP spots, which results in significantly reduced primary and secondary ion currents. The adoption of the stronger O^- rather than O_2^- primary beam when analysing xenotime with a small 5–8 μm SHRIMP spot, increased the precision of individual analyses.

The optimal data acquisition sequence for SHRIMP U–Pb–Th analysis should comprise six scans, analyzing: $^{181}[HoO]^+$, $^{194}[Y_2O]^+$, ^{204}Pb, BG, $^{206}Pb^+$, $^{207}Pb^+$, $^{208}Pb^+$, $^{238}U^+$, $^{248}[ThO]^+$, $^{254}[UO]^+$, $^{264}[ThO_2]$ and $^{270}[UO_2]^+$ (BG=background measured at +0.04 mass units away from the ^{204}Pb peak). The $^{181}[HoO]^+$ and $^{270}[UO_2]^+$ molecules can be used as an alternative to EPMA analysis for the calculation of U and Th abundances. Importantly, the $^{270}[UO_2]^+$ and either the $^{248}[ThO]^+$ or $^{264}[ThO_2]^+$ species are included so that 1-D $^{206}Pb^+/^{270}[UO_2]^+$ and $^{208}Pb^+/^{248}[ThO]^+$ calibrations can be made. The various analytical sessions conducted in this study demonstrate that SHRIMP Th/U calibration factor can vary by a few percent between sessions, and therefore, like the U–Pb–Th

matrix corrections, should be determined for each analytical session if $^{206}Pb/^{238}U$ and $^{208}Pb/^{232}Th$ ratios are not independently calibrated.

The SHRIMP xenotime U–Pb–Th matrix correction technique developed here differs in a number of respects from those used by Fletcher et al. (2004) and Li et al. (2013). Their studies related the SHRIMP U–Pb–Th matrix effects to chemical contrasts between the U–Pb–Th calibration reference materials and 'unknown' xenotime. In contrast, the simplicity of the 1-D $^{206}Pb^{+}/^{270}[UO_2]^{+}$ and $^{208}Pb^{+}/^{248}[ThO]^{+}$ calibration used here allows for a unique matrix correction procedure that corrects all of the reference materials simultaneously to determine correction coefficients for U and ΣREE (i.e. f(U) and f(ΣREE)), prior to U–Pb–Th calibration against the primary reference material. Additionally, 1-D calibrations that independently determine $^{206}Pb/^{238}U$ and $^{208}Pb/^{232}Th$ ratios avoid possible contrasts in slope between various combinations of Pb/UO_x : UO_x and Pb/ThO_x : ThO_x calibrations that will further reduce the effectiveness of U–Pb–Th matrix corrections. Both the studies of Fletcher et al. (2004) and Li et al. (2013) related SHRIMP xenotime U–Pb–Th matrix effects to contrasts in U, Th, and ΣREE. This study indicates that the contribution of Th to the U–Pb–Th matrix effects is insignificant and that only U and ΣREE play an important role in SHRIMP xenotime U–Pb–Th matrix effects.

This study has shown the need to determine SHRIMP xenotime U–Pb–Th matrix correction factors for each analytical session. Slight differences in instrumental conditions between analytical sessions are likely to be responsible for this. Having to determine U–Pb–Th matrix correction factors for each SHRIMP dating experiment necessarily requires that all reference materials and unknown xenotimes be analysed by EPMA prior to the SHRIMP U–Pb–Th dating experiment. The results of this study show that the SHRIMP U–Pb–Th xenotime analyses using the matrix correction technique developed here can be expected to result in $^{206}Pb/^{238}U$ and $^{208}Pb/^{232}Th$ analyses with an accuracy of between 1.5 and 3.0%. Our matrix correction technique allows $^{206}Pb/^{238}U$ dating of Phanerozoic xenotime where it is unlikely that a precise $^{207}Pb/^{206}Pb$ age could be obtained. This ability to date relatively young xenotime has major significance for dating clastic, unfossiliferous sedimentary sequences.

Acknowledgements

We thank Ken Ludwig for all his useful advice and strong support throughout this project. We are also grateful to Ian Fletcher who was always willing to share his knowledge of SHRIMP U–Pb–Th xenotime dating. Trevor Ireland, Peter Holden, Peter Lanc, John Aleinikoff and David Huston also played a big part in the success of this project. This work was undertaken while A.J. Cross was a Ph.D. student at the ANU, which was supported by Geoscience Australia. This contribution greatly benefited from thoughtful reviews by Geoff Fraser and Richard Armstrong. John Aleinikoff and an anonymous reviewer also provided

insightful advice and suggestions that greatly improved this manuscript. It is published with permission from the Chief Executive Officer, Geoscience Australia.

References

Aleinikoff, J.N. & Grauch, R.I., (1990). U–Pb Geochronologic constraints on the origin of a unique monazite-xenotime gneiss, Hudson Highlands, New York. *American Journal of Science*, **290**, 522-546.

Aleinikoff, J.N., Southworth, S., Fanning, C.M., & Mazdab, F.K., (2010) Evidence for Late Neoproterozoic deposition of the Ocoee Supergroup: SHRIMP U-Pb and trace element analysis of diagenetic xenotime and monazite: *Geological Society of America Abstracts with Programs*, v. 42, n. 1, p. 59.

Aleinikoff, J.N., Grauch, R.I., Mazdab, F.K., Kwak, L., Fanning, C.M. & Kamo, S., (2012). Origin of an unusual monazite-xenotime gneiss, Hudson Highlands, New York: SHRIMP U-Pb geochronology and trace element geochemistry. *American Journal of Science*, v. **312**, 723-765.

Aleinikoff, J.N., Lund, K., and Fanning, C.M., 2015, SHRIMP U-Pb and REE data pertaining to the origins of xenotime in Belt Supergroup rocks: Evidence for ages of deposition, hydrothermal alteration, and metamorphism: Canadian Journal of Earth Sciences, v. 52, p. 722–745.

AMLI, R., (1975). MINERALOGY AND RARE EARTH GEOCHEMISTRY OF APATITE AND XENOTIME FROM THE GLOSERHEIA PEGMATITE, FROLAND, SOUTHERN NORWAY. *AMERICAN MINERALOGIST*, **60**, 607–620.

Andersen, C.A. & Hinthorne, J.R., (1973). Thermodynamic approach to the quantitative interpretation of sputtered ions in mass spectra. *Analytical Chemistry*, **45**, 1421-1438.

Bea, F. & Montero, P., (1999). Behaviour of accessory phases and redistribution of Zr, REE, Y, Th and U during metamorphism and partial melting of metapelites in the lower crust: an example from the Kinzigate Formation of Ivrea–Verbano, NW Italy. *Geochimica et Cosmochimica Acta*, **63**, 1133–1153.

Benninghoven, A., Rūdenauer, F.G. & Werner, H.W., (1987). Secondary ion mass spectrometry: Chemical analysis, **86**, 1227p.

Black, L.P., Kinny, P.D. & Sheraton, J.W., (1991). The difficulties of dating mafic dykes: An Antarctic example. *Contributions to Mineralogy and Petrology*, **109**, 183-194.

Butera, K.M., Williams, I.S., Blevin, P.L. & Simpson, C.J., (2001). Zircon U–Pb dating of Early Palaeozoic monzonitic intrusives from the Goonumbla area, New South Wales. *Australian Journal of Earth Sciences*, **48**, 457–464.

Brown, S.M., Fletcher, I.R., Stein, H.J., Snee, L.W. & Grooves, D.I., (2002). Geochronological constraints on pre–, post–mineralization events at the world–class Cleo gold deposit, eastern goldfields province, Western Australia. *Economic Geology*, **97**, 541–559.

Cherniak, D.J., (2006). Pb and rare earth element diffusion in xenotime. *Lithos*, **88**, 1–14.

Claoué-long, J.C., Compston, W., Roberts, J. & Fanning, C.M., (1995). Two Carboniferous ages: A comparison of SHRIMP zircon dating with conventional zircon ages and $^{40}Ar/^{39}Ar$ analysis. *In*: Berggren, W.A., Kent, D.V., Aubry, M-P. & Hardenbol, J. (Editors): Geochronology, time scales and global stratigraphic correlation. *SEPM (Society for Sedimentary Geology) Special Publication*, **54**, 3–21.

Cross, A.J., Fletcher, I.R., Crispe, A.J., Huston, D.L. & Williams, N., (2005). New constraints on the timing of deposition and mineralisation in the Tanami Group. *Annual Geoscience Exploration Seminar (AGES) Record of Abstracts, Northern Territory Geological Survey Record* **2005-001**.

Cross, A. & Williams, I., (2008). SHRIMP U-Th-Pb dating of xenotime. 4th SHRIMP Workshop, Saint Petersburg, Russia. June 29–July 4, 2008.

Demartin, F., Pilati, T., Diella, V., Donzelli, S. & Gentile, O., Gramaccioli, C.M., (1991). The chemical composition of xenotime from fissures and pegmatites in the Alps. *Canadian Mineralogist*, **29**, 69–75.

Fletcher, I.R., Rasmussen B. & McNaughton, N.J., (2000). SHRIMP U–Pb geochronology of authigenic xenotime and its potential for dating sedimentary basins. *Australian Journal of Earth Sciences*, **47**, 845–860.

Fletcher, I.R., McNaughton, N.J., Aleinikoff, J.A., Rasmussen, B. & Kamo, S.L., (2004). Improved calibration procedures and new standards for U–Pb and Th–Pb dating of Phanerozoic xenotime by ion microprobe. *Chemical Geology*, **209**, 295–314.

Fletcher, I.R., McNaughton, N.J., Davis, W.J. & Rasmussen, B., (2010). Matrix effects and calibration limitations in ion probe U–Pb and Th–Pb dating of monazite. *Chemical Geology*, 270, 31–44.

Förster, H.–J., (1998). The chemical composition of REE–Y–Th–U rich accessory minerals in peraluminous granites of the Erzgebirge–Fichtelgebirge region, Germany. Part II. Xenotime. *American Mineralogist*, **83**, 1302–1315.

Harrison, T.M., McKeegan, K.D. & LeFort, P., (1995). Detection of inherited monazite in the Manaslu leucogranite by $^{208}Pb/^{232}Th$ ion microprobe dating: crystallisation age and tectonic implications. *Earth and Planetary Science Letters*, **133**, 271-282.

HARRISON, M.T., CATLOS, E.J. & MONTEL, J.M., (2002). U-TH-PB DATING OF PHOSPHATE MINERALS. IN: KOHN, M.J., RAKOVAN, J., HUGHS, J.M., (EDS) *PHOSPHATES GEOCHEMICAL, GEOBIOLOGICAL, AND MATERIALS IMPORTANCE*. MINERALOGICAL SOCIETY OF AMERICA. REVIEWS IN MINERALOGY AND GEOCHEMISTRY, 523–558.

Hoskin, P.W.O. & Schaltegger, U., (2003). The composition of Zircon in Igneous and Metamorphic Petrogenesis. In: Hanchar, J.M. & Hoskin, P.W.O. (Eds). *Zircon*. Mineralogical Society of America. Reviews in Mineralogy and Geochemistry, **53**, 27-62.

Huston, D.L., Maas, R., Cross, A., Hussey, K.J., Mernagh, T.P., Fraser, G. and Champion, D.C. (2016). The Nolans Bore rare-earth element-phosphorus-uranium mineral system: geology, origin and post-depositional modifications. *Mineralium Deposita*, **51**, 797-822.

Ireland, T.R. & Bukovanská, M., (2003). Initial $^{182}Hf/^{180}Hf$ in meteoritic zircons. *Geochimica Cosmochimica Acta*, **67,** 4849-4856.

Kositcin, N., McNaughton, N.J., Griffin, B.J., Fletcher, I.R., Groves, D.I., and Rasmussen, B., 2003, Textural and geochemical discrimination between xenotime of different origins in the Archaean Witwatersrand basin, South Africa: Geochimica et Cosmochimica Acta, v. 67, p. 709–731.

Li, Q.L., Li, X.H., Lan, Z.W., Guo, C.L., Yang, Y.N., Liu, Y. & Tang, G.Q. (2013). Monazite and xenotime U–Th–Pb geochronology by ion microprobe: dating highly fractionated granites at Xihuashan tungsten mine, SE China. *Contributions to Mineralogy and Petrology*, **166**, 65-80.

McLaren, A.C., Fitzgerald, J.D. & Williams, I.S., (1994). The microstructure of zircon and its influence on the age determination from Pb/U ratios measured by the ion microprobe. *Geochimica Cosmochimica Acta*, **58**, 993-1005.

McNaughton, N.J., Rasmussen, B., Fletcher, I.R., 1999. SHRIMP uranium–lead dating of diagenetic xenotime in siliciclastic sedimentary rocks. Science 285, 78–80.

Rasmussen, B., (1996). Early-diagenetic REE-phosphate minerals (Florencite, Gorceixite, Crandallite, and Xenotime) in marine sandstones: a major sink for oceanic phosphorous. *American Journal of Science*, **296**, 601–632.

Rassmussen, B. & Fletcher, I.R., (2002). Indirect dating of mafic intrusions by SHRIMP U–Pb analysis of monazite in contact metamorphosed shale: an example from the Palaeoproterozoic Capricorn Orogen, Western Australia. *Earth and Planetary Science Letters*, **197**, 287-299.

Shimizu, N. & Hart, S.R., (1982). Applications of the ion microprobe to geochemistry and cosmochemistry: *Annual Reviews of Earth and Planetary Science*, **10**, 483-526.

Schaltegger, U., Pettke, T., Audétat, A., Reusses, E. & Heinrich, A., (2005). Magmatic to hydrothermal crystallisation in the W–Sn mineralised Mole Granite (NSW, Australia) Part I: Crystallisation of zircon and REE phosphates over three million years a geochemical and U–Pb geochronological study. *Chemical Geology*, **220**, 215–235.

Steiger, R.H. & Jäger, E., (1977). Subcommission on geochronology: convention on the use of decay constants in geo-and cosmochronology. *Earth and Planetary Science Letters*, **36**, 359–362.

Stern, R.A. & Berman, R.G., (2000). Monazite U-Pb and Th-Pb geochronology by ion microprobe, with an application to in situ dating of an Archean metasedimentary rock. *Chemical Geology*, **172**, 113-130.

Stern, R.A. and Rayner, N., (2003). Ages of several xenotime megacrysts by ID–TIMS: potential reference materials for ion probe U–Pb geochronology. Geological Survey of Canada, Current Research 2003–F1; Radiogenic age and isotope studies, report 16. 1–7.

Stern, R.A. & Sanborn, N., (1998). Monazite U-Pb and Th-Pb geochronology by high-resolution secondary ion mass spectrometry. Radiogenic Age and Isotopic Studies: Report 11. Geological Survey of Canada, Current Research, 1-18, 1998-F.

Taylor, R., Clark, C., and Reddy, S.M., 2012, The effect of grain orientation on secondary ion mass spectrometry (SIMS) analysis of rutile: Chemical Geology, v. 300-301, p. 81-87.

van Emden, B., Thomber, M.R., Graham, J. & Lincoln, F.J., (1997). The incorporation of actinides in monazite and xenotime from placer deposits in Western Australia. *Canadian Mineralogist*, **35**, 95–104.

Wark, D.A. & Miller, C.F., (1993). Accessory mineral behaviour during differentiation of a granite suite: monazite, xenotime and zircon in the Sweetwater Wash pluton, southeastern California, USA. *Chemical Geology*, **110**, 49–67.

White, L.T. & Ireland, T.R. (2012). High-uranium matrix effect in zircon and its implications for SHRIMP U–Pb age determinations. *Chemical Geology*, **306**, 78–91.

Williams, I.S. & Hergt, J.M., (2000). U–Pb dating of Tasmanian dolerites: a cautionary tale of SHRIMP analysis of high–U zircon. In: Woodhead, J.D., Hergt, J.M. and Noble, W.P. (Eds). Beyond 2000*: New Frontiers in Isotope Geoscience, Lorne, 2000 Abstracts and Proceedings*, pp. 185–188. University of Melbourne, Melbourne.

Williams, I.S., Buick, I.S. & Cartwright, I., (1996). An extended episode of early Mesoproterozoic metamorphic fluid flow in the Reynolds range, central Australia. *Journal of Metamorphic Petrology*, **14**, 29-47.

Wingate, M.T.D. & Compston, W., (2000). Crystal orientation effects during ion microprobe U-Pb analysis of baddeleyite. *Chemical Geology*, **165**, 75-97.

Zhu, X.K., O'Nions, R.K. & Gibb, A.J., (1998). SIMS analysis of U-Pb isotopes in monazite: matrix effects. *Chemical Geology*, **144**, 305-312.

Figure captions

Figure 1a-b. Backscattered Electron (BSE) images of NY/PK 6-80 (a) and D43764 (b) xenotimes. Small white blebs are monazite.

Figure 2. Energy profiles for the xenotime REFERENCE MATERIAL, MG-1 carried out on SHRIMP-RG (a) and SHRIMP II (b). The zero volts position was taken as the maximum transmission of the $^{254}[UO]^{+}$ molecule. Each scan is normalised to the maximum count rate to allow for a better comparison between the two instruments.

Figure 3a-b. Tera-Wasserburg concordia plot of matrix uncorrected xenotime U–Pb analyses for Z6413 (a) and MG-1 (b). (a) demonstrates the effect of a U concentration matrix mismatch, which favours the unknown and results in reversely discordant $^{206}Pb/^{238}U$ ratios and (b), is the opposite situation where the U concentration mismatch favours the calibration reference material and results in the unknown giving normally discordant $^{206}Pb/^{238}U$ ratios. The analyses shown in (a) were calibrated against MG-1 while the analyses in (b) were calibrated against Z6413. Data point error ellipses are 1σ.

Figure 4a-b. Plots showing matrix uncorrected, individually determined SHRIMP $^{206}Pb/^{238}U$ and $^{208}Pb/^{232}Th$ analyses for Z6413 (a) and BS-1 (b). The U–Pb–Th results for Z6413 (a) are within error of each other, strongly correlated (R=0.98) and elevated by ~14%, but the $^{207}Pb/^{206}Pb$ ratios are within error of the reference age for this sample. Similarly, individual SHRIMP U–Pb–Th ages for BS-1 (b) are within uncertainty of each other but elevated by 5% to 6%. All analyses are calibrated against MG-1. The thick black, dashed line in (a) and (b) represents the reference $^{206}Pb/^{238}U$ age. Error bars are 1 σ.

Figure 5a-b. U–Pb–Th concordia plots for BS-1 (a) and Z6413 (b). Both samples are shown to have elevated but concordant U–Pb–Th ratios. Data point error ellipses are 1σ.

Figure 6a-d. Plots demonstrating the correlations between $^{206}Pb^{+}/^{270}[UO_2]^{+}$ and $^{208}Pb^{+}/^{248}[ThO]^{+}$ ratios with $^{254}[UO]^{+}/^{194}[Y_2O]^{+}$ (a-b) and EPMA determined U concentration (c-d) for analyses of the high U xenotime NY/PK 6-80.

Figure 7a-d. Plots demonstrating the correlations between $^{206}Pb^{+}/^{270}[UO_2]^{+}$ and $^{208}Pb^{+}/^{248}[ThO]^{+}$ ratios with $^{190}[YbO]^{+}/^{194}[Y_2O]^{+}$ (a-b) and $^{177}[DyO]/^{194}[Y_2O]^{+}$ ratios for the high U xenotime NY/PK 6-80.

Figure 8. U–Pb–Th concordia plot for NY/PK 6-80, SHRIMP U–Pb–Th analyses. The unfilled ellipses represent matrix uncorrected $^{206}Pb/^{238}U$ and $^{208}Pb/^{232}Th$ ratios while the filled ellipses are matrix corrected ratios. Dark grey ellipses represent analyses of the cores and the light grey ellipses represent rim analyses. Data point error ellipses are 1σ. Session: SHII-(Dec-05).

Figure 9. U–Pb–Th concordia plot for D43764 SHRIMP U–Pb–Th analyses. Uncorrected (unfilled ellipses) and matrix corrected (filled ellipses) U–Pb–Th data are plotted. The two striped ellipses and two pale grey ellipses were excluded from the $^{206}Pb/^{238}U$ and $^{208}Pb/^{232}Th$ weighted mean age calculations respectively. Data point error ellipses are 1σ. Session: RG-(Jun-06).

Figure 10a-b. Tera-Wasserburg concordia plots of U–Pb analyses for D43764. Matrix uncorrected results are shown in (a) and the U and ΣREE matrix corrected results are shown in (b). Data point error ellipses are 1σ. Session: RG-(Jun-06).

Figure 11. Plot showing the excellent correlation (R^2 = 0.94) between the xenotime ∑REE concentration (Nd, Sm, Eu, Gd, Tb, Dy, Ho, Er, Tm, Yb, Lu) and ΣGd,Dy,Er,Yb, for the different types of xenotime analysed in this study.

Table captions

Table 1. REFERENCE AGES FOR XENOTIME SAMPLES USED IN THIS STUDY. UNCERTAINTIES ARE 2σ.

Table 2. EPMA determined average compositions (wt%) for the reference xenotimes used in this study.

Table 3. Table comparing EPMA and SHRIMP-based xenotime U abundance determinations for reference xenotimes analysed in RG-(Sep-06). Of the three techniques presented, $RSF_{(U–Ho)}$ is superior (see text).

Table 4. Representative Th/U calibration factors calculated from MG-1, BS-1 and Z6413 (SHII = SHRIMP II, RG = SHRIMP-RG).

Table 5. Table showing the typical SHRIMP xenotime U–Pb–Th fractionations for the reference xenotimes and the contrasts they have in U, Th and ΣREE concentration with the U–Pb–Th calibration standard MG-1.

Table 6. Table comparing xenotime $^{206}Pb/^{238}U$ fractionations of BS-1 and Z6413, that were collected using an unfiltered and filtered secondary ion beam.

Table 7. U–Pb–Th correction coefficients for U, Th and ΣREE, for nine SHRIMP U–Pb–Th xenotime sessions.

Table 8. U–Pb–Th correction coefficients for U and ΣREE for nine SHRIMP U–Pb–Th xenotime sessions.

APPENDIX A

Electron microprobe settings used for xenotime analysis.

Detection Limits and relative errors are 1σ.
HV: 25kV
Current: 100nA
Beam focus: focussed 5µm
Cameca SX100:Research School of Earth Sciences, ANU

Element	Line	Standard	Crystal	Position	Bg 1	Bg 2	Time (s)	Det. Lim. (ppm)	% relative error
Si	Ka	Quartz	TAP	27741	-1000	1500	150	33	1.7
P	Ka	YP_5O_{14}	PET	70526	-400	400	10	430	2.4
Ca	Ka	$CaAl_2O_4$	PET	38375	-521	400	20	77	13.9
Y	La	YP_5O_{14}	PET	73913	-1600	1500	10	528	5.5
Nd	La	NdP_5O_{14}	PET	27084	290	880	30	230	14
Sm	La	SmP_5O_{14}	PET	25140	315	738	30	262	9
Eu	La	EuP_5O_{15}	PET	24243	-505	-190	30	342	9.4
Gd	La	GdP_5O_{14}	PET	23398	-385	400	30	552	7.2
Tb	La	TbP_5O_{14}	PET	22593	-365	430	30	610	10.9
Dy	La	DyP_5O_{14}	LLIF	47391	-885	826	30	200	2.3
Ho	Lb	HoP_5O_{14}	LLIF	40895	-2495	5610	30	407	4.6
Er	La	ErP_5O_{14}	LLIF	44318	-5918	2200	30	203	2.7
Tm	La	TmP_5O_{14}	LLIF	42868	-4468	3637	30	184	4.1
Yb	La	YbP_5O_{14}	LLIF	41502	-3102	4950	30	209	1.6
Lu	Lb	LuP_5O_{14}	LLIF	35336	-2008	3064	30	399	5.4
U	Mb	UO_2	LPET	42463	-1060	550	60	210	7-60
Th	Ma	ThO_2	LPET	47294	-1170	560	60	161	6-15

APPENDIX B

ID TIMS results for NY/PK 6-80

Analyst: Dr. Sandra Kamo
Royal Ontario Museum

Table B.1. U–Pb data for single xenotime crystal fragments from NY/PK 6-80

Analysis No.	Weight (mg)	U (ppm)	Pb (ppm)	Th/U	PbCom (pg)	206/204	206/238	2σ	207/235	2σ	207/206	2σ	206/238 Age (Ma)	2σ	207/206 Age (Ma)	2σ	% Disc	Corr Coeff
Sk17p90[a]	0.0020	21355	3518	0.24	10.7	43025	0.16732	0.00070	1.6763	0.0072	0.072663	0.000094	997.3	3.9	1004.6	2.6	0.8	0.954
Sk17p120[a]	0.0036	6942	1148	0.23	6.8	39854	0.16829	0.00044	1.6870	0.0043	0.072707	0.000068	1002.7	2.4	1005.8	1.9	0.3	0.934
Sk17p121[a]	0.0022	5469	902	0.24	3.2	40769	0.16748	0.00061	1.6717	0.0063	0.072392	0.000102	998.2	3.4	997.0	2.9	-0.1	0.928
Sk17p116[b]	0.0050	4293	714	0.27	2.7	85254	0.16744	0.00039	1.6769	0.0041	0.072636	0.000096	998.0	2.2	1003.8	2.7	0.6	0.849
Sk17p118[a]	0.0058	4289	722	0.29	3.4	80425	0.16888	0.00038	1.6942	0.0043	0.072760	0.000068	1005.9	2.1	1007.3	1.9	0.1	0.930
Sk17p119[a]	0.0044	7575	1248	0.22	3.6	99866	0.16819	0.00041	1.6863	0.0045	0.072716	0.000072	1002.1	2.2	1006.0	2.0	0.4	0.930
Sk17p117[b]	0.0022	5558	908	0.19	3.2	41413	0.16815	0.00042	1.6854	0.0047	0.072696	0.000066	1001.9	2.3	1005.5	1.8	0.4	0.947
Sk17p166[c]	0.0100	16734	2742	0.24	9.1	197021	0.16646	0.00072	1.6727	0.0075	0.072879	0.000068	992.6	4.0	1010.6	1.9	1.9	0.978
Sk17p167[c]	0.0040	11142	1840	0.26	4.8	100141	0.16692	0.00037	1.6683	0.0043	0.072485	0.000058	995.1	2.1	999.6	1.6	0.5	0.956
Sk17p168[c]	0.0040	7883	1280	0.30	8.9	36986	0.16243	0.00035	1.6042	0.0039	0.071626	0.000078	970.3	1.9	975.3	2.2	0.6	0.894
Sk17p169[c]	0.0040	12695	2113	0.24	5.7	97235	0.16897	0.00046	1.6974	0.0051	0.072860	0.000062	1006.4	2.5	1010.1	1.7	0.4	0.960
Sk17p170[c]	0.0040	7899	1285	0.17	9.1	37421	0.16839	0.00037	1.6880	0.0043	0.072703	0.000064	1003.2	2.0	1005.7	1.8	0.3	0.941
Sk17p171[c]	0.0040	8000	1327	0.27	6.8	50124	0.16693	0.00042	1.6691	0.0045	0.072517	0.000082	995.2	2.3	100.5	2.3	0.6	0.909

Superscript a: not abraded—large fragments were broken apart and small internal fragments were selected for analysis
Superscript b: abraded
Superscript c: extensively abraded (significant volume reduction)
PbCom: Common Pb
Th/U: calculated from radiogenic $^{208}Pb/^{206}Pb$ ratio and $^{207}Pb/^{206}Pb$ age
Pb/U corrected for spike, fractionation, blank; 206/204 corrected for spike and fractionation
% Disc: per cent discordance for the given $^{207}Pb/^{206}Pb$ age
Uranium decay constants are from Jaffey et al. (1971)

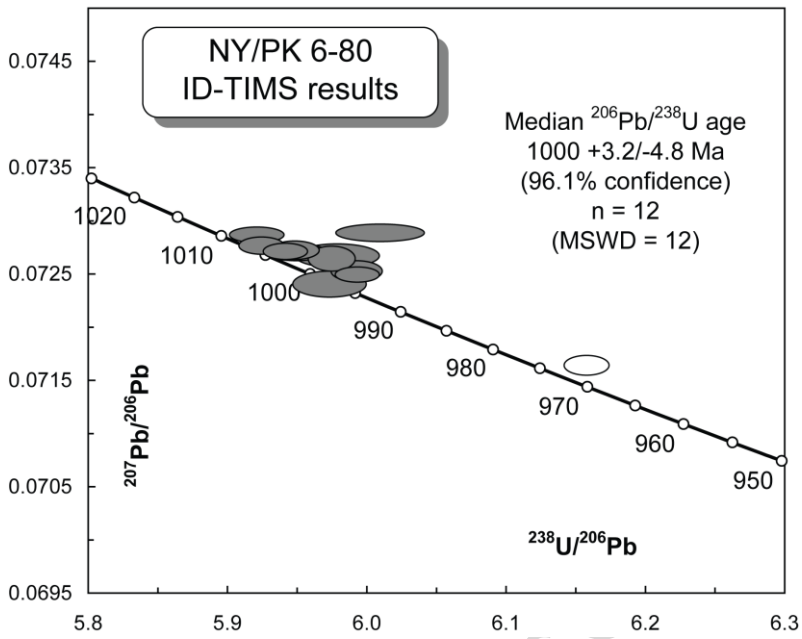

Figure B.1. Tera-Wasserburg concordia plot for NY/PK 6-80 ID-TIMS analyses. The unfilled ellipse was excluded from the median $^{206}Pb/^{238}Pb$ age calculation (Sk17p168). Data point error ellipses are 2σ.

APPENDIX C

ELECTRON MICROPROBE CHEMICAL U–TH–PB DATING OF REFERENCE XENOTIME D43764

Electron microprobe chemical U–Th–Pb dating was carried out on a single xenotime crystal of D43764 using a Cameca sx100 electron microprobe at the RSES. This experiment was undertaken as a means to independently determine the age of D43764 and therefore provide a check for the SHRIMP determined $^{207}Pb/^{206}Pb$ age of 2622 ± 3 Ma (95% confidence). D43764 xenotime is a good candidate for electron probe U–Th–Pb dating having a high U concentration (~1.5 wt%) and Archaean age. This experiment was conducted under the basic assumptions that underpin electron microprobe chemical U–Th–Pb dating. These are (1) common Pb is negligible and, (2) there has been no modification of the U/Th/Pb ratios except by radioactive decay (Montel et al. 1996). Before analysis, BSE imaging of the xenotime was carried out to determine whether different growth domains exist and also to identify the most pristine areas for analysis. The xenotime was analysed for U, Th, Pb and Y, using a 15 kV electron beam regulated at 200 nA. The X–ray lines were Pb*M*β, Th*M*α, U*M*β and Y*L*α. Counting times for Pb, Th and U were 200 s and 90 s for Y. Background count times were done at half of the peak time. Prior to analysis, a WDS scan of xenotime D43764 was carried out in order to select background positions for the analysed elements. The background intensity under the U, Th, Pb and Y peaks was then calculated by an exponential regression of the background regions. Under these operating conditions the detection limit (2σ) is 150 ppm, 215 ppm and 130 ppm for Pb, Th and U respectively. Single-point xenotime age calculations were done with the EPMA dating excel add–in of Pommier et al. (2002) which uses the U–Th–Pb age calculation equation of Montel et al. (1996). Thirty-two analyses were undertaken on a single crystal of D43764 (Fig. 1 and Table 1). All analyses have the same weighted mean U–Th–Pb chemical age within analytical error and combine to give an age of **2637 ± 22 Ma** (MSWD=0.11; 95% confidence). The U–Th–Pb chemical age calculation is within error of the SHRIMP $^{207}Pb/^{206}Pb$ age of 2622 ± 3 Ma for this sample (MSWD = 1.8, POF = 0.18) and supports it being used as reference age for D43764 xenotime.

References

Montel, J.-M., Foret, S., Veschambre, M.C.N., Provost, A., 1996. Electron microprobe dating of monazite. *Chemical Geology*, **131**, 37–53.

Pommier, A., Cocherie, A. & Legendre, O., 2002. EPMA Dating User's Manual: Age calculation from Electron Probe Microanalyser Measurements of U–Th–Pb. BRGM, 9 pp.

Williams, M.L. & Jercinovic, M.J., 2002. Age dating and mapping of monazite on the electron probe: Deconvoluting multistage tectonic histories. *Geology* **27**, 1023–1026.

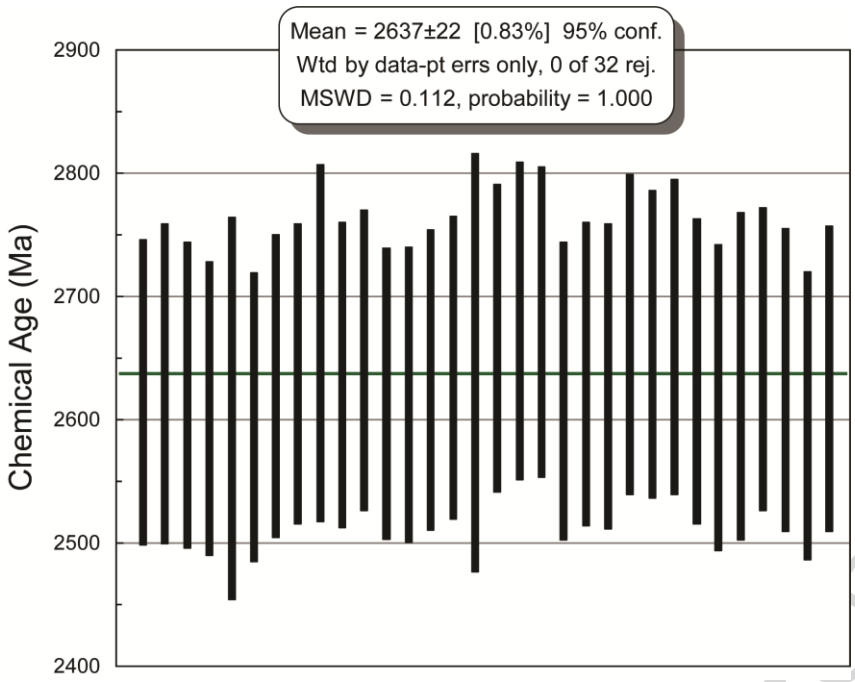

Figure C.1. Diagram showing EPMA chemical U-Th-Pb ages for xenotime standard D42764. Box heights are 2σ.

Table C.1. EPMA chemical U-Th-Pb ages and results for D43764.

Spot name	Th (ppm)	Pb (ppm)	U (ppm)	Th/U	Chemical age (±2σ %)	
1 / 1 .	3788	8003	14796	0.26	2623	124
2 / 1 .	4407	7151	12921	0.34	2630	130
3 / 1 .	3699	7939	14714	0.25	2621	124
4 / 1 .	6047	8934	16205	0.37	2610	119
5 / 1 .	7202	5800	9719	0.74	2610	155
6 / 1 .	5528	10323	19158	0.29	2603	117
7 / 1 .	3923	8196	15102	0.26	2628	123
8 / 1 .	3919	8974	16530	0.24	2638	122
9 / 1 .	2190	6576	12104	0.18	2663	145
10 / 1 .	3234	8216	15226	0.21	2637	124
11 / 1 .	4413	9181	16709	0.26	2649	122
12 / 1 .	4320	11051	20675	0.21	2622	118
13 / 1 .	3191	9859	18610	0.17	2621	120
14 / 1 .	2930	9722	18282	0.16	2633	122
15 / 1 .	2664	9204	17240	0.15	2643	123
16 / 1 .	3749	5506	9765	0.38	2647	170
17 / 1 .	3274	8521	15543	0.21	2667	125
18 / 1 .	2352	7737	14151	0.17	2681	129
19 / 1 .	3319	8639	15646	0.21	2680	126
20 / 1 .	3729	9173	17101	0.22	2624	121
21 / 1 .	3180	8882	16532	0.19	2638	123
22 / 1 .	3426	8421	15592	0.22	2636	124
23 / 1 .	2756	7577	13834	0.20	2670	130
24 / 1 .	3277	8418	15395	0.21	2662	125
25 / 1 .	2785	7716	14110	0.20	2668	128
26 / 1 .	3185	8585	15937	0.20	2640	124
27 / 1 .	3087	8107	15208	0.20	2619	124
28 / 1 .	2571	7067	13157	0.20	2636	133
29 / 1 .	3624	8977	16491	0.22	2650	123
30 / 1 .	3237	8959	16720	0.19	2633	123
31 / 1 .	4842	10969	20600	0.24	2604	117
32 / 1 .	3745	8126	14952	0.25	2634	124

APPENDIX D

Least squares $^{206}Pb^{+}/^{270}[UO_2]^{+}$ matrix correction technique

For simplicity, the following methodology uses SHRIMP xenotime $^{206}Pb^{+}/^{270}[UO_2]^{+}$ ratios to describe the matrix correction procedure developed; this technique is identical to that used to matrix-correct $^{208}Pb^{+}/^{248}[ThO]^{+}$ ratios.

The SHRIMP U–Pb matrix effect causes a breakdown in the basic assumption underpinning all SIMS $^{206}Pb/^{238}U$ ages, i.e. that the emission of secondary $^{206}Pb^{+}$ and $^{238}U_xO_x^{+}$ ions relative to the true $^{206}Pb/^{238}U$ in both the calibration reference material and unknown is identical.

For SHRIMP $^{206}Pb/^{238}U$ analysis, this means that:

$$\frac{\left(\frac{206Pb+}{270[UO2]+}std\right)}{\left(\frac{206Pb}{238U}std\right)} \neq \frac{\left(\frac{206Pb+}{270[UO2]+}unk\right)}{\left(\frac{206Pb}{238U}unk\right)} \qquad \text{(A)}$$

To correct for the SHRIMP U–Pb matrix effect we need to correct both sides of (A) by a factor, **F** that relates the $^{206}Pb^{+}/^{270}[UO_2]^{+}$ matrix effect to the chemical contrasts in the three reference materials (MG-1, BS-1 and Z6413) (B).

$$\frac{\left(\frac{206Pb+}{270[UO2]+}std\right)*F}{\left(\frac{206Pb}{238U}std\right)} = \frac{\left(\frac{206Pb+}{270[UO2]+}unk\right)*F}{\left(\frac{206Pb}{238U}unk\right)} \qquad \text{(B)}$$

Where **F** = 1-(f(U) * epmaU)-(f(Th) * epmaTh)-(f(ΣREE) * epmaΣREE) (see below)

Finding the correction coefficients f(U), f(Th) and f(ΣREE)

1. Normalise the $^{206}Pb^{*+}/^{270}[UO_2]^{+}$ ratios for the RMs by their reference $^{206}Pb/^{238}U$ ratios:

$^{206}Pb^{*+}/^{270}[UO_2]^{+}$_norm = ($^{206}Pb^{*+}/^{270}[UO_2]^{+}$)/($^{206}Pb/^{238}U$_ref) (1)

(Note that * denotes common Pb corrected)

2. Determine the session $^{206}Pb^{+}/^{270}[UO_2]^{+}$, U-, Th- and ΣREE-induced, U, Th and ΣREE correction coefficients, **f(U)**, **f(Th)** and **f(ΣREE)** respectively. The correction coefficients are used together with the spot-specific U, Th and ΣREE, EPMA concentrations to determine the overall matrix correction factor, **F** for each analysis.
    - Reference **f(U)**, **f(Th)** and **f(ΣREE)** to three cells where the initial values are set to zero.

F = 1-(**f(U)** * epmaU)- (**f(Th)** * epmaTh)-((**f(ΣREE)** * epmaREE) (2)

3. Multiply the $^{206}Pb^{*+}/^{270}[UO_2]^+$_norm ratios of the RMs by the matrix correction factor **F**.

   $^{206}Pb^{*+}/^{270}[UO_2]^+$_norm_mc = $^{206}Pb^{*+}/^{270}[UO_2]^+$_norm * F (3)

4. Calculate a robust Biweight mean for the combined RMs

   mean$^{206}Pb^{*+}/^{270}[UO_2]^+$_norm_mc (4)

5. Remove the normalisation of the $^{206}Pb^{*+}/^{270}[UO_2]^+$ ratios carried out in step 1:

   $^{206}Pb^{*+}/^{270}[UO_2]^+$_mc = $^{206}Pb^{*+}/^{270}[UO_2]^+$_norm_mc * $^{206}Pb/^{238}U$_ref (5)

6. Convert matrix corrected ratios ($^{206}Pb^{*+}/^{270}[UO_2]^+$_mc) to $^{206}Pb^*/^{238}U$ ratios and ages.

   $^{206}Pb^*/^{238}U$_true = ($^{206}Pb^{*+}/^{270}[UO_2]^+$_mc) /(mean$^{206}Pb^{*+}/^{270}[UO_2]^+$_norm_mc) (6)

7. Calculate robust Biweight mean ages for each of the RMs: mean_BS1_$^{206}Pb/^{238}U$_true; mean_MG1_$^{206}Pb/^{238}U$_true and; mean_Z6413_$^{206}Pb/^{238}U$_true.

8. Calculate the Residual Sum of Squares (**RSS**) of the deviations between the Biweight mean $^{206}Pb/^{238}U$_true (age) and $^{206}Pb/^{238}U$_ref (age) for each of the RMs

   RSS = (mean_BS1_$^{206}Pb/^{238}U$_true/BS1_$^{206}Pb/^{238}U$_ref-1)^2 +
   (mean_MG1_$^{206}Pb/^{238}U$_true/MG1_$^{206}Pb/^{238}U$_ref-1)^2 +
   (mean_Z6413_$^{206}Pb/^{238}U$_true/Z6413_$^{206}Pb/^{238}U$_ref-1)^2 (7)

9. Find the combination of **f(U)**, **f(Th)** and **f(ΣREE)** that minimises the RSS. For MS Excel solver, 'Set Target Cell' (Excel 2003) or 'Set Objective' (Excel 2010) should be assigned to the 'RSS' cell and the cells assigned to f(U), f(Th) and f(ΣREE) (initially set to zero) should be set to 'By Changing Cells:' (Excel 2003) or 'By Changing Variable Cells:' (Excel 2010).

Once the correction coefficients are found, F is calculated for all analyses and the $^{206}Pb^{*+}/^{270}[UO_2]^+$ ratios are matrix corrected before SHRMP U–Pb–Th processing using 1-D, $^{206}Pb^{*+}/^{270}[UO_2]^+$ and $^{208}Pb^{*+}/^{248}[ThO]^+$ calibrations (Stage 2). The additional uncertainty associated with the above procedure results in total, pooled-age $^{206}Pb/^{238}U$ and $^{208}Pb/^{232}Th$ uncertainties of between 1.5% to 3.0 %. An excel spread sheet is available from the authors on request that details both the uncertainty propagation methodology and the matrix correction procedure described above. Additionally, SQUID2 tasks (for processing SHRIMP .pd files) are also available that automatically calculate matrix corrected $^{206}Pb/^{238}U$ and $^{208}Pb/^{232}Th$ ages.

APPENDIX E

Table E.1. Generalised EPMA (WDS) results for session SHII-(Dec-05). (ΣREE = Nd, Sm, Eu, Gd, Tb, Dy, Ho, Er, Tm, Yb, Lu).

Grain.area	U (wt%)	±1σ (%)	ΣREE (wt%)	±1σ (%)
MG-1-2.10	0.0781	23.94	13.44	4.38
MG-1-2.11	0.1045	18.66	13.64	4.35
MG-1-2.12	0.1142	16.99	13.69	4.33
MG-1-2.13	0.1021	18.81	13.59	4.36
MG-1-2.6	0.1120	17.41	13.73	4.33
MG-1-2.7	0.1013	18.95	13.16	4.42
MG-1-2.8	0.0883	21.52	13.19	4.44
MG-1-2.9	0.1064	18.05	13.08	4.44
MG-1-3.2	0.0993	19.23	13.66	4.34
MG-1-3.3	0.0924	20.45	13.68	4.33
MG-1-3.4	0.1254	15.87	13.92	4.29
MG-1-4.1	0.0966	19.77	13.11	4.24
MG-1-4.2	0.1030	18.64	13.15	4.41
MG-1-4.3	0.0936	20.19	13.02	4.43
MG-1-4.4	0.1024	18.75	13.10	4.43
BS-1-2.10	0.0189	96.30	17.81	3.50
BS-1-2.8	0.0230	76.96	17.96	3.55
BS-1-2.9	0.0388	46.65	17.93	3.57
BS-1-3.1	0.0363	49.31	17.87	3.57
BS-1-3.2	0.0372	47.85	17.86	3.57
BS-1-3.3	0.0518	35.33	18.02	3.57
BS-1-3.4	0.0515	35.34	17.52	3.56
BS-1-3.5	0.0565	32.39	17.47	3.57
BS-1-4.1	0.0493	37.12	18.64	3.66
BS-1-4.2	0.0611	30.28	18.08	3.57
BS-1-4.3	0.0791	23.51	17.77	3.55
BS-1-4.4	0.0376	48.14	18.49	3.64
BS-1-5.1	0.0604	30.46	18.17	3.60
BS-1-5.2	0.0360	50.56	18.61	3.58
Z6413-5.1	1.3156	6.64	16.22	3.55
Z6413-5.2	1.2436	6.67	16.26	3.56
Z6413-5.3	1.5045	6.58	16.19	3.56
Z6413-5.4	1.2920	6.64	16.16	3.57
Z6413-6.1	1.2411	6.66	16.33	3.54
Z6413-6.2	1.2452	6.66	16.39	3.53
Z6413-6.3	1.1592	6.70	16.36	3.53

Grain.area	U (wt%)	±1σ (%)	ΣREE (wt%)	±1σ (%)
Table E.1. continued				
Z6413-6.4	1.2116	6.68	16.33	3.54
Z6413-6.5	1.5431	6.57	16.50	3.53
Z6413-6.6	1.6180	6.55	16.39	3.53
Z6413-7.1	1.3210	6.63	16.38	3.53
Z6413-7.2	1.2815	6.65	16.45	3.52
NYPK-3.2r	1.2782	6.65	16.99	3.68
NYPK-3.3r	1.2442	6.66	17.09	3.67
NYPK-4.1c	1.5679	5.40	17.84	3.51
NYPK-4.10c	1.5305	6.72	17.64	3.63
NYPK-4.11r	1.3083	7.69	17.21	3.69
NYPK-4.12r	1.2738	6.81	17.09	3.69
NYPK-4.2c	1.7252	6.53	17.97	3.61
NYPK-4.3c	1.7492	6.53	17.68	3.61
NYPK-4.4c	1.0538	6.76	17.21	3.66
NYPK-4.5c	1.2671	6.65	17.51	3.63
NYPK-4.6c	1.4494	6.60	17.58	3.60
NYPK-4.7c	1.7101	6.54	17.25	3.64
NYPK-4.8c	1.3095	6.64	17.56	3.60
NYPK-4.9c	1.7983	6.52	17.61	3.61
NYPK-5.1c	1.4169	6.61	17.70	3.59
NYPK-5.2c	1.3404	6.63	17.56	3.61
NYPK-5.3r	2.2728	6.46	17.52	3.64
NYPK-7.1r	1.3453	6.63	17.30	3.65
NYPK-7.2r	1.7898	6.52	17.97	3.58
NYPK-7.3c	1.7553	6.53	17.70	3.59
NYPK-8.1c	1.4692	6.59	17.70	3.58
NYPK-8.2r	1.3585	6.62	17.38	3.64
NYPK-8.3c	1.5783	6.56	17.85	3.58
NYPK-8.4c	1.8349	6.51	17.66	3.61
NYPK-8.5r	1.3739	6.61	17.30	3.64

Table E.2. Table showing the xenotime matrix uncorrected and matrix corrected $^{206}Pb/^{238}U$ ratios for session SHII-(Dec-05).

Grain.area	$^{206}Pb/^{238}U$ ± 1σ (Ma)	% δ^1	$^{206}Pb/^{238U}$_mc ± 1σ (Ma)	% $^{206}Pb/^{238}U$ correction	% δ^2
BS-1-2.10	547±18.8	7.5	523±15.4	4.6	2.8
BS-1-2.8	526.4±19.2	3.4	499.1±14.5	5.5	-1.9
BS-1-2.9	538.3±13.7	5.8	515.9±12.4	4.3	1.4
BS-1-3.1	530.4±15.3	4.2	509.4±13.1	4.1	0.1
BS-1-3.2	542.4±14.7	6.6	520.3±13.1	4.2	2.2
BS-1-3.3	538.2±13.6	5.7	514.3±12.2	4.6	1.0
BS-1-3.4	508.4±13	-0.1	489.6±11.8	3.8	-3.8
BS-1-3.5	536±14.6	5.3	516.5±12.4	3.8	1.5
BS-1-4.1	550.5±13.9	8.2	525.7±12.7	4.7	3.3
BS-1-4.2	530.6±14	4.2	505.6±12	4.9	-0.7
BS-1-4.3	526.7±16.3	3.5	499.3±12.2	5.5	-1.9
BS-1-4.4	531.7±13.9	4.5	513.1±12.6	3.6	0.8
BS-1-5.1	524.4±14.2	3.0	497±11.9	5.5	-2.4
BS-1-5.2	520.5±13.6	2.3	497.3±12.4	4.7	-2.3
Z6413-5.1	1170.5±25.2	17.8	979.9±23.1	19.5	-1.4
Z6413-5.2	1203.8±25.7	21.1	1009.9±22.1	19.2	1.6
Z6413-5.3	1229.6±26.2	23.7	994.2±22.4	23.7	0.0
Z6413-5.4	1195.7±25.6	20.3	999.3±22.1	19.7	0.5
Z6413-6.1	1214.7±26	22.2	1012±22.3	20.0	1.8
Z6413-6.2	1208.9±26.1	21.6	1011.1±23.6	19.6	1.7
Z6413-6.3	1173.3±25.2	18.0	997.4±21.7	17.6	0.3
Z6413-6.4	1176.1±25.4	18.3	990.1±22.1	18.8	-0.4
Z6413-6.5	1216.3±26	22.4	974±22.1	24.9	-2.0
Z6413-6.6	1232±26.3	23.9	975.5±22.1	26.3	-1.9
Z6413-7.1	1203.1±25.7	21.0	996.3±22.3	20.8	0.2
Z6413-7.2	1192.5±25.5	20.0	992.2±22.3	20.2	-0.2
NYPK-3.2r	1235.6±26.4	27.4	1016.8±22.9	21.5	4.8
NYPK-3.3r	1218±26	25.6	1011.5±22.5	20.4	4.3
NYPK-4.1c	1326.4±28.1	32.6	1040.2±22.8	27.5	2.8
NYPK-4.10c	1230.7±26.3	23.1	972.7±22	26.5	-3.9
NYPK-4.11r	1196.7±25.7	23.4	982.9±23	21.7	1.3
NYPK-4.12r	1171.6±25.1	20.8	964.4±21.2	21.5	-0.6
NYPK-4.2c	1421.2±29.9	42.1	1087.5±24.9	30.7	7.5
NYPK-4.3c	1308.7±28.2	30.9	1001.7±24.1	30.6	-1.0
NYPK-4.4c	1191.3±25.5	19.1	1014.3±22.8	17.5	0.2
NYPK-4.5c	1222.7±26.1	22.3	1009.3±22	21.1	4.1
NYPK-4.6c	1243.6±26.6	24.4	995.4±22.1	24.9	2.6
NYPK-4.7c	1252.6±26.7	25.3	971.2±23	29.0	0.1

δ^1 percent deviation of the matrix uncorrected ratios from their reference age.
δ^2 percent deviation of the matrix corrected ratios from their reference age.

Table E.2. continued.

Grain.area	$^{206}Pb/^{238}U$ ± 1σ (Ma)	% δ^1	$^{206}Pb/^{238U}$_mc ± 1σ (Ma)	% $^{206}Pb/^{238}U$ correction	% δ^2
NYPK-4.8c	1224.3±26.2	22.4	1003.6±24.3	22.0	3.5
NYPK-4.9c	1319.8±28	32.0	1003.1±23.3	31.6	3.4
NYPK-5.1c	1268.6±27	26.9	1020.2±22.8	24.4	5.2
NYPK-5.2c	1234.1±26.7	23.4	1004.8±23.9	22.8	3.6
NYPK-5.3r	1350.7±28.5	39.2	951.9±24.9	41.9	-1.9
NYPK-7.1r	1203.8±25.8	24.1	985.3±22.9	22.2	1.6
NYPK-7.2r	1287.1±27.3	32.7	974.7±22.7	32.1	0.5
NYPK-7.3c	1323.1±28	32.3	1011.4±23.6	30.8	-0.1
NYPK-8.1c	1247.8±26.6	24.8	997.5±22.2	25.1	-1.4
NYPK-8.2r	1150.7±24.7	18.6	935.4±21	23.0	-3.6
NYPK-8.3c	1251.8±26.7	25.2	980±22.3	27.7	-3.2
NYPK-8.4c	1316.2±27.9	31.6	994.8±23.5	32.3	-1.7
NYPK-8.5r	1146.4±24.6	18.2	930.6±21.1	23.2	-4.1

δ^1 percent deviation of the matrix uncorrected ratios from their reference age.
δ^2 percent deviation of the matrix corrected ratios from their reference age.

Table E.3. Table showing the xenotime matrix uncorrected and matrix corrected $^{208}Pb/^{232}Th$ ratios for session SHII-(Dec-05).

Grain.area	$^{208}Pb/^{232}Th$ ± 1σ (Ma)	% δ^1	$^{208}Pb/^{232}Th$_mc ± 1σ (Ma)	% $^{208}Pb/^{232}Th$ correction	% δ^2
BS-1-2.10	560.9±19.1	10.2	530±15.8	5.8	4.1
BS-1-2.8	542.1±20.2	6.5	505.1±15	7.3	-0.8
BS-1-2.9	548.1±14.4	7.7	513.1±14.5	6.8	0.8
BS-1-3.1	549.4±16.2	7.9	516.7±14.3	6.3	1.5
BS-1-3.2	557.9±15.5	9.6	521.5±14.1	7.0	2.4
BS-1-3.3	545.1±14.5	7.1	508.2±13.5	7.3	-0.2
BS-1-3.4	538±14.3	5.7	506.7±14.3	6.2	-0.4
BS-1-3.5	530.5±15.1	4.2	500.9±15	5.9	-1.6
BS-1-4.1	564.5±14.8	10.9	523.5±13.8	7.8	2.9
BS-1-4.2	539.9±14.8	6.1	502.8±14.4	7.4	-1.2
BS-1-4.3	524.6±16.4	3.1	492±13	6.6	-3.3
BS-1-4.4	547.4±14.5	7.5	511.5±14.5	7.0	0.5
BS-1-5.1	531.3±14.7	4.4	492.1±13	8.0	-3.3
BS-1-5.2	535±14.2	5.1	496.3±14.6	7.8	-2.5
Z6413-5.1	1133.8±29.2	14.1	936.2±25	21.1	-5.8
Z6413-5.2	1221.3±31.6	22.9	1022.2±27	19.5	2.8
Z6413-5.3	1231±31.5	23.8	993.7±26.7	23.9	0.0
Z6413-5.4	1201.6±31.1	20.9	1001.4±26.6	20.0	0.7
Z6413-6.1	1222.4±31.5	23.0	1027±27.4	19.0	3.3
Z6413-6.2	1224.9±31.7	23.2	1015.7±27	20.6	2.2
Z6413-6.3	1183.8±30.9	19.1	998.4±26.6	18.6	0.4
Z6413-6.4	1175.6±30.4	18.3	981.8±26.2	19.7	-1.2
Z6413-6.5	1219.1±31.6	22.6	974.6±27.6	25.1	-2.0
Z6413-6.6	1239.7±31.7	24.7	986.9±27.6	25.6	-0.7
Z6413-7.1	1193±30.8	20.0	985.1±28	21.1	-0.9
Z6413-7.2	1182.9±30.7	19.0	981.6±28.5	20.5	-1.2
NYPK-3.2r	1249.8±31.7	28.8	1027.5±27.1	21.6	5.9
NYPK-3.3r	1227.8±31.3	26.6	1010.6±26.7	21.5	4.2

NYPK-4.1c	1343.2±34	34.3	1046.5±29.7	28.4	3.4
NYPK-4.10c	1252±31.9	25.2	979.7±27.2	27.8	-3.2
NYPK-4.11r	1194.8±30.6	23.2	977.1±26.4	22.3	0.7
NYPK-4.12r	1133.1±28.9	16.8	929.5±26.2	21.9	-4.2
NYPK-4.2c	1456.5±36.6	45.7	1109±31.6	31.3	9.6
NYPK-4.3c	1322.6±33.5	32.3	1008.4±28	31.2	-0.4
NYPK-4.4c	1185.3±30.3	18.5	1001.1±28.4	18.4	-1.1
NYPK-4.5c	1236.8±32.8	23.7	1016±29.6	21.7	4.7
NYPK-4.6c	1264.3±32.1	26.4	1004.4±28.8	25.9	3.5
NYPK-4.7c	1261.1±32.2	26.1	972.9±28.1	29.6	0.3

δ^1 percent deviation of the matrix uncorrected ratios from their reference age.
δ^2 percent deviation of the matrix corrected ratios from their reference age.

TABLE E.3. CONTINUED.

Grain.area	$^{208}Pb/^{232}Th$ ± 1σ (Ma)	% δ^1	$^{208}Pb/^{232}Th$_mc ± 1σ (Ma)	% $^{208}Pb/^{232}Th$ correction	% δ^2
NYPK-4.8c	1228.5±31.4	22.8	995.8±29.1	23.4	2.7
NYPK-4.9c	1323.5±33.6	32.4	1002.2±29.2	32.1	3.3
NYPK-5.1c	1297.5±33	29.8	1035.6±27.7	25.3	6.8
NYPK-5.2c	1235±31.6	23.5	996.6±29.1	23.9	2.7
NYPK-5.3r	1391±35.1	43.4	986.4±29.3	41.0	1.7
NYPK-7.1r	1225.5±31.2	26.3	992.4±29.5	23.5	2.3
NYPK-7.2r	1322.8±33.6	36.4	998.5±27.4	32.5	2.9
NYPK-7.3c	1355.6±34.6	35.6	1032±28.3	31.4	2.0
NYPK-8.1c	1264.8±32.3	26.5	1001.8±26.9	26.3	-1.0
NYPK-8.2r	1174±30	21.0	954.1±25.6	23.0	-1.6
NYPK-8.3c	1283.7±32.7	28.4	997.5±28.1	28.7	-1.4
NYPK-8.4c	1329.8±33.9	33.0	1000.5±29.1	32.9	-1.1
NYPK-8.5r	1160.8±29.7	19.7	936±26.2	24.0	-3.5

δ^1 percent deviation of the matrix uncorrected ratios from their reference age.
δ^2 percent deviation of the matrix corrected ratios from their reference age.

TABLE E.4. SHRIMP U–PB–TH XENOTIME ISOTOPIC DATA FOR XENOTIME ANALYSED IN SESSION SHII-(Dec-05).

Grain.area	^{206}Pbc %	^{232}Th/^{238}U	^{206}Pb/^{238}U_mc ± 1σ (%)	^{206}Pb/^{238}U_mc ± 1σ (Ma)	^{208}Pb/^{232}Th_mc ± 1σ (%)	^{208}Pb/^{232}Th_mc ± 1σ (Ma)	Disc. %
BS-1-2.10	-2.66	6.52	0.0845±3.1	523±15.4	0.0266±3	530±15.8	-1.3
BS-1-2.8	-2.52	6.32	0.0805±3	499.1±14.5	0.0253±3	505.1±15	-1.2
BS-1-2.9	0.00	10.07	0.0833±2.5	515.9±12.4	0.0257±2.9	513.1±14.5	0.6
BS-1-3.1	1.78	6.89	0.0822±2.7	509.4±13.1	0.0259±2.8	516.7±14.3	-1.4
BS-1-3.2	0.50	6.73	0.0841±2.6	520.3±13.1	0.0261±2.7	521.5±14.1	-0.2
BS-1-3.3	-0.17	7.05	0.083±2.5	514.3±12.2	0.0255±2.7	508.2±13.5	1.2
BS-1-3.4	0.39	6.82	0.0789±2.5	489.6±11.8	0.0254±2.9	506.7±14.3	-3.4
BS-1-3.5	-0.20	6.86	0.0834±2.5	516.5±12.4	0.0251±3	500.9±15	3.1
BS-1-4.1	-0.19	10.40	0.085±2.5	525.7±12.7	0.0262±2.7	523.5±13.8	0.4
BS-1-4.2	0.93	7.81	0.0816±2.5	505.6±12	0.0252±2.9	502.8±14.4	0.6
BS-1-4.3	0.65	7.70	0.0805±2.5	499.3±12.2	0.0246±2.7	492±13	1.5
BS-1-4.4	-0.63	9.82	0.0828±2.6	513.1±12.6	0.0256±2.9	511.5±14.5	0.3
BS-1-5.1	0.82	8.30	0.0801±2.5	497±11.9	0.0246±2.7	492.1±13	1.0
BS-1-5.2	1.07	10.49	0.0802±2.6	497.3±12.4	0.0249±3	496.3±14.6	0.2
Z6413-5.1	0.00	0.19	0.1642±2.5	979.9±23.1	0.0474±2.7	936.2±25	4.7
Z6413-5.2	0.00	0.18	0.1696±2.4	1009.9±22.1	0.0519±2.7	1022.2±27	-1.2
Z6413-5.3	0.01	0.18	0.1668±2.4	994.2±22.4	0.0504±2.8	993.7±26.7	0.1
Z6413-5.4	0.01	0.18	0.1677±2.4	999.3±22.1	0.0508±2.7	1001.4±26.6	-0.2
Z6413-6.1	-0.01	0.18	0.17±2.4	1012±22.3	0.0521±2.7	1027±27.4	-1.5
Z6413-6.2	-0.01	0.18	0.1698±2.5	1011.1±23.6	0.0515±2.7	1015.7±27	-0.5
Z6413-6.3	0.02	0.18	0.1673±2.3	997.4±21.7	0.0506±2.7	998.4±26.6	-0.1
Z6413-6.4	0.02	0.18	0.166±2.4	990.1±22.1	0.0498±2.7	981.8±26.2	0.8
Z6413-6.5	0.00	0.19	0.1631±2.4	974±22.1	0.0494±2.9	974.6±27.6	-0.1
Z6413-6.6	-0.01	0.19	0.1634±2.4	975.5±22.1	0.05±2.9	986.9±27.6	-1.2
Z6413-7.1	0.01	0.18	0.1671±2.4	996.3±22.3	0.0499±2.9	985.1±28	1.1
Z6413-7.2	0.00	0.18	0.1664±2.4	992.2±22.3	0.0498±3	981.6±28.5	1.1
NYPK-3.2r	0.01	0.34	0.1709±2.4	1016.8±22.9	0.0521±2.7	1027.5±27.1	-1.0
NYPK-3.3r	0.01	0.34	0.1699±2.4	1011.5±22.5	0.0513±2.7	1010.6±26.7	0.1
NYPK-4.1c	0.02	0.25	0.1751±2.4	1040.2±22.8	0.0531±2.9	1046.5±29.7	-0.6
NYPK-4.10c	-0.01	0.24	0.1629±2.4	972.7±22	0.0497±2.8	979.7±27.2	-0.7
NYPK-4.11r	0.04	0.30	0.1647±2.5	982.9±23	0.0495±2.8	977.1±26.4	0.6
NYPK-4.12r	-0.01	0.33	0.1614±2.4	964.4±21.2	0.0471±2.9	929.5±26.2	3.8
NYPK-4.2c	0.01	0.31	0.1838±2.5	1087.5±24.9	0.0564±2.9	1109±31.6	-1.9
NYPK-4.3c	0.02	0.25	0.1681±2.6	1001.7±24.1	0.0512±2.8	1008.4±28	-0.7
NYPK-4.4c	0.02	0.32	0.1704±2.4	1014.3±22.8	0.0508±2.9	1001.1±28.4	1.3
NYPK-4.5c	-0.01	0.26	0.1695±2.4	1009.3±22	0.0516±3	1016±29.6	-0.7
NYPK-4.6c	0.00	0.25	0.167±2.4	995.4±22.1	0.0509±2.9	1004.4±28.8	-0.9
NYPK-4.7c	0.00	0.19	0.1626±2.5	971.2±23	0.0493±3	972.9±28.1	-0.2

Table E.4. continued.

Grain.area	^{206}Pbc %	^{232}Th/^{238}U	^{206}Pb/^{238}U_mc ± 1σ (%)	^{206}Pb/^{238}U_mc ± 1σ (Ma)	^{208}Pb/^{232}Th_mc ± 1σ (%)	^{208}Pb/^{232}Th_mc ± 1σ (Ma)	Disc. %
NYPK-4.8c	0.01	0.26	0.1685±2.6	1003.6±24.3	0.0505±3	995.8±29.1	0.8
NYPK-4.9c	0.00	0.25	0.1684±2.5	1003.1±23.3	0.0508±3	1002.2±29.2	0.1
NYPK-5.1c	0.02	0.24	0.1715±2.4	1020.2±22.8	0.0526±2.7	1035.6±27.7	-1.5
NYPK-5.2c	0.02	0.24	0.1687±2.6	1004.8±23.9	0.0505±3	996.6±29.1	0.8
NYPK-5.3r	0.01	0.23	0.1591±2.8	951.9±24.9	0.05±3	986.4±29.3	-3.5
NYPK-7.1r	-0.01	0.31	0.1651±2.5	985.3±22.9	0.0503±3.1	992.4±29.5	-0.7
NYPK-7.2r	0.02	0.26	0.1632±2.5	974.7±22.7	0.0506±2.8	998.5±27.4	-2.4
NYPK-7.3c	0.00	0.17	0.1699±2.5	1011.4±23.6	0.0524±2.8	1032±28.3	-2.0
NYPK-8.1c	0.01	0.20	0.1673±2.4	997.5±22.2	0.0508±2.8	1001.8±26.9	-0.4
NYPK-8.2r	0.00	0.28	0.1562±2.4	935.4±21	0.0483±2.7	954.1±25.6	-2.0
NYPK-8.3c	-0.01	0.24	0.1642±2.5	980±22.3	0.0506±2.9	997.5±28.1	-1.7
NYPK-8.4c	0.02	0.19	0.1669±2.6	994.8±23.5	0.0507±3	1000.5±29.1	-0.6
NYPK-8.5r	0.01	0.34	0.1553±2.4	930.6±21.1	0.0474±2.9	936±26.2	-0.6

1. 2σ error of mean = 1.191%. This should be added in quadrature to the uncertainty of the pooled ^{206}Pb/^{238}U ages (see section 2.1).
2. 2σ error of mean = 1.559%. This should be added in quadrature to the uncertainty of the pooled ^{208}Pb/^{232}Th ages (see section 2.1).

TABLE E.5. GENERALISED EPMA (WDS) RESULTS FOR SESSION RG-(JUN-06). (ΣREE = Nd , Sm, Eu , GD, TB, DY, HO, ER, TM, YB, LU).

Grain.area	U (wt%)	±1σ (%)	ΣREE (wt%)	±1σ (%)
MG-1-1.2	0.1103	17.41	12.57	3.31
MG-1-11.1	0.1025	18.54	12.12	3.32
MG-1-11.2	0.0956	19.67	12.27	3.34
MG-1-11.3	0.1169	16.51	12.32	3.33
MG-1-3.1	0.0908	20.59	12.39	3.34
MG-1-3.2	0.0854	21.78	12.63	3.30
MG-1-7.1	0.0842	21.85	12.85	3.28
MG-1-7.2	0.0912	20.50	12.75	3.30
MG-1-7.3	0.1195	16.32	12.68	3.30
BS-1-1.1	0.0246	70.73	17.23	2.50
BS-1-1.2	0.0213	81.69	16.99	2.48
BS-1-2.1	0.0548	32.85	16.80	2.61
BS-1-2.2	0.0573	31.59	16.99	2.62
BS-1-3.1	0.0467	38.12	16.82	2.55
BS-1-3.2	0.0558	32.08	16.88	2.56
BS-1-4.1	0.0405	43.95	17.34	2.67
BS-1-4.2	0.0372	47.85	17.46	2.69
Z6413-1.1	1.3644	6.61	15.53	2.37
Z6413-2.1	0.6207	7.27	15.54	2.36
Z6413-3.1	1.3750	6.61	15.70	2.35
Z6413-3.2	1.3632	6.62	15.76	2.34
Z6413-3.3	1.4225	6.59	15.84	2.34
Z6413-3.4	1.4422	6.59	15.70	2.35
Z6413-4.1	1.0806	6.74	15.72	2.35
Z6413-4.2	1.0632	6.74	15.73	2.35

D43764-2A.1	1.4957	6.59	16.83	2.50
D43764-2A.2	0.8966	6.87	17.86	2.50
D43764-2A.3	0.9035	6.87	17.85	2.53
D43764-2B.1	1.0509	6.77	17.81	2.49
D43764-2B.2	1.1416	6.71	16.84	2.49
D43764-3A.1	2.1060	6.48	17.32	2.53
D43764-3A.2	1.6161	6.55	17.58	2.51
D43764-3A.3	0.6546	7.21	17.07	2.45
D43764-6A.1	1.2616	6.66	17.13	2.51
D43764-6A.3	1.4447	6.60	16.89	2.55
D43764-6A.2	0.9234	6.84	16.76	2.48
D43764-6B.1	1.4173	6.60	17.65	2.38
D43764-6B.2	1.4134	6.60	17.55	2.38
D43764-6B.3	1.6935	6.54	17.60	2.38
D43764-7B.1	1.1486	6.70	17.21	2.50
D43764-7B.2	2.0221	6.49	16.72	2.59
D43764-7C.1	1.1914	6.68	17.73	2.58
D43764-7C.2	1.2311	6.67	17.53	2.56
D43764-8A.1	0.9729	6.81	17.46	2.51

Table E.6. Table showing the xenotime matrix uncorrected and matrix corrected $^{206}Pb/^{238}U$ ratios for session RG-(Jun-06).

Grain.area	$^{206}Pb/^{238}U$ ± 1σ (Ma)	% δ[1]	$^{206}Pb/^{238}U$_mc ± 1σ (Ma)	% $^{206}Pb/^{238}U$ correction	% δ2
BS-1-1.1	521.7±63.9	2.5	502.6±62.9	3.8	-1.3
BS-1-1.2	525.7±17.8	3.3	507.8±21.3	3.5	-0.2
BS-1-2.1	543.9±12.9	6.9	524.5±18.4	3.7	3.1
BS-1-2.2	541.5±12.9	6.4	521.1±18.4	3.9	2.4
BS-1-3.1	520.9±13.3	2.3	502.7±18.1	3.6	-1.2
BS-1-3.2	526.5±13.6	3.4	507.3±18.4	3.8	-0.3
BS-1-4.1	530.8±13.9	4.3	510±19	4.1	0.2
BS-1-4.2	528.5±13.9	3.8	507.3±19	4.2	-0.3
Z6413-1.1	1214±21	22.2	1033±31	17.6	3.9
Z6413-2.1	1074±20	8.0	990±29	8.5	-0.4
Z6413-3.1	1190±21	19.7	1008±30	18.0	1.4
Z6413-3.2	1185±20	19.2	1005±29	17.9	1.1
Z6413-3.3	1177±20	18.4	991±29	18.8	-0.3
Z6413-3.4	1174±22	18.1	987±30	18.9	-0.7
Z6413-4.1	1129±21	13.6	989±29	14.2	-0.5
Z6413-4.2	1108±20	11.4	972±29	14.0	-2.2
D43764-2A.1*	2644±40	0.8	2222±62	19.0	-15.3
D43764-2A.2	3023±45	15.3	2687±71	12.5	2.5
D43764-2A.3	3041±48	16.0	2702±73	12.5	3.1
D43764-2B.1	3017±45	15.1	2642±70	14.2	0.8
D43764-2B.2	3071±46	17.1	2690±72	14.2	2.6
D43764-3A.1	3315±69	26.4	2612±84	26.9	-0.4
D43764-3A.2	3090±48	17.9	2558±71	20.8	-2.5
D43764-3A.3	2883±43	10.0	2641±69	9.2	0.7
D43764-6A.1	3040±47	15.9	2623±72	15.9	0.0
D43764-6A.3	3133±48	19.5	2661±74	17.8	1.5
D43764-6A.2	2877±43	9.7	2574±68	11.8	-1.8
D43764-6B.1	3094±45	18.0	2615±69	18.3	-0.3
D43764-6B.2	3059±49	16.7	2587±70	18.2	-1.3

D43764-6B.3	3154±49	20.3	2590±71	21.8	-1.2
D43764-7B.1	3007±45	14.7	2621±70	14.7	0.0
D43764-7B.2*	3055±113	16.5	2437±112	25.4	-7.1
D43764-7C.1	2982±45	13.7	2575±71	15.8	-1.8
D43764-7C.2	2918±51	11.3	2513±73	16.1	-4.2
D43764-8A.1	2922±63	11.4	2585±80	13.0	-1.4

δ^1 percent deviation of the matrix uncorrected ratios from their reference age.
δ^2 percent deviation of the matrix corrected ratios from their reference age.
Analyses marked with an * were not included in the $^{206}Pb/^{238}U$ weighted mean age calculation.

Table E.7. Table showing the xenotime matrix uncorrected and matrix corrected $^{208}Pb/^{232}Th$ ratios for session RG-(Jun-06).

Grain.area	$^{208}Pb/^{232}Th$ ± 1σ (Ma)	% δ^1	$^{208}Pb/^{232}Th$_mc ± 1σ (Ma)	% $^{208}Pb/^{232}Th$ correction	% δ2
BS-1-1.1	528.8±18.1	3.9	497.3±15.3	3.9	-2.3
BS-1-1.2	561.4±14.4	10.3	530.1±11	10.3	4.1
BS-1-2.1	529.5±11	4.0	499.6±7.2	4.0	-1.8
BS-1-2.2	529.5±11	4.0	498.1±7.2	4.0	-2.1
BS-1-3.1	548.2±11.7	7.7	517.6±7.9	7.7	1.7
BS-1-3.2	542.5±11.7	6.6	511.3±8	6.6	0.5
BS-1-4.1	545.5±11.4	7.2	511.4±7.6	7.2	0.5
BS-1-4.2	542±11.3	6.8	507.4±7.5	6.5	-0.3
Z6413-1.1*	1238.5±24.6	24.6	1041.3±14.9	18.9	4.8
Z6413-2.1*	1028.6±29	3.5	935.1±13.3	10.0	-5.9
Z6413-3.1	1202±27	21.0	1006.8±14.9	19.4	1.3
Z6413-3.2	1206±24	21.4	1010.5±13.5	19.4	1.7
Z6413-3.3	1210±24	21.7	1005.2±13.6	20.3	1.1
Z6413-3.4	1201±24	20.8	997.8±16	20.3	0.4
Z6413-4.1	1129±23	13.6	975.8±14.3	15.7	-1.8
Z6413-4.2	1104±23	11.1	955.7±13.6	15.5	-3.9
D43764-2A.1	3079±75	17.4	2517±54	22.4	-4.0
D43764-2A.2	3081±68	17.5	2642±48	16.6	0.8
D43764-2A.3*	2615±56	-0.3	2237±37	16.9	-14.7
D43764-2B.1	3023±57	15.3	2552±36	18.5	-2.7
D43764-2B.2*	2765±49	5.4	2345±29	17.9	-10.6
D43764-3A.1	3391±74	29.3	2566±51	32.2	-2.2
D43764-3A.2	3198±66	22.0	2548±45	25.5	-2.8
D43764-3A.3	2892±55	10.3	2572±35	12.4	-1.9
D43764-6A.1	3100±59	18.2	2587±37	19.8	-1.3
D43764-6A.2	2928±53	11.7	2663±41	9.9	1.6
D43764-6A.3	3241±63	23.6	2545±31	27.3	-2.9
D43764-6B.1	3258±59	24.3	2652±36	22.8	1.2
D43764-6B.2	3188±57	21.6	2600±35	22.6	-0.8
D43764-6B.3	3349±61	27.7	2646±38	26.6	0.9
D43764-7B.1	3101±55	18.3	2616±33	18.5	-0.2
D43764-7B.2	3341±109	27.4	2580±82	29.5	-1.6
D43764-7C.1	3073±55	17.2	2559±33	20.1	-2.4
D43764-7C.2	3064±58	16.9	2549±36	20.2	-2.8
D43764-8A.1	3041±64	16.0	2603±44	16.8	-0.7

δ^1 percent deviation of the matrix uncorrected ratios from their reference age.
δ^2 percent deviation of the matrix corrected ratios from their reference age.
Analyses marked with an * were not included in the $^{208}Pb/^{232}Th$ weighted mean age calculation.

Table E.8. SHRIMP U-Pb-Th xenotime isotopic data, session RG-(Jun-06).

Grain.area	^{206}Pbc %	^{232}Th/^{238}U	^{206}Pb/^{238}U_mc ± 1σ (%)	^{206}Pb/^{238}U_mc ± 1σ (Ma)	^{208}Pb/^{232}Th_mc ± 1σ (%)	^{208}Pb/^{232}Th_mc ± 1σ (Ma)	^{207}Pb/^{206}Pb ± 1σ (%)	^{207}Pb/^{206}Pb ± 1σ (Ma)	Disc. %
BS-1-1.1	0.00	6.28	0.0811±13*	502.6±62.9*	0.0249±3.1	497.3±15.3	-	-	-
BS-1-1.2	1.60	6.18	0.082±4.4	507.8±21.3	0.0266±2.1	530.1±11	-	-	-
BS-1-2.1	0.78	8.45	0.0848±3.6	524.5±18.4	0.025±1.5	499.6±7.2	0.05202±4.6	286±106	-87
BS-1-2.2	0.85	8.28	0.0842±3.7	521.1±18.4	0.025±1.5	498.1±7.2	0.053±4.7	329±106	-61
BS-1-3.1	0.43	6.57	0.0811±3.7	502.7±18.1	0.0259±1.6	517.6±7.9	0.05229±4.1	298±94	-71
BS-1-3.2	0.47	6.83	0.0819±3.8	507.3±18.4	0.0256±1.6	511.3±8	0.05211±4.4	290±102	-78
BS-1-4.1	0.38	9.58	0.0823±3.9	510±19	0.0256±1.5	511.4±7.6	-	-	-
BS-1-4.2	0.37	9.84	0.0819±3.9	507.3±19	0.0254±1.5	507.4±7.5	0.05475±4	402±90	-27
Z6413-1.1	0.01	0.18	0.1737±3.2	1033±31	0.0529±1.5*	1041.3±14.9	0.07306±0.2	1016±5	-2
Z6413-2.1	0.02	0.20	0.166±3.2	990±29	0.0474±1.5*	935.1±13.3	0.07274±0.4	1007±7	2
Z6413-3.1	0.01	0.18	0.1693±3.2	1008±30	0.0511±1.5	1006.8±14.9	0.07246±0.2	999±5	-1
Z6413-3.2	0.00	0.17	0.1686±3.2	1005±29	0.0513±1.4	1010.5±13.5	0.07183±0.2	981±5	-3
Z6413-3.3	0.00	0.17	0.1661±3.2	991±29	0.051±1.4	1005.2±13.6	0.07282±0.2	1009±5	2
Z6413-3.4	0.01	0.17	0.1654±3.3	987±30	0.0506±1.6	997.8±16	0.07177±0.2	979±5	-1
Z6413-4.1	0.02	0.19	0.1658±3.2	989±29	0.0495±1.5	975.8±14.3	0.07175±0.3	979±6	-1
Z6413-4.2	0.02	0.19	0.1627±3.2	972±29	0.0484±1.5	955.7±13.6	0.07157±0.3	974±6	0
D43764-2A.1	0.00	0.59	0.4115±3.3*	2222±62*	0.1326±2.3	2517±54	0.17711±0.1*	2626±2*	18
D43764-2A.2	0.00	0.33	0.5171±3.2	2687±71	0.1397±1.9	2642±48	0.17767±0.1*	2631±2*	-3
D43764-2A.3	0.01	0.24	0.5207±3.3	2702±73	0.117±1.8*	2237±37*	0.17611±0.3	2617±5	-4
D43764-2B.1	0.00	0.80	0.5065±3.2	2642±70	0.1346±1.5	2552±36	0.17701±0.1	2625±2	-1
D43764-2B.2	0.01	0.94	0.5178±3.3	2690±72	0.123±1.3*	2345±29*	0.17648±0.1	2620±2	-3
D43764-3A.1	0.00	0.34	0.4996±3.9	2612±84	0.1353±2.1	2566±51	0.17432±1.1	2600±18	-1
D43764-3A.2	0.00	0.25	0.487±3.4	2558±71	0.1344±1.9	2548±45	0.17649±0.2	2620±3	3
D43764-3A.3	0.01	0.86	0.5062±3.2	2641±69	0.1357±1.4	2572±35	0.17732±0.2	2628±3	-1
D43764-6A.1	0.00	0.59	0.5021±3.3	2623±72	0.1366±1.5	2587±37	0.1768±0.5	2623±8	0

Table E.8. continued.

Grain.area	$^{206}Pb_c$ %	$^{232}Th/^{238}U$	$^{206}Pb/^{238}U$_mc ± 1σ (%)	$^{206}Pb/^{238}U$_mc ± 1σ (Ma)	$^{208}Pb/^{232}Th$_mc ± 1σ (%)	$^{208}Pb/^{232}Th$_mc ± 1σ (Ma)	$^{207}Pb/^{206}Pb$ ± 1σ (%)	$^{207}Pb/^{206}Pb$ ± 1σ (Ma)	Disc. %
D43764-6A.3	0.01	0.67	0.4907±3.2	2661±74	0.1342±1.3	2663±41	0.17597±0.3	2615±5	2
D43764-6A.2	0.00	0.71	0.511±3.4	2574±68	0.1408±1.6	2545±31	0.17714±0.3	2626±5	-2
D43764-6B.1	0.00	0.17	0.5002±3.2	2615±69	0.1402±1.5	2652±36	0.17585±0.4	2614±6	0
D43764-6B.2	0.00	0.38	0.4939±3.3	2587±70	0.1373±1.4	2600±35	0.17689±0.3	2624±5	2
D43764-6B.3	0.00	0.13	0.4945±3.3	2590±71	0.1399±1.5	2646±38	0.17594±0.5	2615±8	1
D43764-7B.1	0.00	0.61	0.5018±3.3	2621±70	0.1382±1.3	2616±33	0.17585±0.2	2614±4	0
D43764-7B.2	0.01	0.63	0.4594±5.5*	2437±112*	0.1361±3.4	2580±82	0.17005±2.2*	2558±37*	6
D43764-7C.1	0.01	0.83	0.4911±3.3	2575±71	0.1349±1.4	2559±33	0.17786±0.4*	2633±7*	3
D43764-7C.2	0.00	0.60	0.4768±3.5	2513±73	0.1344±1.5	2549±36	0.1766±0.4	2621±7	5
D43764-8A.1	0.00	0.70	0.4933±3.8	2585±80	0.1374±1.8	2603±44	0.17726±1.2	2627±19	2

1. 2σ error of mean = 1.459%. This should be added in quadrature to the uncertainty of the pooled $^{206}Pb/^{238}U$ ages (see section 2.1).
2. 2σ error of mean = 1.373%. This should be added in quadrature to the uncertainty of the pooled $^{208}Pb/^{232}Th$ ages (see section 2.1).
Analyses marked with an * were not included in the respective $^{206}Pb/^{238}U$, $^{208}Pb/^{232}Th$ and $^{207}Pb/^{206}Pb$ weighted mean age calculations.

Table 1. Reference ages for xenotime samples used in this study. Uncertainties are 2σ.

Sample	$^{206}Pb/^{238}U$ (Ma)	$^{207}Pb/^{206}Pb$ (Ma)	$^{208}Pb/^{232}Th$ (Ma) (assumed)
MG-1[1]	490.0 ± 0.3	491.8 ± 0.6	490.0 ± 0.3
BS-1[1]	508.9 ± 0.3	505.5 ± 0.6	508.9 ± 0.3
Z6413[2]	994 ± 1	997 ± 1	994 ± 1
D43764[3]	2622 ± 3	2622 ± 3	2622 ± 3
NY/PK 6-80[4] **- cores**	~1012	~1012	~1012
NY/PK 6-80[4] **- rims**	~970	-~970	~970

1. Source: Fletcher et al. (2004).
2. Source: Stern & Rayner (2003).
3. Reference age interpreted from SHRIMP $^{207}Pb/^{206}Pb$ age and EPMA dating (see Appendix C).
4. Reference ages interpreted from Aleinikoff et al. (2012) (see text). Sample supplied by Dr John Aleinikoff (USGS).

Table 2. EPMA determined average compositions (wt%) for the reference xenotimes used in this study.

	MG-1	BS-1	Z6413	NY/PK 6-80 core	NY/PK 6-80 rim	D43764
	n=30	n=28	n=32	n=22	n=21	n=25
SiO_2	0.15	0.26	0.69	0.58	0.49	0.73
P_2O_5	35.10	33.24	34.27	34.27	34.38	33.87
CaO	0.02	0.01	0.02	0.09	0.08	0.10
Y_2O_3	47.07	42.76	43.58	41.89	42.45	39.35
ThO_2	0.11	0.35	0.26	0.42	0.38	1.00
U_2O_3	0.11	0.05	1.46	1.76	1.43	1.62
Nd_2O_3	0.26	0.16	0.04	0.45	0.44	0.90
Sm_2O_3	0.63	0.52	0.13	0.59	0.58	0.75
Eu_2O_3	0.37	0.21	0.03	0.04	0.05	0.02
Gd_2O_3	3.73	3.08	1.02	2.20	2.25	2.29
Tb_2O_3	0.67	0.74	0.33	0.58	0.61	0.57
Dy_2O_3	5.24	6.63	4.30	5.73	5.90	4.79
Ho_2O_3	1.07	1.46	1.19	1.36	1.36	1.10
Er_2O_3	2.26	3.99	4.37	4.18	4.05	3.68
Tm_2O_3	0.24	0.52	0.71	0.60	0.57	0.53
Yb_2O_3	0.72	2.52	5.30	3.54	3.20	3.83
Lu_2O_3	0.33	0.58	1.07	0.81	0.77	0.12
total	98.07	97.09	98.78	99.09	98.98	95.25
av. U/Th	0.96	0.15	5.79	4.19	3.76	1.62
total REE oxide	15.51	20.42	18.49	20.09	19.78	18.57

Table 3. Table comparing EPMA and SHRIMP-based xenotime U abundance determinations for reference xenotimes analysed in RG-(Sep-06). Of the three techniques presented, $RSF_{(U–Ho)}$ is superior (see text).

Labels	U ppm (EPMA)	U ppm (EPMA) %error (σ)	U ppm Fletcher et al. (2004)	% diff. to EPMA value	U ppm RSF (U-Y)	% diff. to EPMA value	U ppm RSF (U-Ho)	% diff. to EPMA value
MG-1-1.2	852	22	861	1	865	2	865	1
MG-1-1.1	853	22	860	1	865	1	892	5
MG-1-1.3	946	20	881	-7	877	-7	854	-10
MG-1-1.4	1006	19	1027	2	1012	1	973	-3
MG-1-1.5	941	20	922	-2	935	-1	955	1
MG-1-1.6	891	21	893	0	903	1	935	5
MG-1-1.8	968	20	973	1	981	1	996	3
MG-1-1.9	1104	18	1173	6	1173	6	1167	6
MG-1-1.10	1125	17	1096	-3	1076	-4	1036	-8
Z6413-1.1	13479	6	16128	16	14858	10	12924	-4
Z6413-1.11	10453	7	12526	17	11500	10	10294	-2
Z6413-1.2	16480	6	21145	22	19345	17	16034	-3
Z6413-1.3	10472	7	12387	15	11338	8	10268	-2
Z6413-1.5	15273	6	19113	20	17392	14	14666	-4
Z6413-1.6	17082	6	22717	25	20663	21	16463	-4
Z6413-1.7	8122	7	9348	13	8539	5	7989	-2
Z6413-1.8	7483	7	8597	13	7961	6	7404	-1
Z6413-1.9	7091	7	7679	8	7177	1	6996	-1
NYPK-1.1	13815	6	18157	24	16097	17	13178	-5
NYPK-1.2	14394	6	18900	24	16744	16	13912	-3
NYPK-2.1	10950	7	13850	21	12526	14	10851	-1
NYPK-3.1	11543	6	15139	24	13571	18	11343	-2
NYPK-4.1	12908	6	16049	20	14379	11	12171	-6
NYPK-5.1	17493	6	23876	27	20869	19	16191	-7
NYPK-6.1	12894	6	15590	17	14069	9	11992	-7
NYPK-6.2	13166	6	16698	21	14930	13	12406	-6
NYPK-9.1	15538	6	18347	15	16286	5	13416	-14
BS-1-1.10	225	78	291	23	270	20	249	11
BS-1-1.3	360	50	400	10	366	2	325	-10
BS-1-1.4	156	114	332	53	304	95	260	67
BS-1-1.5	226	79	368	39	338	50	304	35
BS-1-1.6	162	109	174	7	161	0	152	-6
BS-1-1.7	332	54	539	38	493	49	421	27
BS-1-1.8	363	49	440	17	406	12	357	-2
BS-1-1.9	262	67	303	14	283	8	263	0
BS-1.2	568	32	578	2	534	-6	492	-13

Table 4. Representative Th/U calibration factors calculated from MG-1, BS-1 and Z6413 (SHII = SHRIMP II, RG = SHRIMP RG).

session	MG1	BS1	Z6413	average
SHII-(Apr-05a)	0.869	0.867	0.873	0.870
SHII-(Apr-05b)[1]	0.850	0.838	0.849	0.846
SHII-(Dec-05)[2]	0.836	0.830	0.834	0.833
RG-(Jun-06)	0.928	0.912	0.942	0.927
RG-(Sep-06)	0.964	0.907	0.941	0.937
RG-(Nov-06)	0.903	0.935	0.934	0.924
RG-(Oct-06a)	0.917	0.926	0.932	0.925
RG-(Oct-06b)	0.895	0.929	0.910	0.911
RG-(Feb-07)	0.919	0.926	0.947	0.931
RG-(Apr-07)	0.936	0.927	0.947	0.937

1. Energy filter 50% (low energy ions)
2. Energy filter 90% (low energy ions)

Table 5. Table showing the typical SHRIMP xenotime U–Pb–Th fractionations for the reference xenotimes and the contrasts they have in U, Th and ΣREE concentration with the U–Pb–Th calibration standard MG-1.

Sample	Typical % $^{206}Pb/^{238}U$ fractionation	Typical % Pb/Th fractionation	Average U ppm diff. to MG1	Average Th ppm diff. to MG1	Average ΣREE wt% diff. to MG1
Z6413	17	17	12000	1000	2.8
BS-1	4–6	4–6	-500	2500	4.7
NY/PK 6-80	24	24	14400	2760	4.0
D43764	16	7	11600	5300	4.0

Table 6. Table comparing xenotime $^{206}Pb/^{238}U$ fractionations of BS-1 and Z6413, that were collected using an unfiltered and filtered secondary ion beam.

session	Sample	% Energy filter	% $^{206}Pb/^{238}U$ δ
SHII-(Apr-05a)	Z6413	-	16
SHII-(Apr-05a)	BS-1	-	5
SHII-(Apr-05b)	Z6413	50	14
SHII-(Apr-05b)	BS-1	50	4
SHII-(Dec-05)	Z6413	90	21
SHII-(Dec-05)	BS-1	90	5

% $^{206}Pb/^{238}U$ δ represents the percent deviation from the reference age.

Table 7. U–Pb–Th correction coefficients for U, Th and ΣREE, for nine SHRIMP U–Pb–Th XENOTIME SESSIONS.

	$^{206}Pb^{+}/^{270}[UO_2]^{+}$			$^{208}Pb^{+}/^{248}[ThO]^{+}$		
session	**f(U)**	**f(Th)**	**f(ΣREE)**	**f(U)**	**f(Th)**	**f(ΣREE)**
SHII-(Dec-05)[1]	0.1073	0.0026	0.0091	0.0889	0.0047	0.0124
RG-(Jun-06)	0.0899	-0.0305	0.0098	0.0857	0.0710	0.0090
RG-(Sep-06)	0.0956	-0.0733	0.0164	0.0939	-0.0765	0.0197
RG-(Nov-06)	0.1191	0.0044	0.0086	0.1040	0.0193	0.0172
RG-(Oct-06a)	0.0956	-0.0728	0.0098	0.0869	-0.0021	0.0095
RG-(Oct-06b)	0.1092	0.0864	0.0095	0.0865	0.2338	0.0155
RG-(Nov-06)	0.1000	0.0405	0.0051	0.0789	-0.0240	0.0099
RG-(Feb-07)	0.0982	0.0891	0.0071	0.1039	0.0013	0.105
RG-(Apr-07)	0.1039	0.0635	0.0046	0.0979	-0.0157	0.0085

1. Energy filter 90% (low energy ions)

TABLE 8. U–PB–TH CORRECTION COEFFICIENTS FOR U AND ΣREE FOR NINE SHRIMP U–PB–TH XENOTIME SESSIONS.

	$^{206}Pb^{+}/^{270}[UO_2]^{+}$		$^{208}Pb^{+}/^{248}[ThO]^{+}$	
session	**f(U)**	**f(ΣREE)**	**f(U)**	**f(ΣREE)**
SHII-(Dec-05)[1]	0.1083	0.0094	0.0884	0.0128
RG-(Jun-06)	0.0925	0.0086	0.0801	0.0119
RG-(Sep-06)	0.0974	0.0137	0.0972	0.0166
RG-(Nov-06)	0.1188	0.0089	0.1035	0.0181
RG-(Oct-06a)	0.0988	0.0075	0.0871	0.0091
RG-(Oct-06b)	0.1094	0.0123	0.0936	0.0211
RG-(Nov-06)	0.0954	0.0085	0.0800	0.0121
RG-(Feb-07)	0.1013	0.0089	0.1040	0.0105
RG-(Apr-07)	0.1064	0.0061	0.0970	0.0082

2. Energy filter 90% (low energy ions)

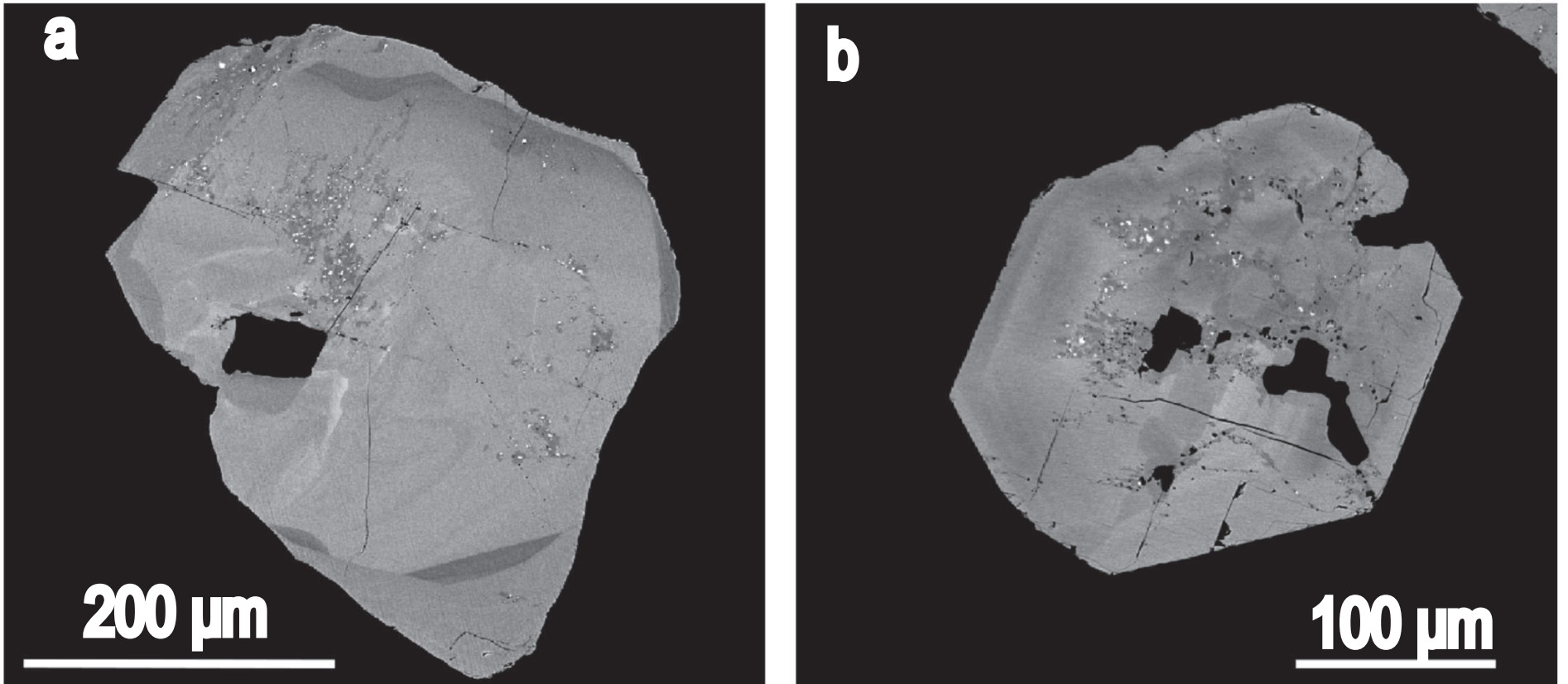

Figure 1

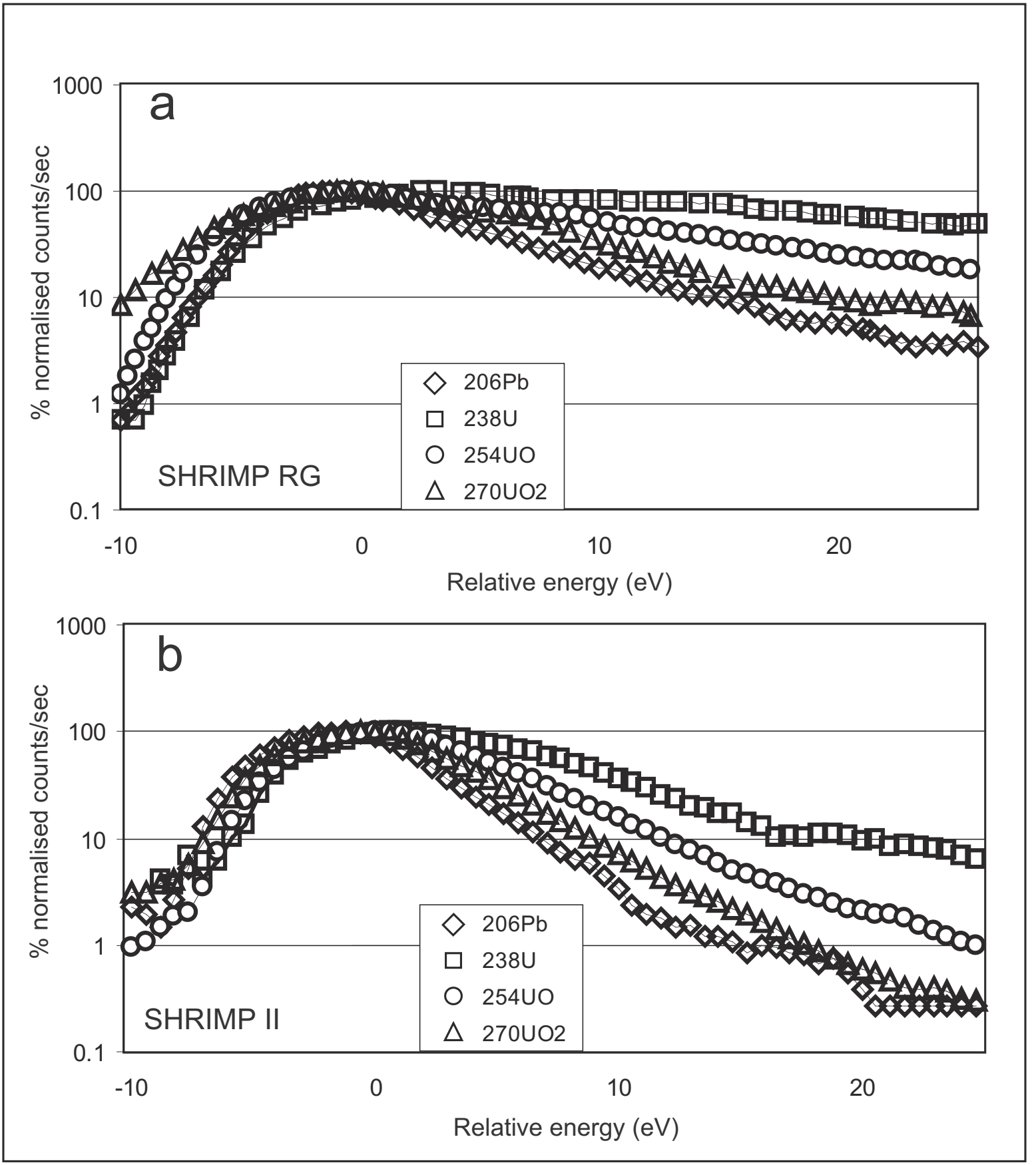
a
1000
100
10
1
0.1
% normalised counts/sec
SHRIMP RG
206Pb
238U
254UO
270UO2
-10
0
10
20
Relative energy (eV)
b
1000
100
10
1
0.1
% normalised counts/sec
SHRIMP II
206Pb
238U
254UO
270UO2
-10
0
10
20
Relative energy (eV)

Figure 2

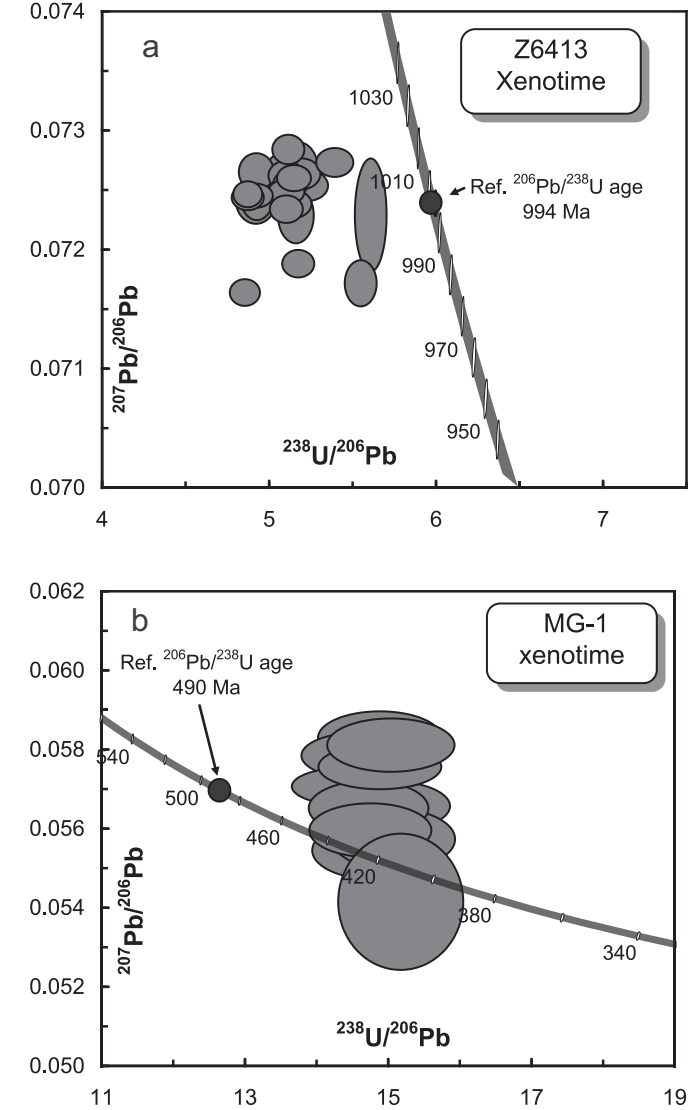
a
Z6413
Xenotime
1030
1010
Ref. 206Pb/238U age
994 Ma
990
970
950
0.074
0.073
0.072
0.071
0.070
4
5
6
7
207Pb/206Pb
238U/206Pb
b
MG-1
xenotime
Ref. 206Pb/238U age
490 Ma
540
500
460
420
380
340
0.062
0.060
0.058
0.056
0.054
0.052
0.050
11
13
15
17
19
207Pb/206Pb
238U/206Pb

Figure 3

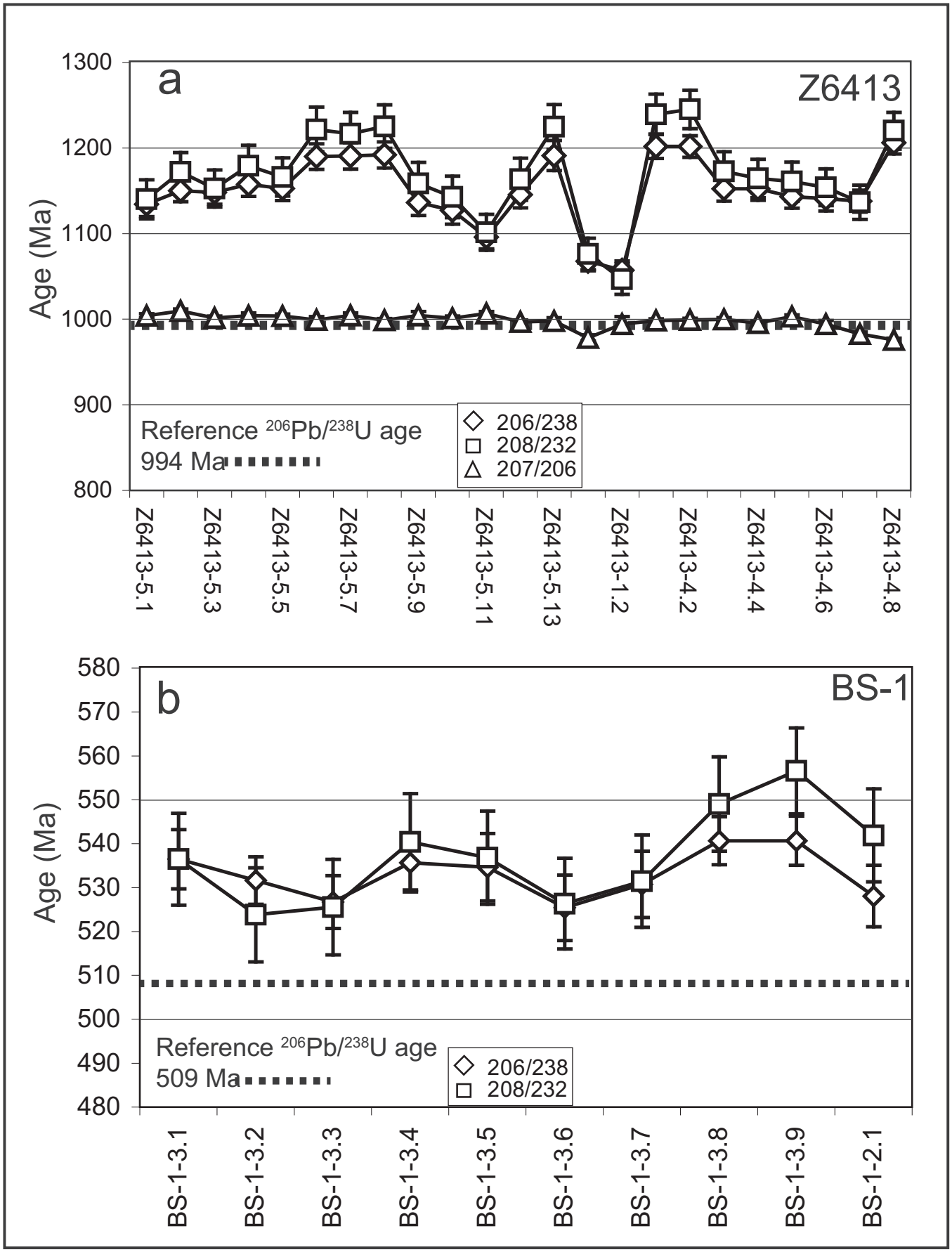
a
Z6413
Age (Ma)
1300
1200
1100
1000
900
800
Reference 206Pb/238U age
994 Ma
206/238
208/232
207/206
Z6413-5.1
Z6413-5.3
Z6413-5.5
Z6413-5.7
Z6413-5.9
Z6413-5.11
Z6413-5.13
Z6413-1.2
Z6413-4.2
Z6413-4.4
Z6413-4.6
Z6413-4.8
b
BS-1
Age (Ma)
580
570
560
550
540
530
520
510
500
490
480
Reference 206Pb/238U age
509 Ma
206/238
208/232
BS-1-3.1
BS-1-3.2
BS-1-3.3
BS-1-3.4
BS-1-3.5
BS-1-3.6
BS-1-3.7
BS-1-3.8
BS-1-3.9
BS-1-2.1

Figure 4

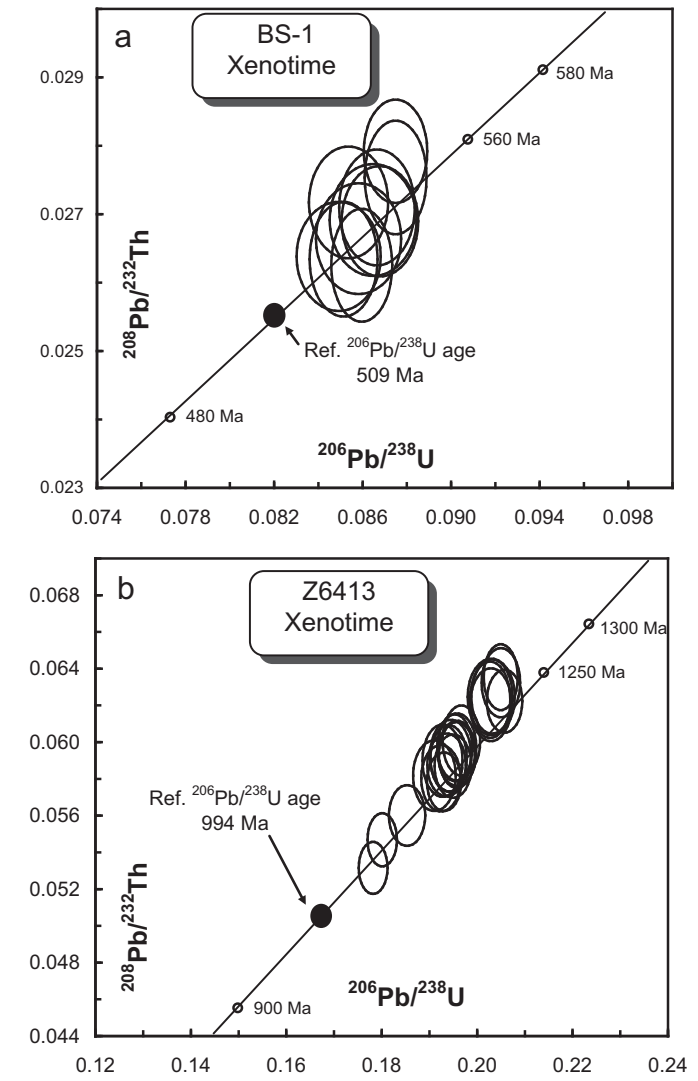
a
BS-1
Xenotime
580 Ma
560 Ma
480 Ma
Ref. 206Pb/238U age
509 Ma
208Pb/232Th
206Pb/238U
0.029
0.027
0.025
0.023
0.074
0.078
0.082
0.086
0.090
0.094
0.098
b
Z6413
Xenotime
1300 Ma
1250 Ma
900 Ma
Ref. 206Pb/238U age
994 Ma
208Pb/232Th
206Pb/238U
0.068
0.064
0.060
0.056
0.052
0.048
0.044
0.12
0.14
0.16
0.18
0.20
0.22
0.24

Figure 5

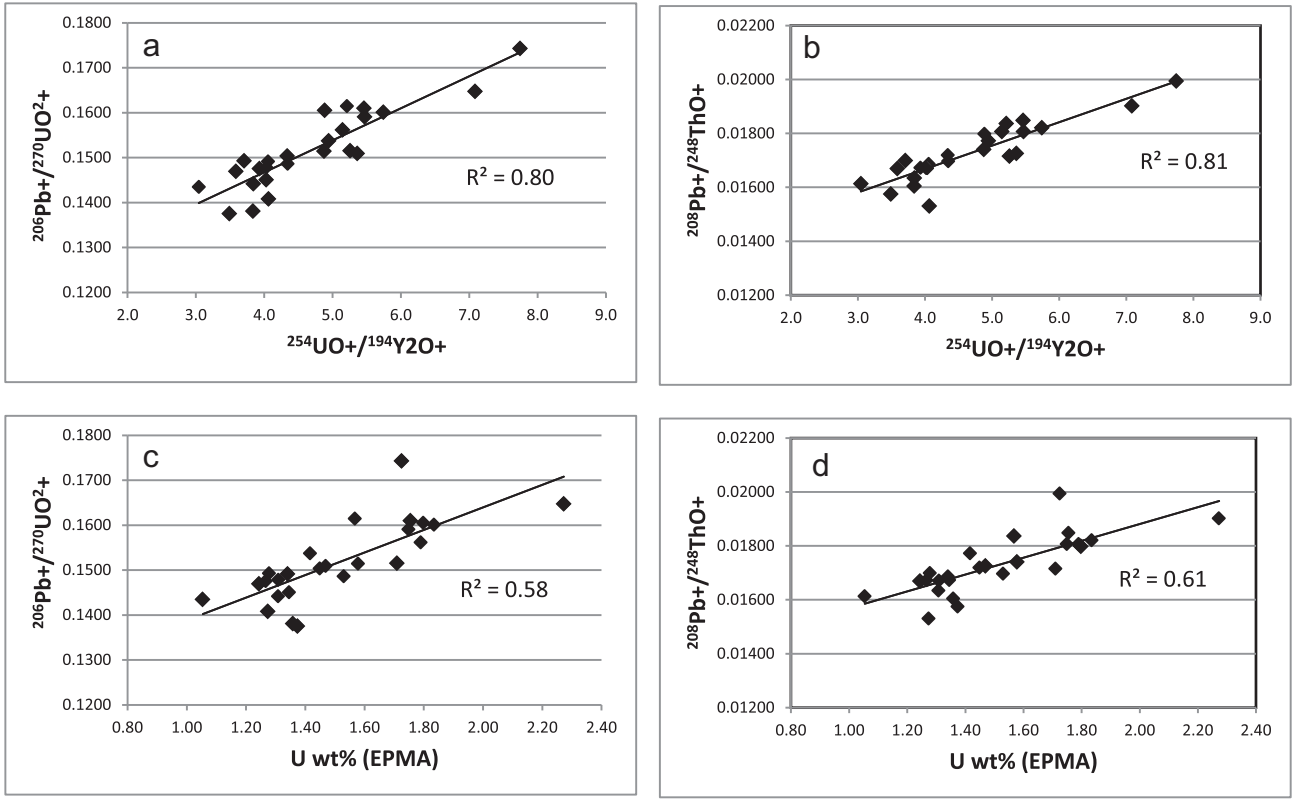
a
$^{206}Pb+/^{270}UO^{2}+$
$^{254}UO+/^{194}Y2O+$
$R^2 = 0.80$
b
$^{208}Pb+/^{248}ThO+$
$^{254}UO+/^{194}Y2O+$
$R^2 = 0.81$
c
$^{206}Pb+/^{270}UO^{2}+$
U wt% (EPMA)
$R^2 = 0.58$
d
$^{208}Pb+/^{248}ThO+$
U wt% (EPMA)
$R^2 = 0.61$

Figure 6

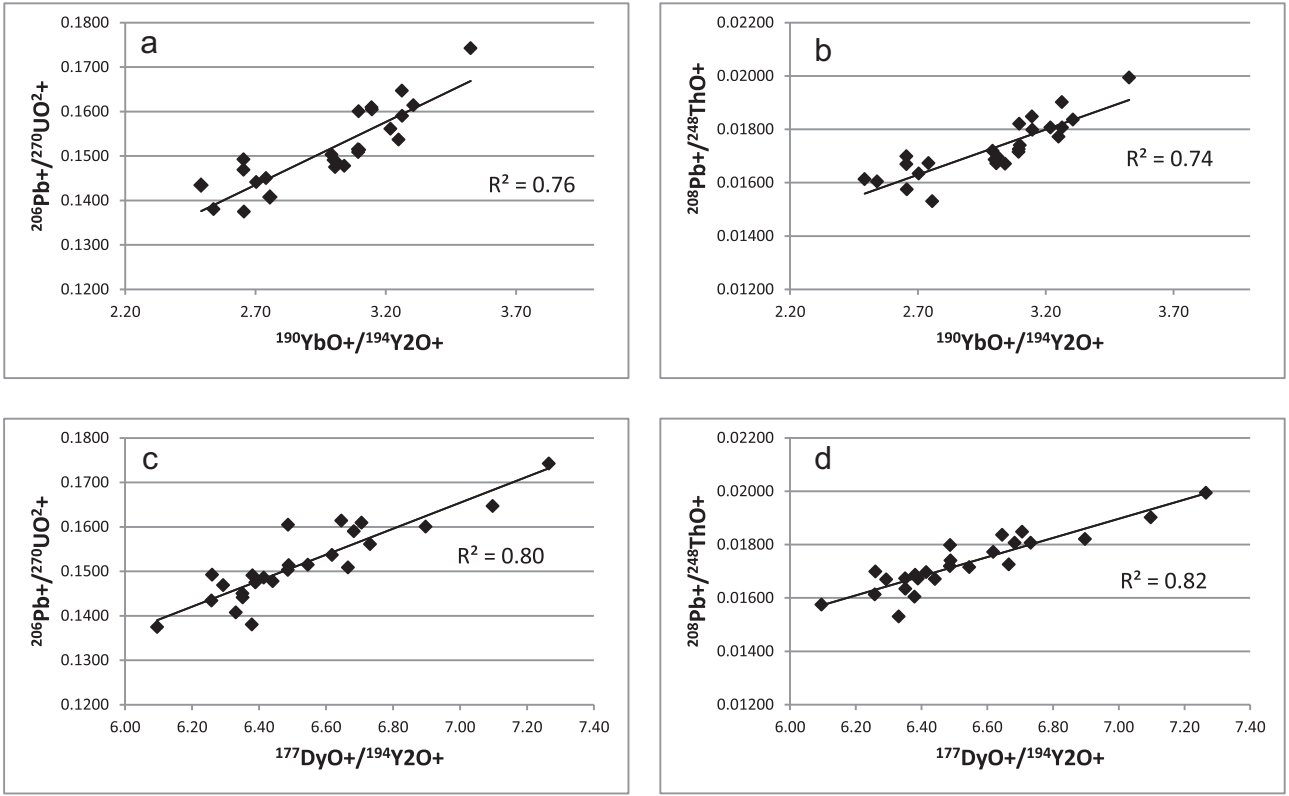
a
0.1800
0.1700
0.1600
0.1500
0.1400
0.1300
0.1200
2.20
2.70
3.20
3.70
$^{206}Pb+/^{270}UO^{2}+$
$^{190}YbO+/^{194}Y2O+$
$R^2 = 0.76$
b
0.02200
0.02000
0.01800
0.01600
0.01400
0.01200
2.20
2.70
3.20
3.70
$^{208}Pb+/^{248}ThO+$
$^{190}YbO+/^{194}Y2O+$
$R^2 = 0.74$
c
0.1800
0.1700
0.1600
0.1500
0.1400
0.1300
0.1200
6.00
6.20
6.40
6.60
6.80
7.00
7.20
7.40
$^{206}Pb+/^{270}UO^{2}+$
$^{177}DyO+/^{194}Y2O+$
$R^2 = 0.80$
d
0.02200
0.02000
0.01800
0.01600
0.01400
0.01200
6.00
6.20
6.40
6.60
6.80
7.00
7.20
7.40
$^{208}Pb+/^{248}ThO+$
$^{177}DyO+/^{194}Y2O+$
$R^2 = 0.82$

Figure 7

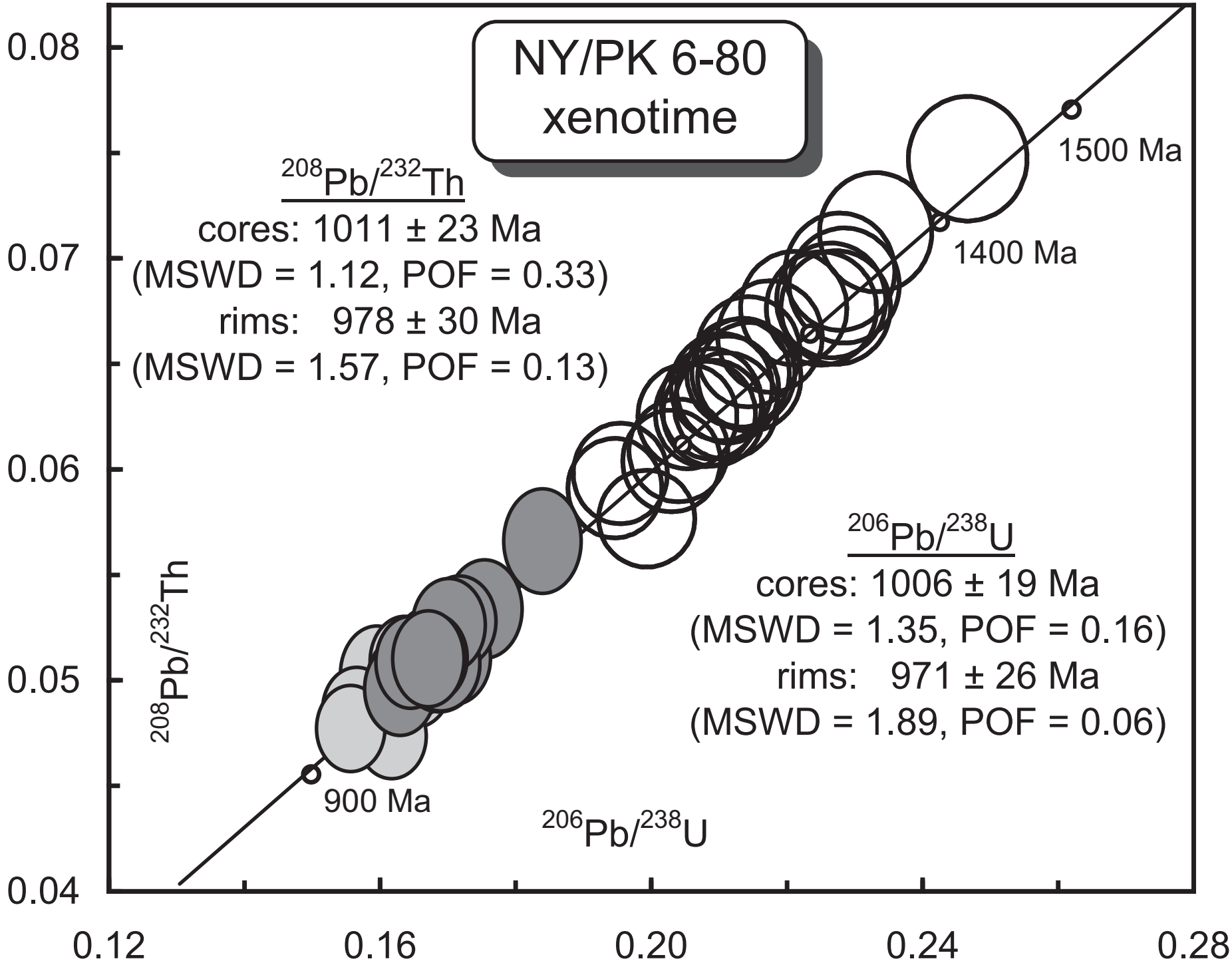
NY/PK 6-80
xenotime
208Pb/232Th
cores: 1011 ± 23 Ma
(MSWD = 1.12, POF = 0.33)
rims: 978 ± 30 Ma
(MSWD = 1.57, POF = 0.13)
206Pb/238U
cores: 1006 ± 19 Ma
(MSWD = 1.35, POF = 0.16)
rims: 971 ± 26 Ma
(MSWD = 1.89, POF = 0.06)
1500 Ma
1400 Ma
900 Ma
208Pb/232Th
206Pb/238U
0.08
0.07
0.06
0.05
0.04
0.12
0.16
0.20
0.24
0.28

Figure 8

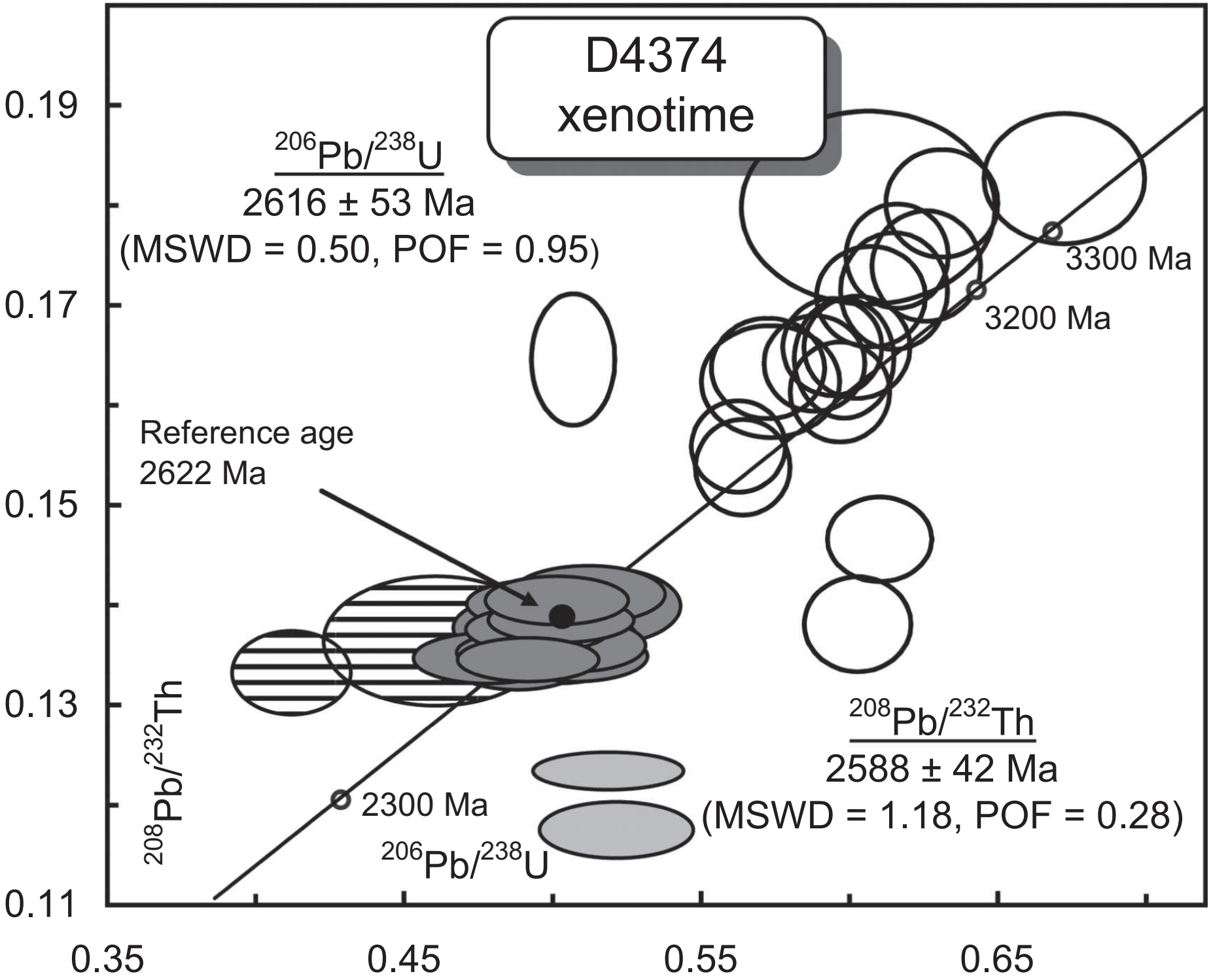
D4374
xenotime
$^{206}Pb/^{238}U$
2616 ± 53 Ma
(MSWD = 0.50, POF = 0.95)
3300 Ma
3200 Ma
Reference age
2622 Ma
$^{208}Pb/^{232}Th$
2588 ± 42 Ma
(MSWD = 1.18, POF = 0.28)
2300 Ma
$^{208}Pb/^{232}Th$
$^{206}Pb/^{238}U$
0.19
0.17
0.15
0.13
0.11
0.35
0.45
0.55
0.65

Figure 9

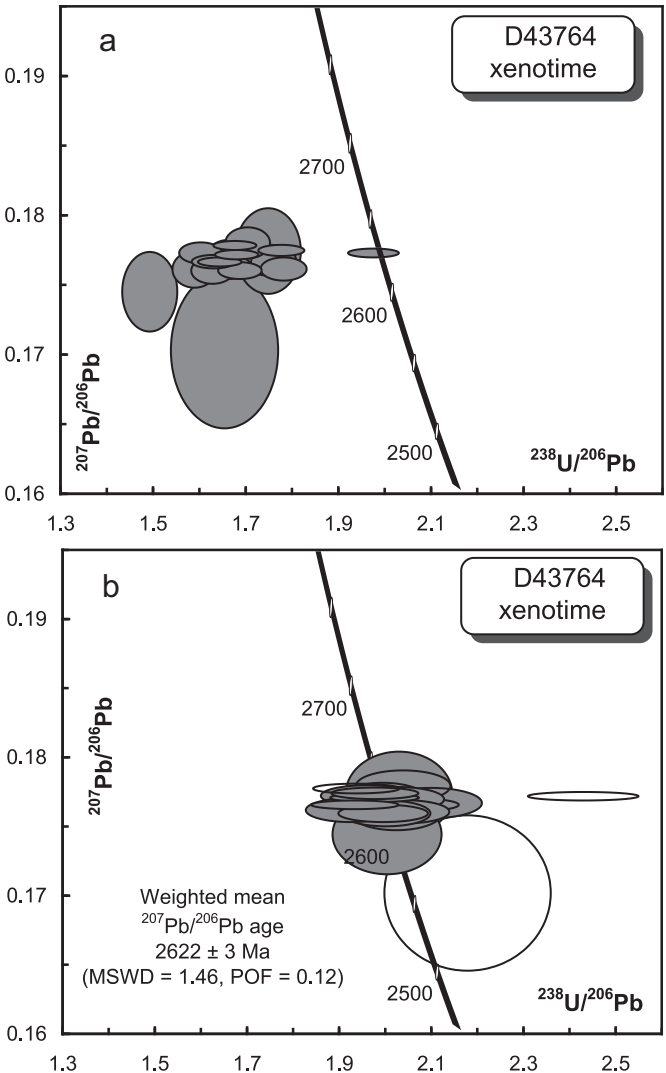
a
D43764
xenotime
2700
2600
2500
0.19
0.18
0.17
0.16
$^{207}Pb/^{206}Pb$
$^{238}U/^{206}Pb$
1.3
1.5
1.7
1.9
2.1
2.3
2.5
b
D43764
xenotime
2700
2600
2500
Weighted mean
$^{207}Pb/^{206}Pb$ age
2622 ± 3 Ma
(MSWD = 1.46, POF = 0.12)

Figure 10

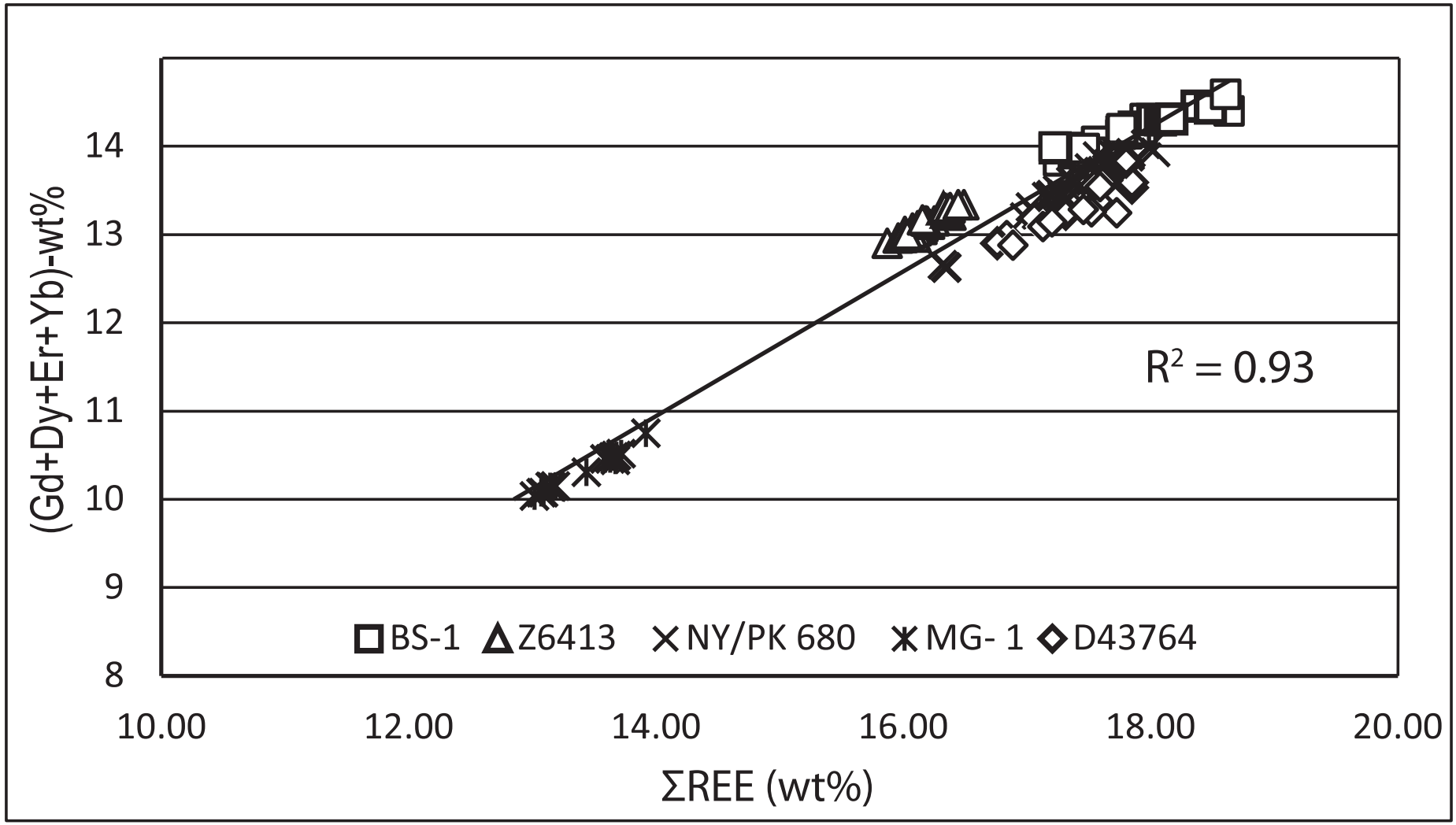
(Gd+Dy+Er+Yb)-wt%
14
13
12
11
10
9
8
10.00
12.00
14.00
16.00
18.00
20.00
ΣREE (wt%)
R² = 0.93
BS-1
Z6413
NY/PK 680
MG- 1
D43764

Figure 11